

SCAVENGING OF PARTICLES BY CLOUD DROPLETS WITH VARYING  
PARTICLE DENSITY AND RELATIVE HUMIDITY

by

Liang Zhang

APPROVED BY SUPERVISORY COMMITTEE:

---

Dr. Brian A. Tinsley, Chair

---

Dr. Phillip C. Anderson

---

Dr. Roderick A. Heelis

---

Dr. Lunjin Chen

---

Dr. Joseph M. Izen

Copyright 2017

Liang Zhang

All Rights Reserved

To my wife, Xiumei Fan, and my parents for their unwavering support and love.

SCAVENGING OF PARTICLES BY CLOUD DROPLETS WITH VARYING  
PARTICLE DENSITY AND RELATIVE HUMIDITY

by

Liang Zhang, BS, MS

DISSERTATION

Presented to the Faculty of  
The University of Texas at Dallas  
in Partial Fulfillment  
of the Requirements  
for the Degree of

DOCTOR OF PHILOSOPHY IN PHYSICS

THE UNIVERSITY OF TEXAS AT DALLAS

August 2017

## ACKNOWLEDGMENTS

I would like to express my special appreciation to everyone who has ever helped and supported me during my journey, without whom I could not complete this dissertation. The following individuals deserve my recognition and thanks for their contribution in the last five years.

I am very grateful to Dr. Brian Tinsley, my advisor, for his patience and guidance in this new area that I had never touched before. I will always remember that he read the code to me line by line, he would print and explain each important paper and text book, and his comments and suggestions on my research are priceless. He has been a tremendous mentor for me in his own work: I'm able to meet with him in early morning, late night or weekends, the joy and enthusiasm he has for his research is motivational for me. Furthermore, I own thanks to Dr. Limin Zhou, a previous PhD student of Dr. Brian Tinsley, his excellent work is the base of my current research, and every time he came the UTD I could deepen my understanding of the model.

I thank my committee members, Drs. Roderick Heelis, Lunjin Chen, Joe Izen, and Phillip Anderson, for their willingness, time, and insightful comments. In particular, Dr. Joe Izen could always propose hard but suggestive questions which gave me the incentive to think twice before jumping to any conclusion. Dr. Heelis has always been supportive to me and his suggestions always widen my perspectives. Dr. Anderson has been kind and helpful to me during the last five years, and he showed and stressed a variety of rules in research and study which will benefit me in my future career. Dr. Lunjin Chen is always ready to help me, and he showed me how to better present my logic and main points.

I am additionally thankful for the help and friendship from other students in physics department. Lyndon Bastatas has always been ready to discuss with me about the computational skills, pushing

me to learn more about the efficiency and accuracy of each algorithms. I'm grateful to Jessica Smith who gave me a lot of suggestions to start the manuscript of my proposal. I thank Zewdie Gebreab who has always shown curiosity and interest in my research and likes to discuss my progress with me. Thanks to the students who provide me cherished friendship and some joyful social activity: Yang Gao, YunJu Chen, Weikang Lin, Kuoyao Lin, Ji Yao, Xinyu Zhao, Zhiyang Xia, Daji Wu and XunLiu, I'm lucky to meet so many outstanding and helpful guys.

My sincere thanks also goes to Barbara Burbey, she is very nice and guides me to complete every administrative process that I'm not familiar with. Additionally, I repeatedly served as TA for several courses and I learned a lot from them each time, and I owe thanks to the instructors: Drs. Yuri Gartstein, Paul MacAlevey, Fan Zhang, Chuanwei Zhang, and Lindsay King.

May 2017

# SCAVENGING OF PARTICLES BY CLOUD DROPLETS WITH VARYING PARTICLE DENSITY AND RELATIVE HUMIDITY

Liang Zhang, PhD  
The University of Texas at Dallas, 2017

Supervising Professor: Brian A. Tinsley

Results of a Monte Carlo trajectory model calculating collision rate coefficients between electrically charged  $3.0\text{ }\mu\text{m}$  radius cloud droplets and aerosol particles are presented in this work. For particles with radius less than  $0.2\text{ }\mu\text{m}$  the collision rate coefficients are mainly determined by diffusion and electric forces, and if the electric force is a purely inverse square Coulomb force there exists an analytic solution, however, the image electric force induced by a particle charge can significantly enhance the collision rate coefficient. As particle radius increases the results become complicated, the effect of flow around particle ('fap') on the droplet's movement becomes significant, and the intercept effect and the weight effect also become important. These can increase or decrease the collision rate coefficient. Especially, if the particle density is greater than the droplet density, as the particle radius increases its fall speed will approach to the fall speed of the droplet, and then collisions occur at the rear-side of the droplet due to the effect of the region of low flow speed around the droplet, which will also influence other effects. When the droplet and particle charges are same-sign, for large particles with density less than that of the droplet the

predominant effect is electro-scavenging due to the short-range image electric force induced by droplet charge, but for particles with density greater than that of droplet the effect of a stagnation region below the droplet becomes significant and can reduce the effect of short-range image electric forces. The effect of relative humidity reaches maximum for about  $1.0\mu\text{m}$  particle radius and it will dominate over other effects if the relative humidity departs far from 100%; however, for smaller particles the effect of relative humidity will diminish and disappear. The solar wind modulates current flow in the global electric circuit (GEC) through which the solar activity can affect weather and climate, in this link the electrification of the cloud boundaries by the GEC can enhance the microphysical processes in clouds by charging droplets and particles, which in turn affects the microphysical collision rates as simulated in this work, and ultimately affects cloud development. However, this mechanism has still not been incorporated in current climate and cloud models due to the complexity of the microphysics. Our current efforts have been focused on the parameterization of collision rate coefficients for varying droplet radius, droplet charges, particle radius, particle charges, particle density and relative humidity. Our aim is to make the use of collision rate coefficients in cloud models simple, less time consuming and user friendly, by providing a code applying the parameterization. Thus it will be possible to incorporate the role of the global electric circuit into global climate models.



## TABLE OF CONTENTS

ACKNOWLEDGMENTS .....	v
ABSTRACT.....	vii
LIST OF FIGURES .....	xii
CHAPTER 1 CLOUD MICROPHYSICAL PROPERTIES.....	1
1.1 The Properties of Particles In Clouds .....	1
1.1.1 Cloud Condensation Nuclei (CCN) and Ice Forming Nuclei (IFN) .....	1
1.1.2 Density and Concentration of Aerosol Particles .....	2
1.2 Saturation and Relative Humidity in Clouds .....	2
1.3 Global Electric Circuit and Cloud Charging.....	3
1.3.1 Introduction.....	3
1.3.2 Global Electric Circuit and climate change .....	4
1.3.3 Global Electric Circuit and modulation by solar activity .....	6
1.3.4 Electrification of cloud boundary .....	8
1.3.5 Charges attached to droplet and aerosol particles .....	9
1.3.6 Scavenging of charged aerosol particles by droplets in clouds .....	10
CHAPTER 2 SCAVENGING OF PARTICLES BY DROPLET IN FLUX MODEL.....	11
2.1 Analytic solution of Collision Rate Coefficient.....	12
2.1.1 Particle concentration in flux model .....	12
2.1.2 Unventilated Brownian diffusion collision rate coefficient .....	13
2.1.3 Ventilated Brownian diffusion collision rate coefficient .....	16
2.2 Flow field around droplet .....	21
2.3 Thermophoretic force and diffusiophoretic force .....	24
CHAPTER 3 MONTE CARLO TRAJECTORY MODEL .....	26
3.1 Introduction of Monte Carlo trajectory model.....	26
3.1.1 Collision Rate Coefficient and collision efficiency .....	26
3.1.2 Control function of particle movement.....	28
3.1.3 Random movement of particles .....	29
3.1.4 The relaxation time, time step and the inertia of particle. ....	30
3.1.5 The boundary of computational area. ....	36

3.2 Conducting sphere electric force .....	38
3.3 The intercept effect of particle .....	42
3.4 The weight effect and the stagnation region .....	42
3.5 Effects of ‘fap’ and electric force on droplet movement .....	46
3.5.1 Effect of flow around the particle (‘fap’).....	47
3.5.2 Effect of electric forces .....	50
CHAPTER 4 PARAMETERIZATION OF AEROSOL SCAVENGING DUE TO ATMOSPHERIC IONIZATION UNDER VARYING RELATIVE HUMIDITY .....	52
4.1 Approach to Simulation and Parameterization .....	52
4.2 Results and parameterization of collision rate coefficients. ....	54
4.2.1 Parameterization of $R_{0,0,RH}$ (base level) rates for varying relative humidity ..	54
4.2.2 Parameterization of collision rate coefficients $R_{0,q,RH}$ for zero droplet charge. .....	56
4.2.3 Parameterization of collision rate coefficients $R_{Q,0,RH}$ for zero particle charge. .....	60
4.2.4 Parameterization of collision rate coefficients $R_{Q,q,RH}$ for opposite-sign droplet charge and particle charge. ....	63
4.2.5 Parameterization of rate coefficients for same-sign droplet charge and particle charge. ....	68
4.3 Discussion .....	72
4.4 Summary .....	74
CHAPTER 5 PARAMETERIZATION OF AEROSOL SCAVENGING DUE TO ATMOSPHERIC IONIZATION UNDER VARYING PARTICLE DENSITY .....	76
5.1 Approach to Simulation and Parameterization .....	76
5.2 Results and parameterizations of collision rate coefficients. ....	78
5.2.1 Parameterization of collision rate coefficients $R_{0,0,RH,\rho}$ for zero-charged droplet and particle. ....	78
5.2.2 Parameterization of collision rate coefficients $R_{0,q,RH,\rho}$ for charged particles. .....	83
5.2.3 Parameterization of collision rate coefficients $R_{Q,0,RH,\rho}$ for charged droplets.	86
5.2.4 Parameterization of collision rate coefficients $R_{Q,a,RH,\rho}$ for opposite-sign droplet charge and particle charge. ....	89

5.2.5 Parameterization of collision rate coefficients $R_{Q,q,RH,\rho}$ for same-sign droplet charge and particle charge.....	92
5.3 Discussion and Conclusion.....	93
CHAPTER 6 CONCLUSION AND IDEAS FOR FUTURE WORK.....	96
6.1 Conclusion .....	96
6.2 Ideas for future work.....	97
REFERENCES .....	104
APPENDIX.....	108
BIOGRAPHICAL SKETCH .....	147
CURRICULUM VITAE .....	148

## LIST OF FIGURES

Figure 1.1 Effects of global current density on storm invigoration. ....	4
Figure 1.2 Meridional section of the global electric circuit. ....	6
Figure 1.3 The accumulation of electric space charge at the cloud boundary. ....	8
Figure 2.1 The value of $x$ in equation for Coulomb electric force and for phoretic forces ....	20
Figure 3.1 Diagram for the calculation of collision efficiency. ....	27
Figure 3.2 The fall speed of particle relative to undisturbed air ....	31
Figure 3.3 Three formalisms to calculate the electrical force between two spherical objects. ....	38
Figure 3.4 Collision rate coefficient for $A = 6 \text{ } \mu\text{m}$ . ....	40
Figure 3.5 Intercept effect for particle density with small density ....	41
Figure 3.6 Trajectories for particles with different particle density ....	43
Figure 3.7 Trajectory of particle around droplet in consideration of diffusion ....	45
Figure 3.8 Collision rate coefficient calculated with and without ‘fap’ ....	48
Figure 4.1 Simulated rate coefficients with ‘wif’ effect and analytic solution. ....	54
Figure 4.2 Simulated rate coefficients with droplet zero-charged . ....	55
Figure 4.3 Comparison of approximate empirical formula results with simulated rate coefficients with zero charge on droplet. ....	57
Figure 4.4 Simulated results of rate coefficient for zero charge on particle ....	60
Figure 4.5 Comparison of approximate empirical formula results with simulated rate coefficients with zero charge on particle. ....	61
Figure 4.6 Simulated results of rate coefficients for opposite sign charged droplet and particle. ....	63
Figure 4.7 Comparison of approximately empirical formula results with simulated rate coefficients for opposite sign charged droplet and particle ....	64
Figure 4.8 Contributions to rate coefficients by each of the four terms ....	65
Figure 4.9 Simulated results of rate coefficients for same sign charged droplet and particle ....	68
Figure 4.10 Comparison of approximately empirical formula results with simulated rate coefficients for same sign charged droplet and particle. ....	69
Figure 4.11 Demonstration of the fitted results of collision rate coefficient ....	73
Figure 5.1 Simulated collision rate coefficients ....	77
Figure 5.2 Simulated collision rate coefficients for zero charge on particle with varying particle radius. ....	79

Figure 5.3 Simulated collision rate coefficients for zero charge on particle with varying particle density .....	81
Figure 5.4 Comparison of approximate empirical formula results with simulated rate coefficients with zero droplet charge zero-charged.....	82
Figure 5.5 Simulated collision rate coefficients for zero droplet charge .....	83
Figure 5.6 Comparison of approximately empirical formula results with simulated rate coefficients with zero particle charge zero-charged.....	85
Figure 5.7 Simulated results of collision rate coefficient for opposite sign charged droplet and particle.....	87
Figure 5.8 Comparison of approximately empirical formula results with simulated rate coefficients for opposite sign charged droplet and particle .....	89
Figure 5.9 Simulated results of collision rate coefficient $R_{Q,q,RH,\rho}$ for particle charge $q = 10e$ , droplet charge $Q = 0, 10e, 20e, 50e, 100e$ , relative humidity $RH = 100\%$ , and particle density $\rho = 1, 500, 1000, 1500, 2000 \text{ kg} \cdot \text{m}^{-3}$ .....	90
Figure 6.1 The results of collision rate coefficient divided by the fall speed of the droplet, with droplet radius of 3, 6, 9, 12, 15 $\mu\text{m}$ , and particle density of $1 \text{ kg} \cdot \text{m}^{-3}$ .....	97
Figure 6.2 Collision rate coefficient for droplet radius of 6 and 9 $\mu\text{m}$ , with particle density of 1, 500, 1000, 1500, 2000 $\text{kg} \cdot \text{m}^{-3}$ respectively .....	98
Figure 6.3 Collision rate coefficient for droplet radius of 12 and 15 $\mu\text{m}$ , with particle density of 1, 500, 1000, 1500, 2000 $\text{kg} \cdot \text{m}^{-3}$ respectively .....	99
Figure 6.4 Collision rate coefficient for droplet radius of 6 and 9 $\mu\text{m}$ , with different particle densities, droplet not charged, particle charged.....	100
Figure 6.5 Collision rate coefficient for droplet radius of 6 and 9 $\mu\text{m}$ , with different particle densities, droplet charged, particle not charged. ....	100
Figure 6.6 Collision rate coefficient for droplet radius of 6 $\mu\text{m}$ , with different particle densities, droplet and particle are charged by same-sign and opposite-sign .....	101
Figure 6.7 Collision rate coefficient for droplet radius of 12 $\mu\text{m}$ , with different particle densities, droplet and particle are charged by same-sign and opposite-sign .....	101

# **CHAPTER 1**

## **CLOUD MICROPHYSIC PROPERTIES**

### **1.1 The Properties of Particles in Clouds**

#### **1.1.1 Cloud Condensation Nuclei (CCN) and Ice Forming Nuclei (IFN)**

Aerosol particles in clouds range from  $10^{-3}$   $\mu\text{m}$  to 10  $\mu\text{m}$  in radius; the cloud condensation nuclei (CCN) and the ice-forming nuclei (IFN) are the aerosol particles whose surfaces are suitable for the condensation of water vapor and the formation of ice. CCN and IFN can affect the process of cloud formation and precipitation, and largely determine the albedo and radiative properties of clouds (Yin, et al., 2000). The organic aerosols such as formic, acetic, pyruvic and oxalic acids make an important contribution to the cloud condensation nuclei population (Yu Shaocai, 2000; Novakov and Penner, 1993). In regions that are affected by anthropogenic pollutants, sulphate aerosols are good candidates for CCN (Charlson and Schwartz, 1992). Particle formation events observed at many locations ranging from boreal forests to polluted coastal regions can increase the global CCN condensation after considerable growth from nanometer sizes has occurred (Kulmala et al., 2004; Spracklen et al., 2008). Homogeneous freezing of liquid particles in clouds occurs below about  $-36$   $^{\circ}\text{C}$ , but the IFN can trigger heterogeneous ice nucleation at higher temperature by lowering the energy barrier to crystallization (DeMott et al, 2010). The great majority of IFN constitute soil mineral particles, while biogenic and anthropogenic materials also make a non-negligible contribution to IFN (Szyrmer and Zawadzki, 1997).

### 1.1.2 Density and Concentration of Aerosol Particles

The density of particles with diameter greater than  $2.5 \mu\text{m}$  near the earth's surface is dependent on particle species. Jenny and Sonia (2002) showed that the average value of retrieved effective density was  $1.56 \pm 0.12 \text{ g} \cdot \text{cm}^{-3}$ . The aerosol particles can exist in the form of both liquid and solid in the atmosphere and in clouds. If the aerosol particles consist of liquid solutions, their density is typically about  $1125 \text{ kg} \cdot \text{m}^{-3}$ . If particles consist of silicate dust, their representative density is about  $2000 \text{ kg} \cdot \text{m}^{-3}$ . If the shape of particles is irregular and elongated, then the effective density could be as low as  $500 \text{ kg} \cdot \text{m}^{-3}$  (Pruppacher and Klett, 1997). So that in our model, four values of particle density are applied: 500, 1000, 1500 and  $2000 \text{ kg} \cdot \text{m}^{-3}$ .

The number density of particles varies rapidly with size, altitude and location. For the middle troposphere a rough estimate is given approximately by  $-dn/d|\log a| = 3 \times 10^9 \text{ m}^{-3}$  at  $0.02 \mu\text{m}$  and  $-dn/d|\log a| = 10^8 \text{ m}^{-3}$  at  $0.2 \mu\text{m}$ . Then the mean times for  $0.02 \mu\text{m}$  radius particle charged by  $20e$  to collide with 15, 10 and  $6 \mu\text{m}$  radius droplets are  $\sim 10 \text{ min}$ ,  $\sim 30 \text{ min}$  and  $\sim 3 \text{ hr}$  respectively. For  $0.2 \mu\text{m}$  radius particle charged by  $20e$  the times are  $\sim 5 \text{ hr}$ ,  $\sim 14 \text{ hr}$ , and  $\sim 90 \text{ hr}$ . (Zhou et al., 2009). As the concentration of particles is low and mean collision time is long, one droplet can only scavenge one particle during a time interval less than 1 second.

## 1.2 Saturation and Relative Humidity in Clouds

At a given temperature, when the water vapor in the atmosphere is in equilibrium with liquid water then we call its partial vapor pressure the saturation vapor pressure. The relative humidity  $RH$  is defined as the ratio of actual water vapor pressure to the saturation water vapor pressure, and when relative humidity  $RH$  is equal to 100% the atmosphere is considered saturated. Relative humidity

and temperature influence the formation and evolution of clouds (Heymsfield and Miloshevich, 1995). In a cloud a droplet will evaporate and cool when the relative humidity  $RH$  is less than 100% (subsaturation), and water vapor will condense on a droplet surface and release heat when the  $RH$  is greater than 100% (supersaturation). The two processes create gradients of water vapor pressure and temperature around a droplet, and further exert phoretic forces on particles nearby which may influence the movement of particles as a function of size. The detailed calculation of phoretic forces will be introduced in Chapter 2.

### **1.3 Global Electric Circuit and Cloud Charging**

#### **1.3.1 Introduction**

Global thunderstorms and electrified clouds generate an electrical potential between the ionosphere and the ground which is  $\sim 250$  kV with respect to the earth's surface (Wilson, 1920, Fullekrug M., 2004). The potential drives a global vertical current density  $J_z \sim 1 - 4$  pA  $\cdot$  m $^{-2}$  from ionosphere to earth. The conductivity in the mesosphere and upper stratosphere is usually much higher than in the troposphere and lower stratosphere, so that the potential of the ionosphere usually extends to mid-stratospheric levels. The solar wind modulates the cosmic ray flux and fluxes of energetic particles that are the sources of atmospheric conductivity, and the solar wind's velocity and magnetic field determine the polar-cap potential, thus the solar wind is an important external forcing agent for global electric circuit changes. Space charges are accumulated when the downward current density flows through cloud boundaries where the conductivity gradient is large. When the space charge (initially as air ions) is transferred to droplets and aerosol particles, the collisions between them will be enhanced (electro-scavenging) or reduced (electro-



anti-scavenging) depending on the sign and magnitude of the charges. Responses of cloud microphysics to the global electric circuit could cause changes in storm invigoration and cloud cover, which may further affect weather and climate.

### 1.3.2 Global Electric Circuit and climate change

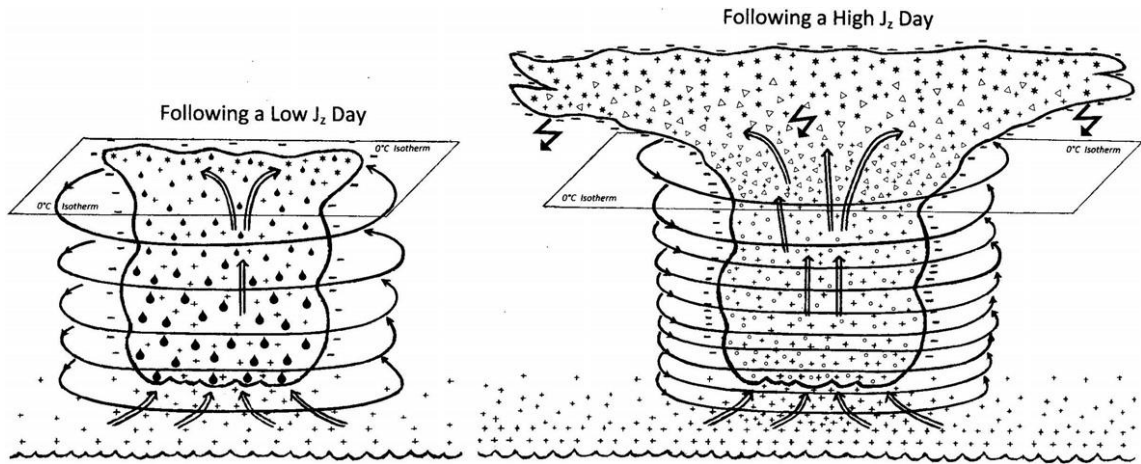


Figure 1.1. Effects of global current density  $J_z$  on storm invigoration (Tinsley, 2012).

In recent decades climate change has become a public concern and a hot topic in scientific research due to the global warming. In addition to human activity and changes in the oceans, solar activity may also be a contributor to climate change. Until now three possible solar mechanisms are proposed, that is, solar activity may affect climate through total solar irradiance, through UV irradiance and through the global electric circuit (Gray et al., 2010). Our interest focuses on the global electric circuit through which solar variability could affect the atmosphere (Lam and Tinsley, 2015). Solar activity modulates the GEC by the solar wind, but the direct energy input is very small compared to the tropospheric dynamical responses, so that large energy amplification is needed. One possible way is that electrical modulation of the continual conversion of thermal energy to

potential energy to latent heat release in clouds could affect atmospheric dynamics such as storms (Tinsley, 2012). The other way is that GEC may affect cloud cover to which the Earth's energy budget is sensitive, so that very small energy inputs from the solar wind could influence the energy flow (Tinsley and Yu, 2004; Kniveton, 2004).

As shown in Figure 1.1, storm invigoration will occur if changes in the concentration and size distribution of cloud condensation nuclei (CCN) cause changes in the size distribution of droplets as updrafts create cooling and condensation (Tinsley, 2012, Rosenfeld et al., 2008). The current density  $J_z$  could affect the electrical charging and scavenging processes and the concentration and size distribution of CCN, and thus could modulate the process of storm invigoration. For larger numbers of smaller CCN, the available water vapor is converted into larger numbers of smaller droplets, and then more liquid water is carried above the freezing level by smaller droplets instead of precipitating, and their freezing releases more latent heat which invigorates the updraft. Also, if  $J_z$  reduces the concentration of large CCN then smaller numbers of large droplets are formed, which also inhibits the coagulation and precipitation process. In addition, collisions of ice forming nuclei (IFN) with liquid droplets above the freezing level can be increased with  $J_z$  and can induce droplet freezing and release latent heat of freezing.

Changes in cloud albedo, cloud cover, and infrared opacity affect the regional energy budget, indirectly affecting regional atmospheric dynamics. This is applicable to layer clouds where the concentration and size distribution of droplets, responding to changes in cloud microphysics, act as a valve on the flow of radiation. The  $J_z$  induced changes in droplet size distribution could directly affect albedo and infrared opacity, and also could indirectly affect cloud cover due to changes in drizzle production and cellular structure in broken clouds. For both of these situations,

the action of the CCN and IFN play a role of catalysts for the partitioning of the energy flows. Electric charges produced by cosmic rays and moved by current flow in the GEC modulate the properties of the catalysts and their regulation of the energy flows.

### 1.3.3 Global Electric Circuit and modulation by solar activity

The electric current injected upward to the ionosphere by tropical thunderstorms is about 1000A, thus the total downward current should be the same amount, while solar wind affects the distribution of current density in three ways (Baumgaertner, 2013).

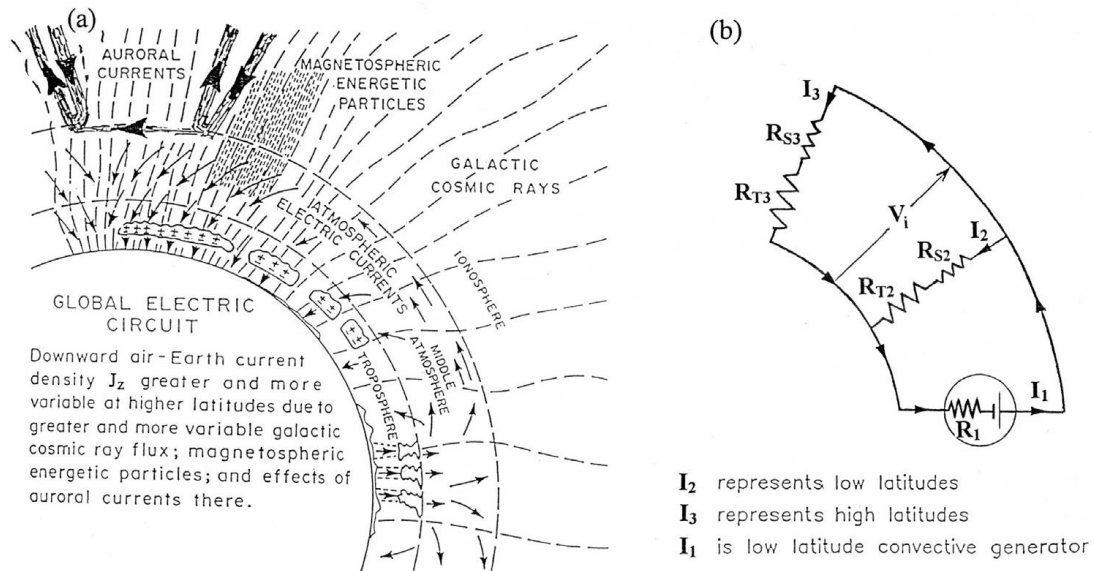


Figure 1.2. (a) Meridional section of the global electric circuit. (b) A simplified equivalent circuit of GEC. (Tinsley, 2000)

The first way is through changes in galactic cosmic ray (GCR) flux which plays a key role in the atmospheric column conductivity. The solar wind can attenuate the lower energy GCR flux, so that the GCR observed on earth shows an opposite phase to the 11-year solar cycle. For short-term solar events such as coronal mass ejection (CME), the corresponding Forbush decrease of GCR

flux usually lasts several days. Due to the shielding of the dipolar geomagnetic field, the flux of GCR is greater at high latitudes, and the changes of GCR in response to solar activity are also greater at high latitudes. In the equivalent circuit shown in Figure 1.2(b), if GCR flux decreases, then the high latitude atmospheric column conductivity will decrease, and as the current  $I_1$  basically remains constant  $I_3$  will decrease but  $I_2$  will increase (Tinsley, 2000). In short, the solar wind can modulate the redistribution of the global electric circuit current density with latitude through GCR flux change.

The second way is through changes in the precipitation of relativistic electrons from the magnetosphere, which is important to the ion production in high altitude. The relativistic electron flux can directly produce ionization above about 50 km and indirectly produce ion production by *X*-ray Bremsstrahlung reaching down to about 20 km (Fang X., 2008). The stratospheric column resistance becomes a significant component of the vertical column resistance after an eruption of a volcano, as then there is more  $\text{H}_2\text{SO}_4$  aerosol in the stratosphere, which promotes ion attachment and recombination. In this situation, the solar wind may affect  $J_z$  through changes in stratospheric resistance by relativistic electron precipitation (Tinsley et al., 1994).

The third way is through changes in the ionospheric potential distribution in the polar caps due to magnetosphere-ionosphere coupling. The solar wind drives the plasma in magnetosphere flows from dayside to night side across the earth's dipolar magnetic field and produces dawn-dusk potential differences averaging about 80 kV. The dawn-dusk potential's magnitude is determined by the solar wind speed and the *z*-component of the magnetic field. The *y*-component of the magnetic field results in an asymmetry of the dawn-dusk potential (Tsyanenko N. A., 2002). The global ionosphere is an equipotential outside the polar cap, while within the polar cap the total

potential is the sum of low latitude ionospheric potential and the superimposed dawn-dusk potential. The value of  $J_z$  is proportional to the total ionospheric potential. Thus the solar wind could influence  $J_z$  through changes in the high latitude ionospheric potential (Tinsley, 2000).

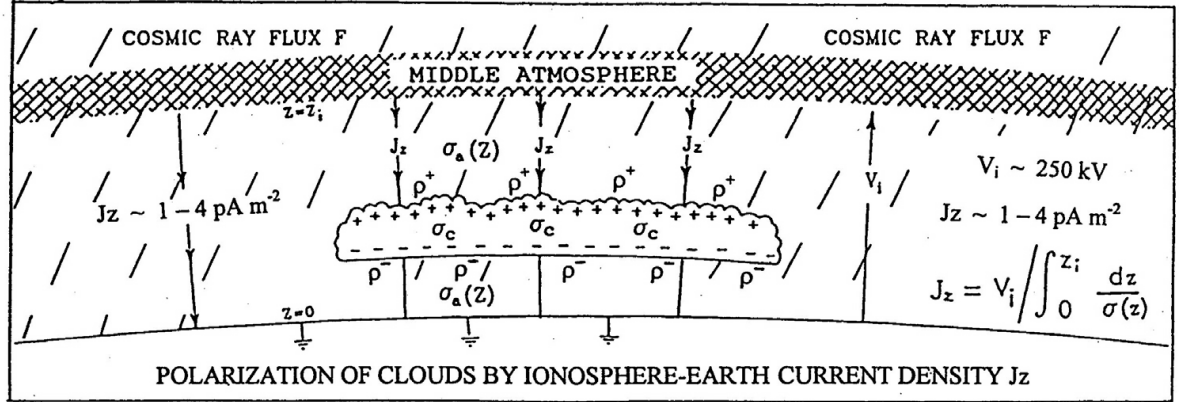


Figure 1.3. The accumulation of electric space charges at the cloud boundaries (Tinsley, 2000)

### 1.3.4 Electrification of cloud boundary

Because of the attachment of ions to droplets within clouds, near the boundaries of the clouds there are large gradients in the concentration of ions, and so large gradients of atmosphere conductivity. When a current density  $J_z$  flows through a gradient of conductivity, a gradient of electric field  $E$  results, and so space charge density  $\rho$  is generated according to Ohm's Law and Gauss's Law. As the current density  $J_z$  is downward, the net space charge in the upper boundary region is positive and in the lower boundary region is negative. Assuming the current density to be  $2 \text{ pA} \cdot \text{m}^{-2}$ , and assuming the conductivity  $\sigma$  decreases by a factor of 10 at the boundary in 10 meters, then the net space charge is estimated to be about  $\rho \sim 10^9 \text{ e} \cdot \text{m}^{-3}$  for a surface charge density of  $\sim 10^{10} \text{ e} \cdot \text{m}^{-2}$ , as shown in Figure 1.3 (Tinsley, 2000).

### **1.3.5 Charges attached to droplet and aerosol particles**

The space charge at cloud boundaries exists in the form of charged ions, charged droplets and charged particles. Due to diffusion of ions and electric field between ions and droplets and large particles, the ions are captured rapidly by droplets and large particles. In tropospheric clouds the typical lifetime of ions is a few seconds before they are captured by a droplet (Zhou and Tinsley, 2007). Measurement shows the charges of small droplets with radius of 8-10  $\mu\text{m}$  in a layer cloud range from 50e to 80e (Beard, et al., 2004). Due to diffusion, the charges on droplets and aerosol particles roughly obey a linear function of radius in an equilibrium space charge region, for example, if a 10  $\mu\text{m}$  radius droplet is charged by 50e, then one could expect a 1  $\mu\text{m}$  radius particle charged by 5e. Also, the ions are mainly captured by large size droplets, but after the droplets evaporate the charges will be left on the residues, which will form small aerosol particles with large charges.

### **1.3.6 Scavenging of charged aerosol particles by droplets in clouds**

When aerosol particles and droplets in clouds are charged, the electric forces between them make the scavenging process complex. The Coulomb electric force of opposite-sign or same-sign charges can increase or decrease the collision rate coefficients, and the image electric force induced by particle charges or droplet charges has an electro-scavenging effect. The observations of the correlation between ground-level pressure in the polar region between the interplanetary magnetic field  $B_y$  or changes in ionospheric potential showed that the weak solar wind variability can impact the earth atmosphere system (Burns et al. 2008; Lam et al., 2013). The effect of electric forces on scavenging provides a possible mechanism to amplify the very small inputs. In the polar region it

is hypothesized that the ultrafine aerosol particles that are present will be charged with same sign as the droplets at the upper boundaries of the clouds there, so that the Coulomb force plays an electro-anti-scavenging role, thus more aerosol particles can grow to CCN rather than be scavenged by droplets. The increased CCN concentration reduces the average size of droplet and increase cloud opacity, results in a stronger ‘greenhouse effect’ which will warm the surface, reduce the katabatic flow, and finally increase the ground-level pressure in polar and sub-polar region (Zhou et al., 2017). The process of aerosol scavenging due to atmospheric ionization can qualitatively explain some observations of the link between the solar variability and the atmospheric activity, and this work calculates and parameterizes the scavenging process by a Monte Carlo Trajectory Model. Then in cloud models and climate models the contribution of the global electric circuit can be quantitatively evaluated.

## **CHAPTER 2**

### **SCAVENGING OF PARTICLES BY DROPLET IN FLUX MODEL**

Scavenging of aerosol particles by cloud droplets is an important process in cloud microphysics. Heavier droplets fall faster than lighter particles due to the gravitational force, so droplets may collect, or scavenge particles along their path. However, in the coordinates of the droplet as origin, air flows upward around its surface and the drag force on small particles will keep their trajectories coinciding with flow lines deviating around the droplet, so that it is very difficult for the droplet to scavenge particles without diffusion. Diffusion allows particles to traverse across flow lines and thus collide with the droplet, therefore diffusion dominates the collision process for small particles. For large particles, the mobility decreases rapidly with increasing particle radius and the collision rates are reduced. If the relative humidity is not equal to 100%, the evaporation or condensation on the droplets will create gradients of temperature and water vapor pressure around the droplets, which will exert phoretic forces on particles. When the relative humidity is greater or less than 100%, the phoretic force will push the particle away from or toward the droplet. In the cloud boundary region, the droplets and particles are often charged, and they will attract each other, via the Coulomb force if they have opposite sign charges, or repel if they have same sign charges. The phoretic force and Coulomb force are both inversely proportional to the square of the distance between the centers of droplet and particle. In this chapter we will introduce the analytic solution of the collision rate coefficient in a flux model, which only takes account of particle diffusion, air flow field around the droplet, and the purely inverse square forces. In the next chapter we will take account of particle density, particle size, particle inertia, the image electric force, and the effect of flow around the particle in a Monte Carlo trajectory model.



## 2.1 Analytic Solution of Collision Rate Coefficient.

### 2.1.1 Particle concentration and flux

The flux of diffusing particles around the droplet is a combination of diffusion and transport,

$$\bar{\Gamma} = -D_p \nabla n + \bar{v}n, \quad (2.1)$$

where  $n$  is the number density of particles,  $\bar{v}$  is the average velocity of particles around droplet, and  $D_p$  is the diffusion coefficient of the particles which can be expressed as,

$$D_p = KTB_p, \quad (2.2)$$

where  $B_p$  is the particle mobility and is given by,

$$B_p = \frac{1 + \alpha N_{Kn}}{6\pi\eta_a a}, \quad (2.3)$$

where  $a$  is the particle radius,  $\alpha = 1.257 + 0.4e^{-1.1/N_{Kn}}$  and  $N_{Kn}$  is the Knudsen number,

$$N_{Kn} = \frac{\lambda}{a}, \quad (2.4)$$

where  $\lambda$  is the mean free path of air molecules,

$$\lambda = \frac{21.55\eta_a T^{0.5}}{P}, \quad (2.5)$$

where  $\eta_a$  is the dynamic viscosity of air and empirically given by,

$$\eta_a = \frac{1.496 \times 10^{-6} T^{1.5}}{T + 120}, \quad (2.6)$$

where  $P$  and  $T$  are the pressure and temperature of the air (Pruppacher and Klett, 1997).

In the non-steady-state the changing of particle concentration with respect to time is determined by the divergence of flux,

$$\frac{\partial n}{\partial t} = \nabla \cdot \bar{\Gamma}, \quad (2.7)$$

and according to the flux given by equation (2.1), it becomes,

$$\frac{\partial n}{\partial t} = D_p \nabla^2 n - \nabla \cdot (\bar{v} n). \quad (2.8)$$

The collision rate coefficient is defined as the rate of collisions per unit volume per unit time per unit concentration of droplets and of particles, and in the flux model the collision rate coefficient  $R_F$  is obtained by integrating the flux of particles around the droplet,

$$R_F = \frac{1}{n_0} \oint \bar{\Gamma} \cdot (-d\bar{S}), \quad (2.9)$$

where  $n_0$  is the particle concentration far from the droplet.

### 2.1.2 Unventilated Brownian diffusion collision rate coefficient

When there is no air flowing around the droplet, the collision rate coefficient is usually defined as unventilated Brownian diffusion collision rate coefficient,  $R_B$ .

#### 2.1.2.1 Diffusion for no forces between particles and droplet

In the steady-state the time-term in the left side of equation (2.8) equals to zero, and the bulk velocity  $\vec{v}$  of particles in equation (2.8) also equals to zero because there is no air flow around droplet and no forces exerted on particles. Then equation (2.8) becomes

$$D_p \nabla^2 n = 0. \quad (2.10)$$

Assuming the particle concentration is spherically symmetric,  $n = n(r)$ , then equation (2.10) becomes,

$$D_p \frac{1}{r^2} \frac{\partial}{\partial r} \left( r^2 \frac{\partial n}{\partial r} \right) = 0. \quad (2.11)$$

The solution of the number density of the particles is,

$$n = \left(1 - \frac{A}{r}\right) n_0, \quad (2.12)$$

where  $A$  is the droplet radius. According to equation (2.1) and (2.9), the value of unventilated Brownian diffusion collision rate coefficient can be obtained by,

$$R_B = \frac{1}{n_0} \oint \left( -D_p \nabla n \right) \cdot \left( -d\vec{S} \right), \quad (2.13)$$

and according to the distribution of particle concentration in equation (2.12),

$$-D_p \nabla n = -D_p \frac{n_0 A}{r^2}. \quad (2.14)$$

Finally, the value of unventilated Brownian diffusion collision rate coefficient is,

$$R_B = 4\pi D_p A. \quad (2.15)$$

#### 2.1.2.2 Purely inverse square force exerted on particles

When an inverse square force  $\vec{f}_{\text{inverse}}$  is exerted on particles, and we assume that the inverse square force is not very strong so that the inertia of small particles can be ignored, then the drag force exerted by air on particle is always equal to the inverse square force, that is,

$$\vec{f}_{\text{drag}} = \vec{f}_{\text{inverse}}. \quad (2.16)$$

The drag force is decided by particle velocity relative to the quiet air and particle mobility in the following way,

$$\vec{f}_{\text{drag}} = \frac{\vec{v}}{B_p}. \quad (2.17)$$

Next, let's define a force constant  $C$  by which the inverse square force can be written as,

$$\vec{f}_{\text{inverse}} = \frac{C}{r^2} \hat{r}. \quad (2.18)$$

Then we can get the average velocity of particles,

$$\bar{v} = \frac{B_p C}{r^2} \hat{r}. \quad (2.19)$$

Again, in the steady-state the time-term in the left side of equation (2.8) is equal to zero, equation (2.8) becomes,

$$\nabla \cdot \bar{\Gamma} = 0. \quad (2.20)$$

The flux is spherically symmetric and can be given as,

$$\bar{\Gamma} \propto \frac{1}{r^2} \hat{r}, \quad (2.21)$$

and the collision rate coefficient in equation (2.9) is a constant,

$$R_F = \frac{1}{n_0} \left( D_p \frac{\partial n}{\partial r} - v_r n \right) 4\pi r^2. \quad (2.22)$$

The average velocity is given by equation (2.19), thus

$$D_p \frac{\partial n}{\partial r} - \frac{B_p C}{r^2} n = \frac{R_F n_0}{4\pi r^2}. \quad (2.23)$$

The solution of particle concentration is,

$$n = -\frac{R_F n_0}{4\pi B_p C} + C_1 e^{-(B_p C)/(D_p r)}, \quad (2.24)$$

where  $C_1$  is a constant. The boundary conditions require the particle concentration to equal  $n_0$  far from the droplet and decrease to zero at the droplet surface, then we can get the value of the constants and finally the particle concentration is,

$$n = n_0 \frac{e^{-(B_p C)/(D_p r)} - e^{-(B_p C)/(D_p A)}}{1 - e^{-(B_p C)/(D_p A)}}, \quad (2.25)$$

and the unventilated Brownian diffusion collision rate coefficient is,

$$R_F = \frac{4\pi B_p C}{\exp(B_p C/(D_p A)) - 1}. \quad (2.26)$$

As shown in equation (2.26), when the inverse square force is attractive, then the force constant  $C$  is negative and the collision rate coefficient changes roughly linearly with the force; When the inverse square force is repulsive, then the force constant  $C$  is positive and the collision rate coefficient decreases roughly exponentially as the force increases; When the force is equal to zero, then the force constant  $C$  is equal to zero, and equation (2.26) reduces to equation (2.15).

Next let's compare the role of inverse square force and diffusion in the collision rate coefficient, and according to equation (2.23) we have,

$$\frac{|n B_p C / r^2|}{|D_p \partial n / \partial r|} = \frac{|B_p C n|}{|B_p C n + R_F n_0 / 4\pi|}. \quad (2.27)$$

It is obvious that the role of transport  $\vec{v}n$  is negligible at the droplet surface as the particle concentration  $n$  is zero there according to equation (2.25), and becomes important far away from the droplet where  $n$  approaches  $n_0$ . Thus the effect of inverse square forces on the collision rate coefficient is a long-range effect.

### 2.1.3 Ventilated Brownian diffusion collision rate coefficient

In the presence of the gravitational force, the droplet falls with speed  $U_{A,\infty}$  relative to undisturbed air. The value of the fall speed  $U_{A,\infty}$  of the droplet should make the drag force equal to the droplet's gravitational force. That is,

$$U_{A,\infty} = B_d m_1 g, \quad (2.28)$$

where  $B_d$  is the droplet mobility and  $m_1$  is the mass of the droplet. In the coordinates with origin point fixed at the droplet center, air flows upward relative to the droplet with speed of  $U_{A,\infty}$  far from the droplet, and the velocity field  $\vec{v}$  of air flow near the droplet will be given in the next

section with more details. If the particles are small enough that their inertia is negligible then the average velocity of particles is always the same as the velocity of the air flow around the droplet assuming there are no other forces.

### 2.1.3.1 Diffusion for no forces between particles and droplet

When the velocity of air flow around the droplet is non-zero, the corresponding collision rate coefficient is named ventilated Brownian diffusion collision rate coefficient,  $N_B$ . When there is no forces exerted on particles, the ventilated Brownian diffusion collision rate coefficient can be obtained by modifying the unventilated Brownian diffusion collision rate coefficient in equation (2.15) by multiplying a factor  $f_p$ ,

$$N_B = 4\pi f_p A D_p, \quad (2.29)$$

with the value of  $f_p$  containing uncertainties due to the approach used to evaluate them. To a first approximation an expression for  $f_p$  was given by Pruppacher and Klett [1997, section 17.4.2.1], and its value has been further improved in the work of Tinsley [2010] and Tinsley and Zhou [2015]. An approximate expression for  $f_p$  use with falling droplets of radii less than about 20  $\mu\text{m}$  is given in terms of the Peclet number ( $N_{Pe,p}$ ) for the particles,

$$f_p = 1 + C_f (N_{Pe,p})^{1/3}, \quad (2.30)$$

where  $C_f$  is the coefficient for first-order variation of  $f_p$  with  $(N_{Pe,p})^{1/3}$ , and has the estimated value of 0.5. The Peclet number is the key parameter and is defined as

$$N_{Pe,p} = \frac{2U_{A,\infty}A}{D_p}. \quad (2.31)$$

It is obvious that  $N_{pe,p}$  is dependent on the particle's size while independent of the particle's density. For  $A = 3 \text{ } \mu\text{m}$  and atmospheric pressure 540 hPa and temperature 256.14 K ( $-17^\circ\text{C}$ ), corresponding to mid-trophospheric conditions,  $N_B$  can be expressed by the polynomial of logarithms of particle radius  $a$ , in  $\mu\text{m}$ .

$$\log_{10} N_B = -14.6845 - 0.8244 \log_{10} a + 0.2086 (\log_{10} a)^2 + 0.0265 (\log_{10} a)^3. \quad (2.32)$$

### 2.1.3.2 Purely inverse square force exerted on particles

If the force between droplet and particle exactly obeys an inverse square law, then the ventilated Brownian diffusion collision rate coefficient can be obtained by modifying the unventilated Brownian diffusion collision rate coefficient in equation (2.26) in the following way (Pruppacher and Klett, 1997),

$$R_F = \frac{4\pi B_p C}{\exp(B_p C / (D_p f_p A)) - 1}, \quad (2.33)$$

where  $C$  is the sum of the force constants for the inverse square forces, and when the sum approaches zero the  $R_F$  will reduce to  $N_B$  in equation (2.29).

The variation of the inverse square Coulomb force between droplet of charge  $Q$  and particle of charge  $q$  with distance of  $r$  between centers is  $f_e = Qq/(4\pi\epsilon_0 r^2)$ . The Coulomb force is repulsive for  $Q$  and  $q$  of the same sign, and attractive if they have opposite sign; the convention used here is that repulsive forces are positive. The electrical force constant  $C_e$  in equation (2.33) is  $Qq/(4\pi\epsilon_0)$  as defined in equation (2.18), where  $\epsilon_0$  is the permittivity of free space. We will show in section 2.3 that when the relative humidity is not equal to 100%, there will be

thermophoretic and diffusiophoretic forces exerted on particles, which are both purely inverse square force. The total inverse square force constant  $C$  is,

$$C = C_e + C_{Th} + C_{Df}, \quad (2.34)$$

where  $C_e$ ,  $C_{Th}$  and  $C_{Df}$  represent the inverse square force constant for the electrical force, the thermophoretic force constant and diffusiophoretic force respectively. The sum of  $C_{Th}$  and  $C_{Df}$  is roughly proportional to the saturation  $s$ , where  $s = RH - 100$  and  $RH$  is the relative humidity, and the sum of  $C_{Th}$  and  $C_{Df}$  is also a function of particle radius.

For a combination of given  $RH$ ,  $A$ ,  $Q$ ,  $q$ , and particle radius  $a$ , we write  $R_F$  in equation (2.33) to be  $N_{Q,q,RH}$ . When droplet and particle are both neutral, and the relative humidity is 100%, then the rate coefficient  $N_{0,0,100\%}$  is only determined by ventilated Brownian diffusion,  $N_B$ , which is the base level of our parameterization. As  $N_B$  is the base level of our parameterization, equation (2.33) could be written in terms of  $N_B$  and  $x$ ,

$$N_{Q,q,RH} = N_B \frac{x}{e^x - 1}, \quad (2.35)$$

where,

$$x = \frac{C}{kTf_p A}. \quad (2.36)$$

For a droplet radius  $A = 3.0 \text{ } \mu\text{m}$ , atmospheric pressure 540 hPa and temperature 256.15 K, the  $x$  value is given in terms of  $Q$ ,  $q$ ,  $s$  and  $a$  by,

$$x = \sum_i A_i \times 10^{-2} (\log_{10} a)^i Qq + \sum_j B_j (\log_{10} a)^j s, \quad (2.37)$$

where  $i = 0, 1, 2, 3, 4$  and  $j = 0, 1, 2, 3, 4, 5, 6$ , and  $A_0 = 0.438$ ,  $A_1 = -0.299$ ,  $A_2 = 0.103$ ,  $A_3 = -0.275$ ,  $A_4 = -0.104$ , and  $B_0 = 7.485$ ,  $B_1 = -0.457$ ,  $B_2 = -15.378$ ,  $B_3 = -6.973$ ,  $B_4 = 6.858$ ,  $B_5 = 6.031$ ,  $B_6 = 1.260$ . If  $x \ll 0$ , the inverse square forces are



attractive, the rate coefficient is roughly linear in  $x$ ; if  $x \gg 0$ , the inverse square forces are repulsive, the rate coefficient is roughly exponential in  $x$ . This indicates the need to fit the collision rate coefficient in a different way for net attractive forces and repulsive forces, i. e., depending on whether  $q$  and  $Q$  are of like sign, and whether the saturation  $s$  is positive (for condensing droplets) or negative (for evaporating droplets).

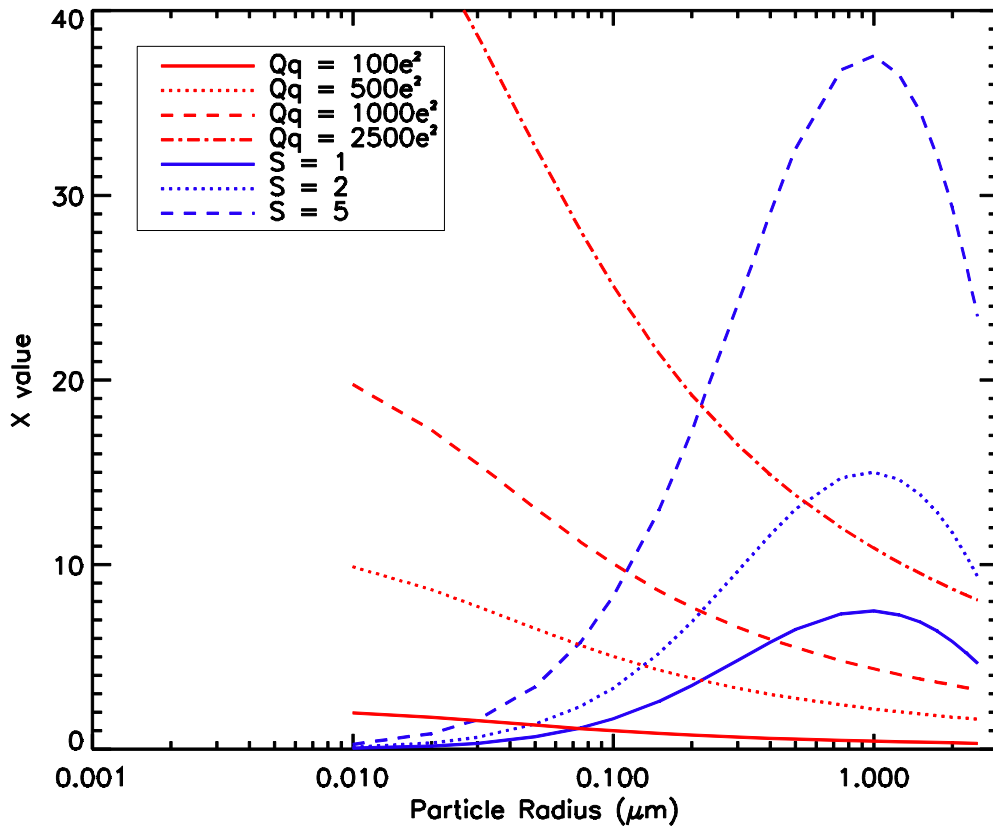


Figure 2.1. The value of  $x$  in equation (2.37) for Coulomb electric force with  $Qq = 100, 500, 1000, 2500e^2$  and for phoretic forces with  $s = 1, 2, 5$ .

Figure 2.1 compares the value of  $x$  in equation (2.37) of Coulomb electric forces and phoretic forces for a droplet radius  $A = 3.0 \mu\text{m}$ , atmospheric pressure 540 hPa and temperature 256.15 K. The electric forces with  $Qq > 0$  and the phoretic forces with  $s > 0$  are both repulsive and the

corresponding  $x$  values are positive. The  $x$  value of phoretic forces for a given saturation  $s$  has a peak at about  $1.0 \mu\text{m}$  as shown in Figure 2.1, because for smaller particle radius the phoretic forces constants  $C_{Th} + C_{Df}$  are roughly proportional to particle radius and become very small; for larger particle radius the particle mobility is small and the value of  $f_p$  is large, thus the  $x$  value of phoretic forces reaches a peak in the middle according to equation (2.36). The Coulomb electric force constant  $C_e$  is a constant for different particle radii, while the value of  $f_p$  decreases as the particle radius decreases, so that the  $x$  value of the Coulomb electric force increase as particle radius decreases. For particle radius at about  $1.0 \mu\text{m}$ , the  $x$  value of phoretic forces can be much greater than that of Coulomb force; for particle radius less than  $0.2 \mu\text{m}$ , the  $x$  value of phoretic forces decreases and the  $x$  value of the Coulomb force increases, thus for small particles the effect of the Coulomb forces are often more important than phoretic forces. Due to the  $x$  value of phoretic forces and of the Coulomb force varying in a different way, in the future chapters when we parameterize the simulated results of collision rate coefficient we deal with cases of particle radius less and greater than  $0.2 \mu\text{m}$  separately.

## 2.2 Flow field around droplet

The exact solution of air flow around a sphere for all stream velocities can be obtained by use of the Navier-Stokes function, while for the limit of very small stream velocities and very small Reynolds numbers, Stokes gave an expression for the stream function when only viscosity needs to be considered, which applies accurately only when the stream velocity or Reynolds number tends to zero. The Reynolds number is  $N_{Re} = \frac{\rho U_{A,\infty} A}{\mu}$ , where  $\rho$  is the density of air,  $A$  is the

droplet radius,  $U_{A,\infty}$  is the velocity of air flow with respect to the droplet as defined in equation (2.28), and  $\mu$  is the dynamic viscosity of air. The Stokes stream function can be written as

$$\psi_{ST} = \frac{U_{A,\infty} A^2 \sin^2 \theta}{2} \left( \frac{b^2}{A^2} - \frac{3b}{A} + \frac{A}{b} \right), \quad (2.38)$$

where  $b$  is the radial distance from the center of the droplet, and  $\theta$  is measured relative to the upstream direction,  $U_{A,\infty}$  is the fall speed of droplet relative to undisturbed air and it is the speed of upward air flow with respect to the droplet. As for any such stream function, the radial velocity  $u_r$  and the tangential velocity  $u_\theta$  are given by,

$$\begin{cases} u_r = -\frac{1}{b^2 \sin \theta} \frac{\partial \Psi}{\partial \theta} \\ u_\theta = \frac{1}{b \sin \theta} \frac{\partial \Psi}{\partial b} \end{cases}. \quad (2.39)$$

These velocities in terms of the normalized radial distance  $r = b/A$  become,

$$\begin{cases} u_{r,ST} = -U_{A,\infty} \cos \theta \left( 1 - \frac{3}{2r} + \frac{1}{2r^3} \right) \\ u_{\theta,ST} = U_{A,\infty} \sin \theta \left( 1 - \frac{3}{4r} - \frac{1}{4r^3} \right) \end{cases}. \quad (2.40)$$

These velocities become 0 for  $r = 1$  and become  $-U_{A,\infty} \cos \theta$  and  $U_{A,\infty} \sin \theta$  respectively for large  $r$ , as required for undisturbed flow.

For non-negligible Reynolds number the inertia of the air needs to be taken account of, and Oseen gave the stream function:

$$\Psi_{OR} = \frac{U_{A,\infty} A^2 \sin^2 \theta}{2} \left( \frac{b^2}{A^2} + \frac{A}{2b} \right) - \frac{3U_{A,\infty} A^2}{N_{Re}} (1 - \cos \theta) \left( 1 - e^{-\frac{bN_{Re}}{4A}(1 - \cos \theta)} \right). \quad (2.41)$$

The radial and tangential velocities in terms of the normalized radial distance are:

$$\begin{cases} u_{r,OR} = -U_{A,\infty} \cos \theta \left(1 + \frac{1}{2r^3}\right) - \frac{3U_{\infty}}{N_{Re} r^2} \left[ e^{-\frac{rN_{Re}}{4}(1+\cos \theta)} \left( \frac{rN_{Re}}{4} (1 - \cos \theta) + 1 \right) - 1 \right] \\ u_{\theta,OR} = U_{A,\infty} \sin \theta \left[ \left(1 - \frac{1}{4r^3}\right) - \frac{3}{4r} e^{-\frac{rN_{Re}}{4}(1+\cos \theta)} \right] \end{cases}. \quad (2.42)$$

Although Oseen expressions represent well the effects of inertia at large  $r$ , they do not give the required zero radial or tangential velocities at  $r = 1$  for non-zero Reynolds number.

For a falling sphere of  $N_{Re} \approx 1$ , both viscosity and inertia must be considered to evaluate the drag. Proudman and Pearson (1957) obtained a stream function, which is a first order approximation in  $N_{Re}$ , and satisfies the zero velocity condition for  $r = 1$ . That is:

$$\Psi_{PP} = \frac{U_{A,\infty} A^2 \sin^2 \theta}{2} \left( \frac{b^2}{A^2} - \frac{2b}{A} + 1 \right) \left[ \left( 1 + \frac{3}{16} N_{Re} \right) \left( 1 + \frac{4}{2b} \right) + \frac{3}{16} N_{Re} \cos \theta \left( 1 + \frac{A}{2b} + \frac{A^2}{2b^2} \right) \right]. \quad (2.43)$$

The corresponding radial and tangential velocities in terms of the normalized radial distance  $r$  are:

$$\begin{cases} u_{r,pp} = -U_{A,\infty} \cos \theta \left( 1 - \frac{3}{2r} + \frac{1}{2r^3} \right) \left( 1 + \frac{3}{16} N_{Re} \right) \\ \quad - \frac{3}{16} U_{A,\infty} N_{Re} \left( \cos^2 \theta - \frac{\sin^2 \theta}{2} \right) \left( 1 - \frac{3}{2r} + \frac{1}{2r^2} - \frac{1}{2r^3} + \frac{1}{2r^4} \right) \\ u_{\theta,pp} = -U_{A,\infty} \sin \theta \left( 1 - \frac{3}{4r} - \frac{1}{4r^3} \right) \left( 1 + \frac{3}{16} N_{Re} \right) \\ \quad + \frac{3}{16} U_{A,\infty} N_{Re} \cos \theta \left( 1 - \frac{3}{4r} + \frac{1}{4r^2} - \frac{1}{4r^3} - \frac{1}{4r^4} \right) \end{cases}. \quad (2.44)$$

These Proudman-Pearson expressions reduce to the Stokes expression for  $N_{Re} = 0$ , but don't satisfy the requirement of  $u_r = -U_{A,\infty} \cos \theta$  and  $u_{\theta} = U_{A,\infty} \sin \theta$  for  $r \rightarrow \infty$ .

The above Proudman-Pearson expressions for velocities are smaller than the Oseen expressions for  $r < 2$  and greater than them for  $r > 5$ , while matching them quite closely in the

range  $2 < r < 5$  in the general region of the droplet. In order to best evaluate the effects of air drag on the particle, we apply the PP expression for  $r < 2$ , and the OS expression for  $r > 5$ , and in the range  $2 < r < 5$  we make a smooth transition between them by using an average with linearly varying weights (Tinsley et al., 2006).

### 2.3 Thermophoretic force and diffusiophoretic force

When the relative humidity is not equal to 100%, there exist the thermophoretic force  $F_{Th}$  and the diffusiophoretic force  $F_{Df}$ . The former is caused by the temperature gradient of the air around the condensing or evaporating droplet and the latter is caused by the water vapor density gradient around the droplet, and the two forces have opposite directions.

The thermophoretic force  $F_{Th}$  can be expressed as

$$F_{Th} = -\frac{12\pi\eta_a a(k_a + 2.5K_p N_{Kn})k_a}{5(1 + 3N_{Kn})(k_p + 2k_a + 5k_p N_{Kn})P} \frac{(T_\infty - T_A)}{Ar^2}, \quad (2.45)$$

where  $k_a$  is the thermal conductivity of moist air that varies with temperature and slightly with relative humidity, and  $k_p$  is the thermal conductivity of the particles,  $P$  is the pressure of air,  $N_{Kn}$  is the Knudsen number and  $\eta_a$  is the dynamic viscosity of air which have been given in equation (2.4) and (2.6). Also  $T_\infty$  is the temperature far from the droplet of radius  $A$ , and  $T_A$  is the temperature at the surface of the droplet, so that the term  $(T_\infty - T_A)/Ar^2$  is the temperature gradient. When the droplet evaporates, the temperature at the surface is lower due to energy loss in the form of latent heat, and so that the thermophoretic force is toward the droplet. On the other hand, when droplet condenses, the thermophoretic force's direction is outward.

The diffusiophoretic force  $F_{Df}$  can be expressed as

$$F_{Df} = -\frac{6\pi\eta_a a(0.74)D_v M_a (\rho_{v,\infty} - \rho_{v,A})}{(1 + \alpha N_{Kn})M_w Ar^2}, \quad (2.46)$$

where  $D_v$  is the diffusivity of water vapor,  $M_a$  and  $M_w$  are the molecular weights of air and water, 28.96 and 18.04 respectively,  $\rho_a$  is the density of air,  $N_{Kn}$  is the Knudsen number,  $\eta_a$  is the dynamic viscosity of air as mentioned above, and  $\alpha = 1.257 + 0.4\exp(-1.1/N_{Kn})$ . The parameters  $\rho_{v,\infty}$  and  $\rho_{v,A}$  are the water vapor densities in the air far from droplet and at the droplet surface respectively, so that the term  $(\rho_{v,\infty} - \rho_{v,A})/Ar^2$  is the water vapor density gradient, which has a vapor partial pressure gradient and will exert a pressure force on the particle. When the droplet evaporates, the water vapor density will increase near droplet's surface, so that the diffusiophoretic force is outward. On the other hand, when droplet condenses, the diffusiophoretic force is inward (Tinsley et al., 2006).

As noted above, the directions of thermophoretic and diffusiophoretic forces are opposite. For the atmosphere at low altitudes whose temperature ranges between 20°C and −56°C, in general the thermophoretic force is stronger, so the net force on the particle is inward if the droplet is evaporating and outward if it is condensing.

## CHAPTER 3

### MONTE CARLO TRAJECTORY MODEL

In our Monte Carlo trajectory model, a large number of particles are released below the droplet and by integrating the probability of collision we get the value of collision rate coefficient. The flux model in Chapter 2 can only deal with the purely inverse square forces of Coulomb and phoretic forces, while our trajectory model further includes the image electrical forces and gravitational forces, which are quite important as shown in the next chapters. In addition, our trajectory model also includes the intercept effect resulting from particle size and the effect of particle inertia. For a small droplet, such as the 3  $\mu\text{m}$  droplet in our work, and a particle not much smaller, the air flow around the particle can affect the movement of the droplet, which is the ‘fap’ effect, and this is included also.

#### 3.1 Introduction of Monte Carlo trajectory model

##### 3.1.1 Collision Rate Coefficient and collision efficiency

The collision rate coefficient  $R_D$  in the Monte Carlo trajectory model, as in the flux model, means the rate of collisions per unit volume per unit time per unit concentrations of droplets and of particles. It can be calculated by,

$$R_D = \pi A^2 E_D (U_{A,\infty} - U_{a,\infty}), \quad (3.1)$$

where  $A$  and  $a$  are the radii of droplet and particle, and  $U_{A,\infty}$  and  $U_{a,\infty}$  are the fall speeds of droplet and particle relative to undisturbed air respectively, and so  $U_{A,\infty}$  and  $U_{a,\infty}$  are their relative speeds.  $E_D$  is the collision efficiency, which is calculated as

$$E_D = \sum P_i \Delta(x_i^2) = 2 \sum P_i x_i \Delta x_i, \quad (3.2)$$

where  $P_i$  is the probability of collision with droplet for the particle starting from a horizontal offset  $x_i$  below droplet, and  $\Delta x_i$  is the increment in  $x_i$ . Figure 3.1 is a diagram of the method to calculate collision efficiency. At a given position  $x_i$ , a number  $N_i$  of particles are released and we trace the trajectory for each of them. Finally, a number  $S_i$  of particles will collide with the droplet and the other  $N_i - S_i$  particles will pass over without collision, thus the probability of collision at position  $x_i$  is  $P_i = S_i/N_i$ . Then we continue to calculate the value of collision probability  $P_{i+1}$  for the position  $x_{i+1}$ , until the probability decreases to 0, and then our calculation stops. In our model, we set the position as  $x_n = x_0 \sqrt{n}$ , and  $x_0$  is a constant number, then  $\Delta(x_n^2) = x_n^2 - x_{n-1}^2 \equiv x_0^2$  is a constant value.

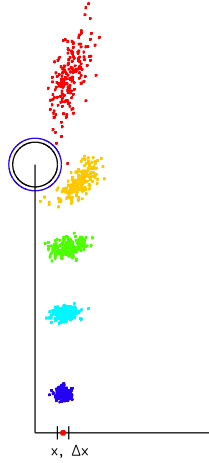


Figure 3.1. Diagram for the calculation of collision efficiency. A large number of particles are released below the droplet at position  $x$  with increment  $\Delta x$ , and some of them could collide with the droplet. The inner black circle represents droplet radius, the outer blue circle represents the sum of droplet and particle radius.



If there is no diffusion, there will exist a value of  $X_{max}$  ensuring  $P_x = 1$  for  $x < X_{max}$  and  $P_x = 0$  for  $x > X_{max}$  due to the intercept effect or the various forces. In this situation,

$$E_D = X_{max}^2. \quad (3.3)$$

If diffusion exists, then particles could traverse flow lines, so that  $P_x$  could be less than 1 within  $X_{max}$  and greater than 0 outside  $X_{max}$ , and usually the collision efficiency with diffusion is greater than  $X_{max}^2$  (Zhou et al., 2009).

### 3.1.2 Control function of particle movement

In the inertial coordinate system centered on a droplet which moves downward with constant fall speed of  $U_{A,\infty}$  relative to undisturbed air, the movement of a particle obeys equation (3.4),

$$m_2 \frac{d\vec{v}}{dt} = -\frac{\vec{v}}{B_p} + \frac{\vec{v}_f}{B_p} + \vec{f}_p + \vec{f}_e + \vec{f}_g, \quad (3.4)$$

where  $m_2$  is the mass of a particle,  $B_p$  is its mobility,  $-\frac{\vec{v}}{B_p} + \frac{\vec{v}_f}{B_p}$  is the drag force  $\vec{f}_{drag}$ ,  $\vec{v}_f$  is the velocity of air flow around droplet,  $\vec{f}_p$  is the phoretic force,  $\vec{f}_e$  is the electric force,  $\vec{f}_g$  is the gravitational force. All of the forces  $\vec{f}_{drag}$ ,  $\vec{f}_e$ ,  $\vec{f}_p$  vary with position along the trajectory.

If the mass of the particle is small and the velocity changes slowly, then the term  $m_2 d\vec{v}/dt$  in equation (3.4) which representing the inertia of particles could be neglected, and the velocity of the particle will reach a balance value  $\vec{v}_b$  where the drag force balances other forces, that is,

$$\vec{v}_b = \vec{v}_f + B_p (\vec{f}_p + \vec{f}_e + \vec{f}_g). \quad (3.5)$$

If the particle is small and its gravity can be neglected, the balance velocity has no relation to particle density, and it makes the calculation simple and less time-consuming to substitute  $\vec{v}_b$

for  $\vec{v}$ . For large particles or where the velocity changes fast, the inertia needs to be taken account of and the real velocity the departs from the balance velocity.

### 3.1.3 Random movement of particles

Besides the above control function in equation (3.4), the trajectories of the particles will also be affected by diffusion, especially for small particles. For a point source of particles, whose concentration will obey equation (2.8) in which the average velocity is zero, the evolution of number density obeys a Gaussian distribution,

$$n(x, y, z, t) = \frac{N_0}{\sqrt{(4\pi D_p t)^3}} e^{-(x^2+y^2+z^2)/(4D_p t)}, \quad (3.6)$$

where  $N_0$  is the total number of particles,  $D_p$  is the diffusion coefficient which has already been defined in equation (2.2), and it is easy to check that equation (3.6) is a solution of equation (2.8).

The particle concentration in equation (3.6) can also be written as,

$$n(x, y, z, t) = \frac{N_0}{\sqrt{(2\pi\sigma^2)^3}} e^{-(x^2+y^2+z^2)/(2\sigma^2)}, \quad (3.7)$$

where  $\sigma$  is the standard deviation and increases with time in the following way,

$$\sigma = \sqrt{2D_p t}, \quad (3.8)$$

and the standard deviation  $\sigma$  describes how far the particles on average move during the time  $t$ .

It needs to be noted that the diffusion coefficient  $D_p$  is only determined by temperature  $T$  and particle mobility  $B_p$ , and has no relation to density as given in Chapter 2. We have described above that for small particles the balance velocity is independent of particle density, so that for small particles whose trajectories are decided by the balance velocity and random movement the

collision rate coefficient will be independent of density. For large particles and particles accelerated by very great electric force or phoretic forces, particle density needs to be considered.

Equation (3.7) and (3.8) indicate that the position of a random-moving particle obeys a normal distribution, and thus in the trajectory model the displacement of a random-moving particle during time step  $dt$  is calculated by,

$$\begin{cases} dx = \sqrt{2D_p dt} f_n \\ dy = \sqrt{2D_p dt} f_n, \\ dz = \sqrt{2D_p dt} f_n \end{cases} \quad (3.9)$$

where  $f_n$  is a function that generates random numbers obeying a normal distribution. The random movement of the particles will bring in some uncertainty to the collision rate coefficient, while if the number of particles released below the droplet is large enough then the uncertainty could be neglected in accordance with Monte Carlo theory. Our calculation releases enough particles to ensure the uncertainty for the value of the collision rate coefficient is less than 1% for most cases, except for situations where only an extremely small fraction of particles collide with droplets.

### 3.1.4 The relaxation time, time step and the inertia of particle.

#### 3.1.4.1 The relaxation time $\Delta t$

According to the balance velocity defined in equation (3.5), the control function in equation (3.4) becomes,

$$\frac{d\bar{v}}{dt} = -\frac{\bar{v} - \bar{v}_b}{m_2 B_p}. \quad (3.10)$$

Assuming all forces change slowly and so  $\vec{v}_b$  could be viewed as a constant, then the solution of velocity of particle in term of time is,

$$\overline{v(t)} = (\overline{v_0} - \overline{v_b}) e^{-t/\Delta t} + \overline{v_b}, \quad (3.11)$$

where  $\vec{v}_0$  is the initial velocity and the  $\Delta t$  is the ‘relaxation time’,

$$\Delta t = m_2 B_p. \quad (3.12)$$

The fall speed  $U_{a,\infty}$  of the particle relative to undisturbed air is reached when the drag force is equal to the gravitational force on the particle,  $U_{a,\infty}/B_p = m_2 g$ , that is,

$$U_{a,\infty} = B_p m_2 g. \quad (3.13)$$

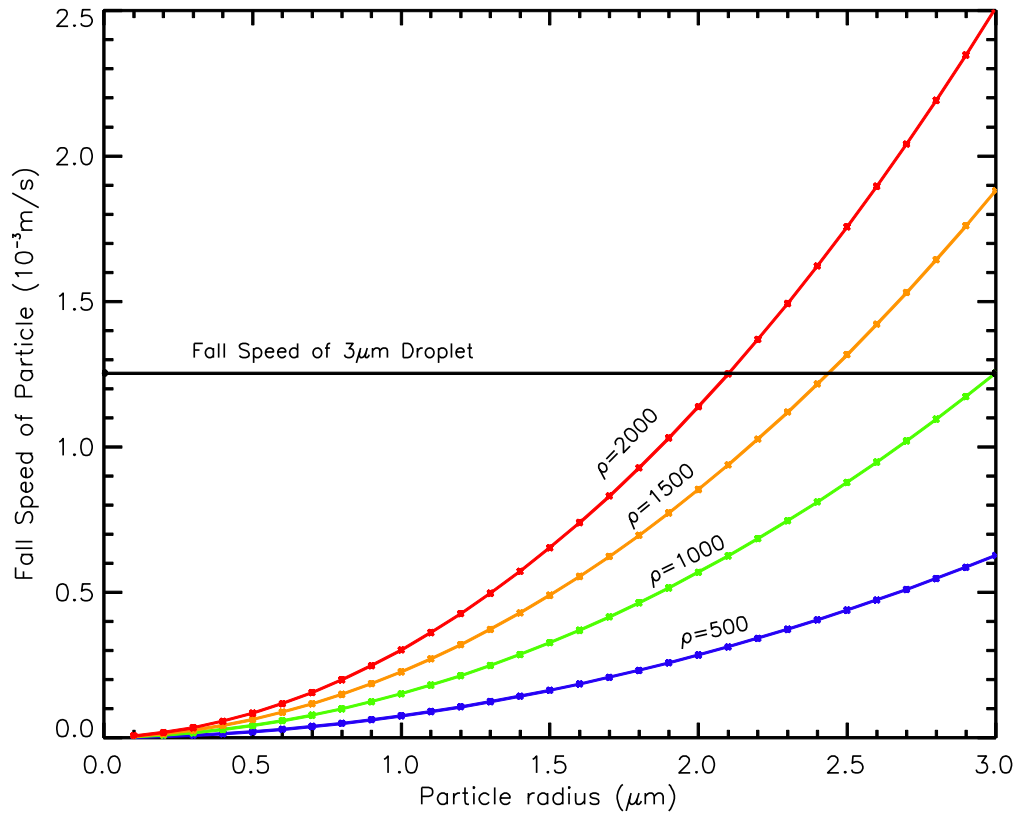


Figure 3.2. The fall speed  $U_{a,\infty}$  of a particle relative to undisturbed air for radius ranges between 0.1 and 3.0  $\mu\text{m}$ , and with density of 500, 1000, 1500, and 2000  $\text{kg} \cdot \text{m}^{-3}$ . The fall speed of a 3.0  $\mu\text{m}$  droplet is shown for comparison.

From equation (3.12) and (3.13) we get the relaxation time in terms of the fall speed of the particle relative to undisturbed air,

$$\Delta t = \frac{U_{a,\infty}}{g}. \quad (3.14)$$

The velocity of the particle will decay to balance velocity from initial velocity during the relaxation time. The value of the relaxation time is important for solving the trajectory of the particles. Figure 3.2 shows the fall speed of particles relative to undisturbed air with density of 500, 1000, 1500, and 2000 kg/m<sup>3</sup>, and the fall speed  $U_{a,\infty}$  is basically proportional to  $\rho a^2$  for  $0.1 \mu\text{m} < a < 3.0 \mu\text{m}$ . For the particles of density  $\rho = 1000 \text{ kg/m}^3$ , several fall speeds and relaxation times are listed as follows,

$$\left\{ \begin{array}{l} a = 0.01 \mu\text{m}, U_{a,\infty} = 2.381 \times 10^{-7} \text{ m} \cdot \text{s}^{-1}, \Delta t = 2.43 \times 10^{-8} \text{ s} \\ a = 0.10 \mu\text{m}, U_{a,\infty} = 3.275 \times 10^{-6} \text{ m} \cdot \text{s}^{-1}, \Delta t = 3.43 \times 10^{-7} \text{ s} \\ a = 1.00 \mu\text{m}, U_{a,\infty} = 1.509 \times 10^{-4} \text{ m} \cdot \text{s}^{-1}, \Delta t = 1.54 \times 10^{-5} \text{ s} \cdot \\ a = 2.00 \mu\text{m}, U_{a,\infty} = 5.688 \times 10^{-4} \text{ m} \cdot \text{s}^{-1}, \Delta t = 5.80 \times 10^{-5} \text{ s} \\ a = 3.00 \mu\text{m}, U_{a,\infty} = 1.254 \times 10^{-3} \text{ m} \cdot \text{s}^{-1}, \Delta t = 1.28 \times 10^{-4} \text{ s} \end{array} \right. \quad (3.15)$$

For the particle with density  $\rho = 500 \text{ kg} \cdot \text{m}^{-3}$  or  $\rho = 2000 \text{ kg} \cdot \text{m}^{-3}$ , the corresponding  $U_{a,\infty}$  and  $\Delta t$  will decrease or increase by two times. The relaxation time of the particle is sensitive to particle radius and density.

#### 3.1.4.2 Time step $dt$ in the trajectory model

Firstly, in our trajectory model the particle is required to move about 1% of droplet's radius during a time step  $dt$ , for the droplet with  $3.0 \mu\text{m}$  radius, the time step when particles are far away from droplet is usually set to be about,

$$dt \approx 0.01 \frac{A}{U_{A,\infty}} = 2.393 \times 10^{-5} \text{ s}. \quad (3.16)$$

Secondly, the diffusion of particles is stronger as particle radius decreases, and the random movement can exceed the transport effect of average velocity for small particles, so that near the droplet surface the time step  $dt$  should be even smaller to ensure the displacement during the time step is less than 1% of droplet radius, and according to equation (3.9) the time step should also meet the following requirement,

$$\sqrt{2D_p dt} \leq 0.01A. \quad (3.17)$$

Besides, in order to limit the uncertainty resulting from the diffusion of small particles, a large number of particles need to be released, so that it is very time-consuming in the trajectory model to calculate the collision rate coefficient for small particles.

Thirdly, for large particles, the relaxation time  $\Delta t$  in equation (3.11) may be greater than time step  $dt$ , and the inertia of the particle needs to be considered by solving the position  $\vec{r}(t)$  and velocity  $\vec{v}(t)$  together, and so we apply a 4th-order Runge-Kutta method to solve for the particle trajectory. On the other hand, the relaxation time  $\Delta t$  is very short for small particles as illustrated in equation (3.15), and the ordinary differential equation (3.4), which is the control function of particle movement, will become very stiff, and it will consume large amounts of computer time because the time step must be smaller than the relaxation time to avoid diverge. On this condition, if the forces exerted on the particle change slowly as the particle moves, it is quite

reliable to assume the real velocity  $\vec{v}(t)$  is equal to the balance velocity  $\vec{v}_b$  in equation (3.5), and then we solve the position  $\vec{r}(t)$  of the particle trajectory using the balance velocity. If the balance velocity  $\vec{v}_b$  changes rapidly, the inertia of the particle needs to be taken into account, and in the next section we will check the property of balance velocity.

### 3.1.4.3 The balance velocity of particles

In this section we will examine if it is appropriate to apply the balance velocity as the real velocity for small particles. If the forces change fast with particle movement, especially near the surface of the droplet, then after time step  $dt$  the balance velocity  $\vec{v}_b(t + dt)$  will departure from the original balance velocity  $\vec{v}_b(t)$  by about

$$\vec{v}_b(t + dt) - \vec{v}_b(t) \approx -dt \frac{\partial \vec{v}_b}{\partial t}. \quad (3.18)$$

And the balance velocity  $\vec{v}_b$  in equation (3.5) are decided by the sum of  $\vec{f}_e$ ,  $\vec{f}_p$ ,  $\vec{f}_g$ , and if we assume the gravitational force  $\vec{f}_g$  and the image electric force are smaller than the inverse-square phoretic forces and inverse-square Coulomb force, then the total force is roughly an inverse-square force and we write it as,

$$|\vec{f}| \approx \frac{C}{r^2}, \quad (3.19)$$

where  $C$  is a constant. Near the droplet surface the inverse-square force increases rapidly and the balance speed in equation (3.5) is mainly decided by the inverse-square force,

$$|\vec{v}_b| = |\vec{f} B_p| \approx \frac{C B_p}{r^2}. \quad (3.20)$$

Then the balance velocity varies with distance between droplet and particle in the following way,

$$|\delta \bar{v}_b| = \left| -2 \frac{CB_p}{r^3} \delta r \right|, \quad (3.21)$$

and distance changes can be roughly written as,

$$|\delta r| \approx |\bar{v}_b \delta t| \quad (3.22)$$

Thus we can estimate how fast the balance speed changes by the following way,

$$\left| \frac{\delta \bar{v}_b}{\delta t} \right| \approx \left| -2 \frac{\bar{v}_b^{-2}}{r} \right|. \quad (3.23)$$

Then equation (3.18) becomes,

$$|\bar{v}_b(t+dt) - \bar{v}_b(t)| = \left| -dt \frac{\partial \bar{v}}{\partial t} \right| \approx \left| -dt \frac{\delta \bar{v}_b}{\delta t} \right| = \left| 2dt \frac{\bar{v}_b^{-2}}{r} \right|. \quad (3.24)$$

Finally we can estimate the increment of balance velocity during the time step,

$$\frac{|\bar{v}_b(t+dt) - \bar{v}_b(t)|}{|\bar{v}_b(t)|} \approx 2 \frac{|\bar{v}_b(t)|}{r} dt \approx 2dt \frac{CB_p}{r^3}. \quad (3.25)$$

If the increment of balance velocity during time step  $dt$  is a small value then the displacement during time step  $dt$  is roughly equal to  $\bar{v}_b dt$ , and if the increment is a large value, then we need to solve the displacement during time step by applying a 4th-order Runge-Kutta method.

Besides, when a small charged particle approaches very close to the droplet surface the image electric force can predominate other forces, and the image electric force is,

$$F = \frac{1}{4\pi\epsilon_0} \frac{q^2 A}{r^3} \left\{ 1 - \frac{1}{(1 - A^2/r^2)^2} \right\}, \quad (3.26)$$

where  $q$  is the particle charge, and  $A$  is the droplet radius. When the distance  $r$  is very close to the droplet radius, then the image electric force is roughly equal to,

$$F \approx \frac{1}{4\pi\epsilon_0} \frac{q^2}{4(r-A)^2} = \frac{C}{(r-A)^2}. \quad (3.27)$$



Obviously the image electric force also obeys the inverse-square law in terms of the separation between the particle and the surface of the droplet, and let's substitute the ' $r$ ' from equation (3.20) to (3.25) by ' $r-A$ ', so that we have,

$$\frac{|\vec{v}_b(t+dt) - \vec{v}_b(t)|}{|\vec{v}_b(t)|} \approx 2 \frac{|\vec{v}_b(t)|}{r-A} dt \approx 2dt \frac{CB_p}{(r-A)^3}. \quad (3.28)$$

So that at a position very near droplet's surface the balance velocity will increase significantly during time step  $dt$ , then we need to decrease the time step and solve the displacement by applying a 4th-order Runge-Kutta method. If the particle charges are large and the image electric force will result in an extreme large balance velocity near droplet surface, then the inertia of even a small particle should be considered and we should solve the displacement and velocity together by applying a 4th-order Runge-Kutta method.

In short, for small particles, the balance velocity can be viewed as the real velocity when the particle is far from the droplet surface, but when the particle approaches very close to the droplet surface the balance velocity may increase fast according to equation (3.25) and (3.28) and we should apply a 4th-order Runge-Kutta method to solve the displacement during time step  $dt$ . Besides, if the image electric force is extremely large then the inertia of the particle needs to be considered by solving the displacement and velocity together by applying a 4th-order Runge-Kutta method.

### 3.1.5 The boundary of computational area.

For small particles whose diffusion coefficient is very large, even when the particle has already passed over the droplet, it could still move back and collide with the droplet due to diffusion, so

that it is useful to describe the boundary of computational area outside of which the particles could hardly collide with droplet.

Assume a new coordinate system in which the droplet falls downward with speed of  $U_{A,\infty}$  and the particle keeps static apart from diffusion. The droplet's initial position is (0,0), and the particle's initial position is  $(x_0, y_0)$ , in which  $x$  and  $y$  represent the horizontal and vertical direction respectively. After a time  $t$ , neglecting diffusion, the distance between droplet and particle becomes,

$$S^2(t) = x_0^2 + (y_0 - U_{A,\infty} \times t)^2. \quad (3.29)$$

If the distance  $S(t)$  is always 3 times greater than standard deviation of diffusion in equation (3.6), that is,  $S(t) > 3\sigma(t)$ , then we could jump to the conclusion that the particles will never collide with droplet by means of diffusion, that is,

$$S^2(t) = x_0^2 + (y_0 - U_{A,\infty} \times t)^2 > 9 \times (2D_p t), \quad (3.30)$$

which could be written as,

$$\left( U_{A,\infty} t - y_0 - \frac{9D_p}{U_{A,\infty}} \right)^2 + x_0^2 + \frac{18D_p}{U_{A,\infty}} y_0 - \left( \frac{9D_p}{U_{A,\infty}} \right)^2 > 0. \quad (3.31)$$

Finally, we get a parabolic computing region outside which the particle is unlikely to collide with the droplet, given as the relation between  $x_0$  and  $y_0$  in the following equation,

$$\frac{y_0}{A} < -\frac{U_{A,\infty} A}{18D_p} \left( \frac{x_0}{A} \right)^2 + \frac{9D_p}{2U_{A,\infty} A} = -\frac{1}{4} \frac{1}{(9/N_{Pe,p})} \left( \frac{x_0}{A} \right)^2 + (9/N_{Pe,p}), \quad (3.32)$$

where  $N_{Pe,p}$  has already has been defined as the Peclet number in equation (2.31). For small particles, the diffusion is strong and the reciprocal of  $N_{Pe,p}$  will be a large number. By setting this parabolic computing boundary, some computing time could be saved, because we stop calculating the trajectory if the particles move out of this boundary.

Taking account of the electric force and phoretic forces, the inverse-square forces decrease fast with the distance between the droplet and the particle, and if the particle lies outside the region of six droplet radii from the droplet then the distance between them is large enough to ensure these forces are negligible. Therefore we require the distance in equation (3.29) should always meet  $S(t) > 3\sigma(t) + 6A$ , and in our model we apply the following boundary,

$$\frac{y_0}{A} < -\frac{1}{4} \frac{1}{(9/N_{Pe,p} + 6)} \left( \frac{x_0}{A} \right)^2 + (9/N_{Pe,p} + 6). \quad (3.33)$$

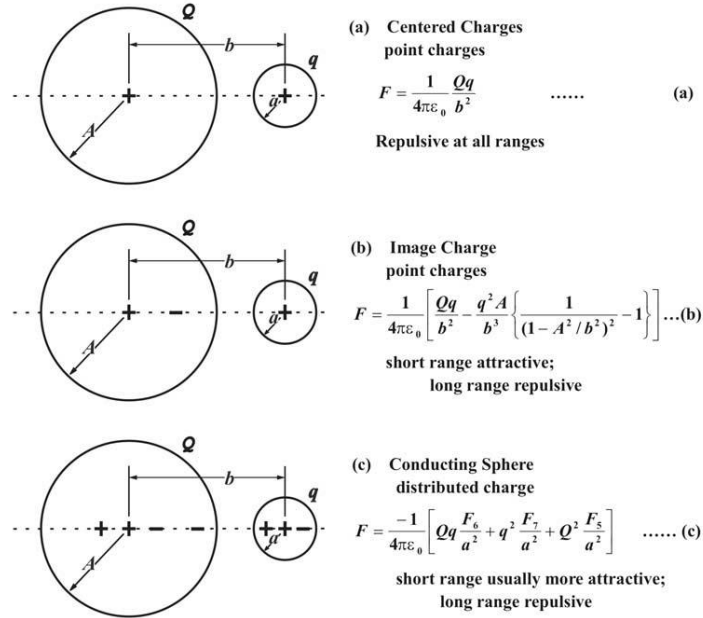


Figure 3.3. Three formalisms that have been used to calculate the electrical force between two charged, spherical, conducting objects. (Tinsley, 2008)

### 3.2 Conducting sphere electric force

There are three approaches to calculate the electric force between two charged conducting spherical objects, the larger with radius  $A$  and charge  $Q$ , and the smaller with radius  $a$  and charge  $q$ . The spacing between the centers is  $b$  as shown in Figure 3.3. When only centered point charges are

considered, as in Figure 3.3(a), there is only the inverse square Coulomb force, which is repulsive for  $Q$  and  $q$  of the same sign, and attractive if they have opposite sign. The convention used here is that repulsive forces are positive, and the force is given by

$$F = \frac{1}{4\pi\epsilon_0} \frac{Qq}{b^2}. \quad (3.34)$$

When the small sphere is still viewed as point charge but the large sphere is not, then the image charge induced on the large object needs to be considered, together with an opposite charge at the droplet center (Tinsley et al, 2000; Tripathi and Harrison, 2002). In Figure 3.3 there is a short range attractive force proportional to  $q^2$ , in addition to the long-range force. In the limit of  $a \rightarrow 0$ , it has an expression as,

$$F = \frac{1}{4\pi\epsilon_0} \left[ \frac{Qq}{b^2} - \frac{q^2 A}{b^3} \left\{ \frac{1}{(1 - A^2/b^2)^2} - 1 \right\} \right]. \quad (3.35)$$

When the smaller object has a non-negligible radius, then the image charge (actually a multipole) inside the small object induced by the charge on the large droplet also needs to be considered (Figure 3.3(c)). In this situation, the exact conducting spheres (CS) formulation is utilized. There is an additional term in the force expression that is proportional to  $Q^2$ , due to the multipole induced on the smaller object by the charges on the larger, which makes the expression on the larger also a multipole, and makes the expression symmetric for sizes and charges. This term provides an attractive force for the cases of smaller charged objects or for different amounts of charge. For objects of nearly equal size and nearly equal charges of the same sign, the near symmetry requires a repulsive force at large distances with the change from attractive to repulsive given by Tinsley and Zhou (2014). For exactly equal sizes and charges the force goes to zero as

the objects approach each other, as the repulsive Coulomb force is balanced by the rapidly increasing multipole forces.

Davis [1964a, 1964b] gave the CS force as following,

$$F = \frac{-1}{4\pi\epsilon_0} \left[ Qq \frac{F_6}{a^2} + q^2 \frac{F_7}{a^2} + Q^2 \frac{F_5}{a^2} \right]. \quad (3.36)$$

The function  $F_5$ ,  $F_6$  and  $F_7$  are dimensionless complex polynomial expressions which depend only on the radii of the two objects and the spacing between their surfaces  $s = b - (A + a)$ , as in Figure 3.3(c).

In our trajectory model, we apply the conducting sphere force which is calculated by using pre-calculated lookup tables, with 316 fixed values of  $b/A$  in a given table, and making a spline fit between the fixed values. Each table was for a given ratio of  $A/a$  whose value ranges from 1 to 150, and was used to generate one point on a curve in the results (Tinsley, 2008).

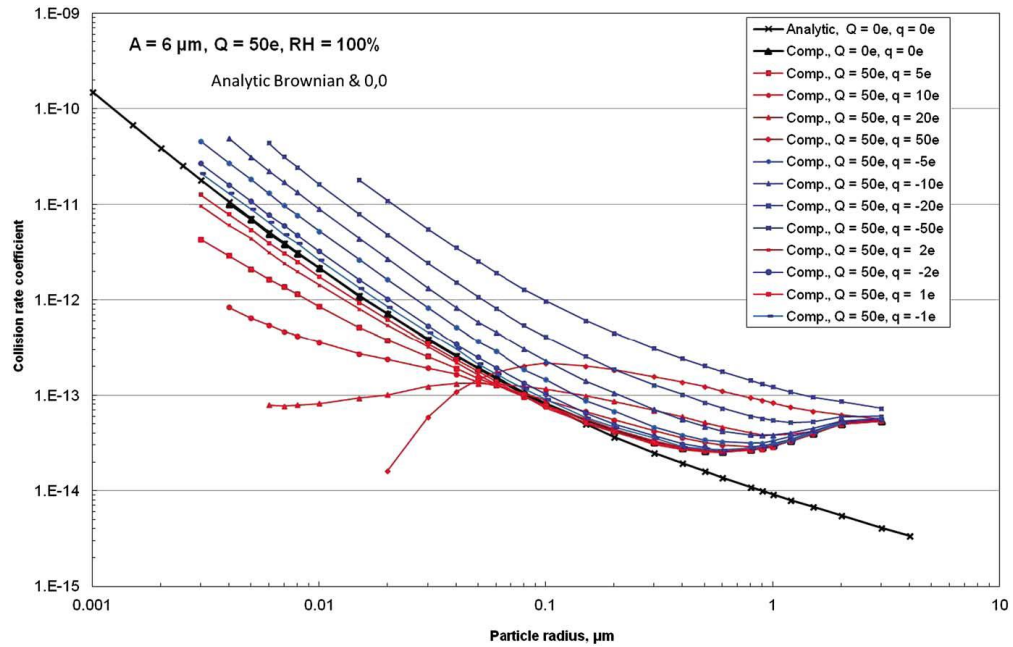


Figure 3.4. Collision rate coefficient for  $A = 6 \mu\text{m}$ ,  $Q = 50e$ ,  $q$  varying from  $-50e$  to  $50e$ , and particle density of  $500 \text{ kg} \cdot \text{m}^{-3}$ . (Tinsley and Leddon, 2013).

For the droplets and particles charged by same sign charge, the conducting sphere electric force will be repulsive in long range while it will become attractive in short range. So that for the large particles whose diffusion is weak, the electric force will enhance the scavenging, while for small particles with strong diffusion the effect of the electric force tends to be anti-scavenging (Tinsley, 2004). Figure 3.4 shows the scavenging and anti-scavenging effect. The red lines represent the collision rate coefficient of particles charged by same sign charges as droplet, and its value is higher than analytic Brownian value for large size particles so that the net effect of the image and Coulomb forces is scavenging. While for small particles the value of the collision rate coefficient is lower than for analytic Brownian scavenging, which corresponds to the anti-scavenging effect. (Tinsley and Leddon, 2013).

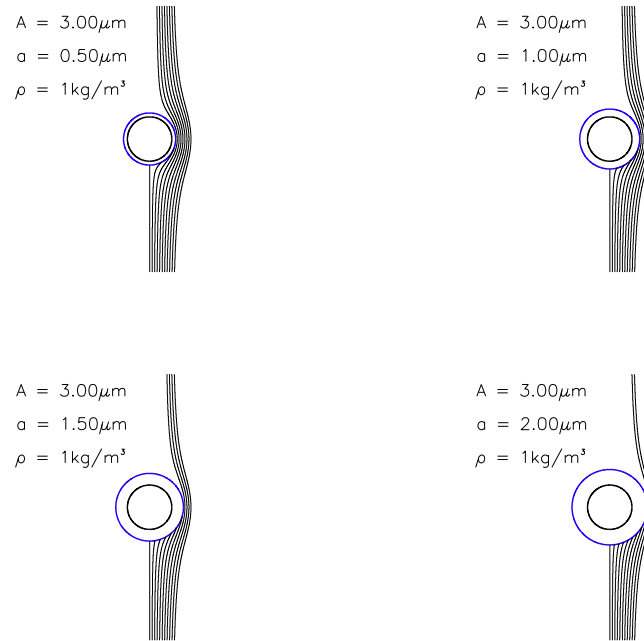


Figure 3.5. Intercept effect for particle density  $\rho_p = 1 \text{ kg} \cdot \text{m}^{-3}$  with radius equal to 0.5, 1.0, 1.5 and 2.0  $\mu\text{m}$ . The inner circle represents the radius of droplet, and the outer circle represents the sum of droplet radius and particle radius. The lines outside are trajectories of particles.

### 3.3 The intercept effect of particle

When the radius of the particle is non-negligible compared to the droplet, the cross sectional area for collisions increases from  $A^2$  to  $(A + a)^2$ . Then in accordance with the analytic solution mentioned before, the collision rate coefficient will increase by  $1 + a/A$  times, which is called the ‘intercept effect’. Figure 3.5 shows that when the size of particles increases, more particles will be intercepted by the droplet due to the extended cross sectional area. In Figure 3.5 the particle density is set to be very small such that the inertia effect and the weight effect are negligible. For low density particles, when the radius is very large then the collision rate coefficient is dominated by the ‘intercept effect’, and the effect of diffusion will be negligible (Tinsley and Leddon, 2013).

### 3.4 The weight effect and the stagnation region

In our trajectory model, the coordinate frame is centered on the droplet. In this frame, the air flows upward around the droplet. The speed of air flow is  $U_{A,\infty}$  far from droplet and gradually decreases toward the droplet, until it becomes zero at the droplet surface, as shown in section 2.2. The particles are released below the droplet in our model, and then move upward due to the drag force of air in conjunction with other forces. As shown in equation (3.4), the drag force exerted on particle is

$$\vec{F}_{drag} = \frac{\vec{v}_f - \vec{v}}{B_p}, \quad (3.37)$$

where  $\vec{v}_f$  is the velocity of the air flow,  $\vec{v}$  is the velocity of the particle, thus  $\vec{v}_f - \vec{v}$  is the relative velocity between the particle and the air flowing around the droplet. The drag force only depends on the relative speed and particle radius, and is not related to particle density. If only the

gravitational force is present, the drag force should be equal to the gravitational force, according to equation (3.13) and equation (3.37), we have,

$$|\vec{v}_f - \vec{v}| = U_{a,\infty}. \quad (3.38)$$

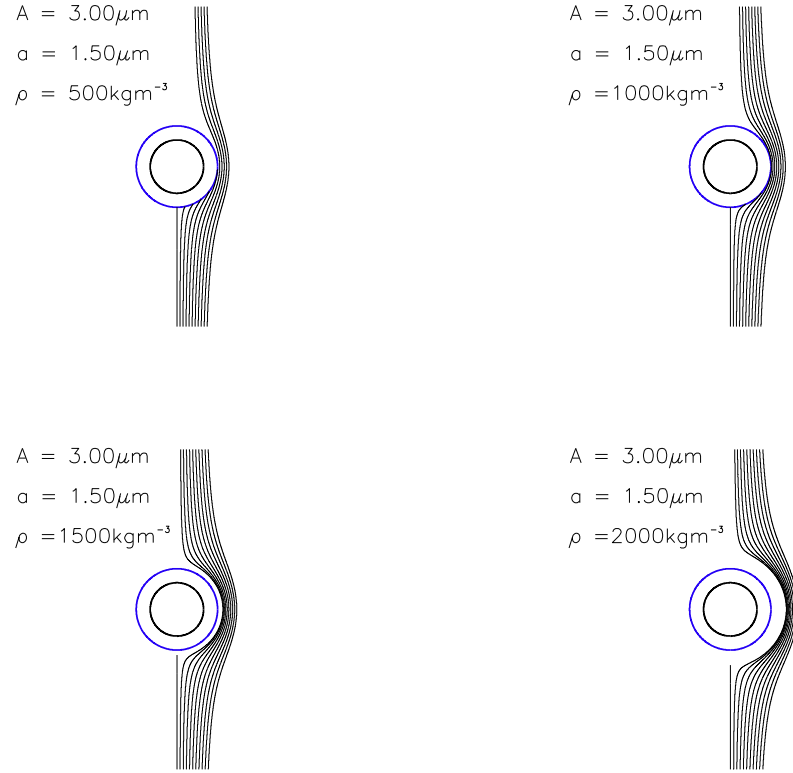


Figure 3.6. Trajectories for  $1.5 \mu\text{m}$  radius particles, with particle density of 500, 1000, 1500, and  $2000 \text{ kg} \cdot \text{m}^{-3}$ .

The velocity of air flow is roughly equal to the fall speed of droplet relative to undisturbed air except for the position very close to droplet surface, thus

$$\frac{|\vec{v}_f - \vec{v}|}{|\vec{v}_f|} \approx \frac{U_{a,\infty}}{U_{A,\infty}}, \quad (3.39)$$



and we have already illustrated the fall speed relative to undisturbed air of droplet and particles in Figure 3.2. As the particle radius decreases the fall speed of particle  $U_{a,\infty}$  decreases rapidly, consequently if the particle radius is small enough the particle velocity is very close to the velocity of air flow in our trajectory model, and thus the collision rate coefficients of small particles do not dependent on particle density. For very small particles, the trajectories without diffusion will coincide with the flow line due to the fall speed of particles,  $U_{a,\infty}$ , being negligible compared with the fall speed of the droplet. However, for large particles the trajectories without diffusion will depart from the flow lines if the weight of the particle is considerable, and normally the weight effect will reduce the collision rate coefficient through pulling the particle away from the droplet.

In the coordinates of the droplet, the speed of air flow will decrease to zero at the droplet surface, and immediately below the droplet there must exist a stagnation point where the upward drag force on the particle at rest is equal to the weight of the particle, and there also exists a stagnation region within which the drag force on the particle at rest is less than the particle weight and into which particles could not enter without diffusion, inertial or attractive forces, so that the stagnation region prevents particles from colliding on the front side of droplet and the flow diverts them to the side. Tinsley et al. (2006) have investigated the effect of the stagnation region in consideration of the inertia of particles and electric forces for a 20  $\mu\text{m}$  droplet. Figure 3.6 illustrates the trajectories of particles around a droplet in the absence of electric forces, phoretic forces and diffusion, with droplet radius  $A = 3.0 \mu\text{m}$ , particle radius  $a = 1.5 \mu\text{m}$ , and particle density  $\rho = 500, 1000, 1500, 2000 \text{ kg} \cdot \text{m}^{-3}$ . The inner circle represents the droplet radius, the outer circle corresponds to the sum of droplet and particle radius, and particle will collide with the droplet when the trajectories reach the outer circle. As shown in Figure 3.6, for particles with

density of  $500 \text{ kg} \cdot \text{m}^{-3}$  the trajectories are roughly aligned with flow lines as the weight of particle is small, and collisions occur at the front side of droplet. As particle density increases, the trajectories of particles fall outside the flow lines due to the increasing weight effect, and it is more difficult for particles to collide at the front side of droplet. For particles with higher density the particle could not collide on the front surface of droplet without diffusion, as shown by the cases for particles with density of 1500 and 2000  $\text{kg} \cdot \text{m}^{-3}$  in Figure 3.6.

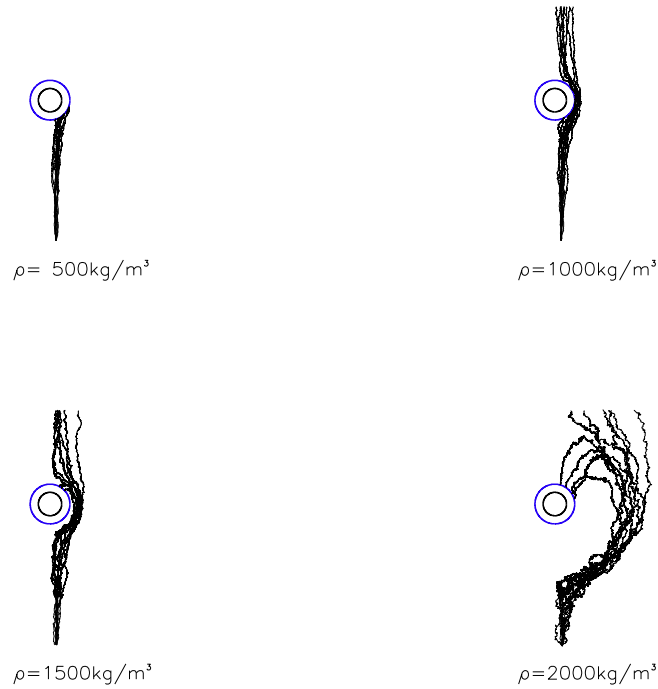


Figure 3.7. Trajectory of  $2.0 \text{ } \mu\text{m}$ -particle around  $3.0 \text{ } \mu\text{m}$ -droplet taking into account diffusion, with particle densities of 500, 1000, 1500 and 2000  $\text{kg} \cdot \text{m}^{-3}$  respectively.

When particles are carried into the low flow region behind the falling droplet, the gravitational force will move the particle toward the droplet. In the presence of diffusion, particles can enter the low flow region through random movement, and with the downward gravitational force can collide

with the back side of droplet. Figure 3.7 illustrates the trajectories of particles around a droplet in consideration of diffusion, with droplet radius  $A = 3.0 \text{ } \mu\text{m}$ , particle radius  $a = 2.0 \text{ } \mu\text{m}$ , and particle density  $\rho = 500, 1000, 1500, 2000 \text{ kg} \cdot \text{m}^{-3}$ . It can be seen that collisions occur at the front side of droplet for particle density  $\rho \leq 1000 \text{ kg} \cdot \text{m}^{-3}$  and at back side for  $\rho > 1000 \text{ kg} \cdot \text{m}^{-3}$ . The process of back-side collision is quite non-linear, and increases the collision rate coefficient for particles with large weight. Besides, when the fall speed of a particle in quiet air approaches to that of the droplet, the relative speed between droplet and particle becomes smaller, and more time is needed for the droplet to encounter the particles released below, in other words, there is more time for diffusion which allows some of the particles to traverse the flow lines and reach the upper boundary of the low-flow region, and increase the collision rate coefficient in this way. In section 3.5 we can see that the ‘fap’ effect can further interact with the stagnation region effects.

### 3.5 Effects of ‘fap’ and electric force on droplet movement

In the flux model the droplet falls downward at a constant speed  $U_{A,\infty}$ , while in our Monte Carlo Trajectory Model the effect of the drag force on the droplet exerted by the air flow around the particle and the electric and other forces on the droplet are considered. The velocity of the droplet is not now a constant, and similarly as in equation (3.4), we can write the control function of the droplet in the coordinate of a particle falling with constant speed  $U_{a,\infty}$  as,

$$m_1 \frac{d\bar{v}}{dt} = -\frac{\bar{v}}{B_d} + \frac{\bar{v}_f}{B_d} + \bar{f}_e + \bar{f}_g, \quad (3.40)$$

where  $m_1$  is the mass of the droplet,  $\vec{v}_f$  is the flow around the particle,  $(\vec{v}_f - \vec{v})/B_d$  is the drag force exerted on the droplet,  $B_d$  is the droplet mobility,  $\vec{f}_e$  are the electric forces,  $\vec{f}_g$  is the gravitational force, and  $m_1 g = U_{A,\infty}/B_d$ . We can write equation (3.40) as,

$$\frac{d\vec{v}}{dt} = -\frac{\vec{v}}{m_1 B_d} + \frac{\vec{f}_e}{m_1} + \frac{\vec{v}_f - U_{A,\infty} \mathbf{y}}{m_1 B_d}. \quad (3.41)$$

Similarly as with equation (3.12), the relaxation time of 3  $\mu\text{m}$  droplet is,

$$\Delta t = m_1 B_d = \frac{U_{A,\infty}}{g} = 1.283 \times 10^{-4} \text{ s}. \quad (3.42)$$

The relaxation time is large and so the inertia of droplet can not be neglected, and the position  $\vec{r}(t)$  and velocity  $\vec{v}(t)$  of droplet in the ordinary differential equation (3.40) have to be solved together, unless the droplet and particle are far enough apart that the drag force and electric force change slowly, then we can simply substitute the balance velocity  $\vec{v}_b$  for the velocity  $\vec{v}$  in equation (3.5).

### 3.5.1 Effect of flow around the particle ('fap')

In order to estimate the drag force exerted on the droplet by the air flow around the particle, assuming the electric force is absent, we compare the effects of the drag force caused by the air flow around particle and the droplet weight,

$$\frac{|\vec{f}_{drag}|}{|\vec{f}_g|} \approx \frac{|\vec{v}_f|/B_d}{|\vec{f}_g|}. \quad (3.43)$$

Assume the relative speed is similar as the fall speed of particle relative to quiet air when the droplet and particle are close,

$$|\vec{v}_f| \sim U_{a,\infty}. \quad (3.44)$$

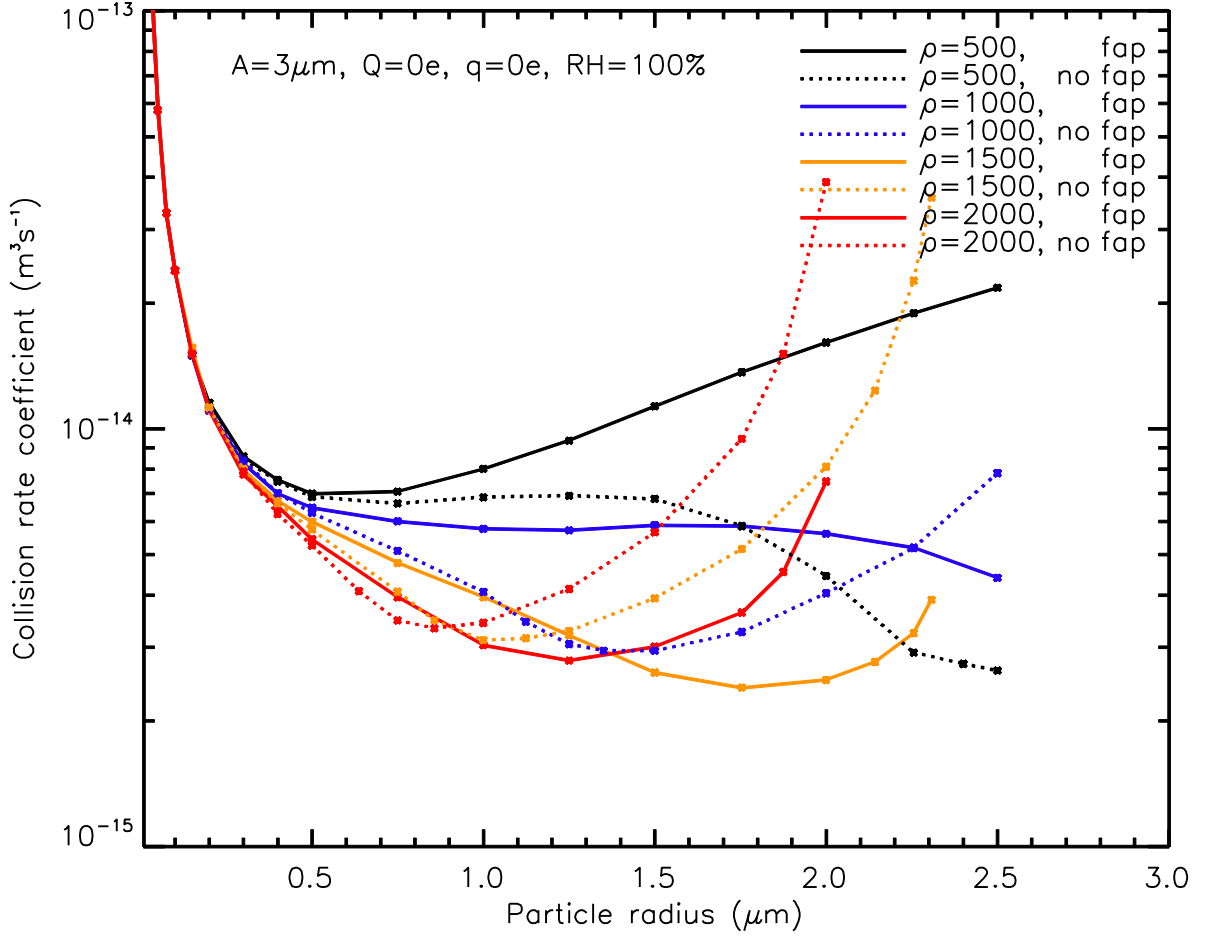


Figure 3.8. Collision rate coefficient ( $\text{m}^3 \cdot \text{s}^{-1}$ ) calculated with (solid lines) and without (dashed lines) ‘fap’, with particle density of 500, 1000, 1500, and 2000  $\text{kg} \cdot \text{m}^{-3}$  respectively.

Then,

$$\frac{|\bar{f}_{drag}|}{|\bar{f}_g|} \approx \frac{U_{a,\infty}}{U_{A,\infty}} \approx \frac{\rho_p a^2}{\rho_d A^2}, \quad (3.45)$$

where  $\rho_p$  is the particle density and  $\rho_d$  is the droplet density. The disturbance of droplet velocity is roughly linearly dependent on the drag force caused by flow around particle, it is about the same order of magnitude as the particle fall speed  $U_{a,\infty}$  when a larger droplet is near to the particle,

and is weak and negligible if the distance is far. If the fall speed of particle  $U_{a,\infty}$  is much smaller than the fall speed of the droplet  $U_{A,\infty}$ , then the ‘fap’ effect could be neglected. In our model, we neglect ‘fap’ effect when

$$\frac{U_{a,\infty}}{U_{A,\infty}} < 0.01. \quad (3.46)$$

If the particle density is equal to that of the droplet, then,

$$a < 0.1A = 0.3 \mu\text{m}. \quad (3.47)$$

For particles with higher density the ‘fap’ effect starts to take effect at smaller particle radius. For example, if the particle density is  $2000 \text{ kg} \cdot \text{m}^{-3}$ , two times of the droplet density, then

$$a < 0.1A/\sqrt{2} = 0.21 \mu\text{m}. \quad (3.48)$$

Figure 3.8 shows the collision rate coefficient calculated by our Monte Carlo Trajectory Model in the absence of electric forces and phoretic forces with and without ‘fap’ by the solid and dashed lines, for particles with density of 500, 1000, 1500, 2000  $\text{kg} \cdot \text{m}^{-3}$ . We can see that the ‘fap’ effect disappears for  $a < 0.3 \mu\text{m}$  for all of particle density. When  $a > 0.3 \mu\text{m}$ , for particles with density of  $500 \text{ kg} \cdot \text{m}^{-3}$ , the collision rate coefficient with ‘fap’ is always greater than without ‘fap’, and the difference will be more significant for larger particle radius. This is because the drag force exerted on the droplet caused by flow around the particle tends to drag the droplet downward, and as shown in Figure 3.7 the collision occurs at the front side of droplet for particle density less than that of the droplet, so that the ‘fap’ effect drags the droplet toward the particle and enhances collision rates, and the larger the particle radius, the greater the ‘fap’ effect becomes. For particles with density equal to or greater than that of the droplet, the collision rate coefficient with ‘fap’ will

first tend to be greater than that without ‘fap’ for the same reason as that of  $500 \text{ kg} \cdot \text{m}^{-3}$  particles, that is, the collision occurs at the front side of droplet for small particles with large density. However, as shown in Figure 3.7 the results of the collision rate coefficient with ‘fap’ tend to be smaller than without ‘fap’ when the particle radius is large. There are two possible reasons, one reason is that the drag force exerted on the droplet caused by ‘fap’ is always downward, and for a large particle with density greater than that of the droplet the collision mainly occurs at the back-side of the droplet, and the drag force tends to push the droplet away from the particle in this case and thus decrease the collision rate coefficients; the other reason is that for particles with larger radius and great density their fall speed  $U_{a,\infty}$  is comparable with droplet fall speed  $U_{A,\infty}$ . Then their relative speed is smaller and there is more time for random movement transporting the particle close to the droplet. So diffusion becomes important and tends to increase the collision rate coefficient. However, the ‘fap’ effect tends to increase the relative speed between the droplet and particles and so decreases the time for diffusion, so that particles far from the droplet do not move so close to the droplet by random movement; thus the collision rate coefficient with ‘fap’ is smaller than without ‘fap’ in this case.

### 3.5.2 Effect of electric forces

In the above section we have shown that the ‘fap’ effect needs to be considered for large particle radii,  $a > 0.1A$ , and in the process of dealing with the drag force caused by ‘fap’ the electrical forces are also included. Now let’s estimate the effect of electric force on the droplet for  $a < 0.1A$ , where the ‘fap’ effect can be neglected. If the electric force  $\vec{f}_e$  is exerted between the droplet and

particle, it may cause droplet's new balance velocity to change by  $\delta\vec{v}_1$  from its old balance velocity, and cause particle's new balance velocity change by  $\delta\vec{v}_2$  from its old balance velocity,  $\delta\vec{v}_1/B_d$  and  $\delta\vec{v}_1/B_p$  are the drag forces which roughly counteract the electric forces  $\vec{f}_e$ , thus

$$|\delta\vec{v}_1| \approx B_d \times |\vec{f}_e|, \quad (3.49)$$

and

$$|\delta\vec{v}_2| \approx B_p \times |\vec{f}_e|, \quad (3.50)$$

then,

$$\frac{|\delta\vec{v}_1|}{|\delta\vec{v}_2|} \approx \frac{B_d}{B_p} \approx \frac{1/A}{1/a} = \frac{a}{A}. \quad (3.51)$$

In our model, we neglect the electric force on droplet when  $|\delta\vec{v}_1|/|\delta\vec{v}_2| < 0.01$ , that is

$$a < 0.01A = 0.03 \mu\text{m}. \quad (3.52)$$

In our Monte Carlo Trajectory Model, for particles with radius  $0.01A < a < 0.1A$ , the electric forces on the droplet are considered and the 'fap' effect is neglected; for particles with radius  $a > 0.1A$ , the electric force and the drag force caused by 'fap' are both taken into account.



## CHAPTER 4

### PARAMETERIZATION OF AEROSOL SCAVENGING DUE TO ATMOSPHERIC IONIZATION UNDER VARYING RELATIVE HUMIDITY

#### 4.1 Approach to Simulation and Parameterization

The analytic solution in equation (2.33) is inaccurate because the electrical forces necessarily include the image-charge forces, which increase rapidly as the particles approach the droplet surface. Besides, for particle sizes approaching that of the droplet, the ‘wif’ (weight, intercept, ‘fap’) effects become important [Tinsley et al., 2006], and these are not included in the flux model.

The rate coefficients obtained with the trajectory model are designated as  $R_{Q,q,A,a,RH}$ , (where, as before,  $Q$  is the droplet charge,  $q$  is the particle charge,  $A$  is the droplet radius,  $a$  is the particles radius,  $RH$  is the relative humidity) and where convenient, the rate coefficient is abbreviated as  $R_{Q,q,RH}$ . The value of  $A$  used was 3  $\mu\text{m}$ , and so the ‘flow around the particle’ effect is important in this work. Values of  $a$  used were 0.01, 0.02, 0.03, 0.05, 0.075, 0.1, 0.15, 0.2, 0.3, 0.4, 0.5, 0.75, 1.0, 1.25, 1.5, 1.7543, 2.0, 2.2556, and 2.5  $\mu\text{m}$ . The particle charges  $q$  were 0, 10, 20 and 50e, and the droplet charges  $Q$  were 0,  $\pm 10\text{e}$ ,  $\pm 20\text{e}$ ,  $\pm 50\text{e}$ ,  $\pm 100\text{e}$ , where e is the elementary charge. The values of relative humidity  $RH$  were 95%, 98%, 99%, 100%, 101%. In this work the atmospheric pressure and temperature were 540 hPa, 256.15 K respectively, and the particle densities 500  $\text{kg} \cdot \text{m}^{-3}$ . The computational uncertainties of collision rate coefficient in the present simulations depend on the number of trials, and are less than 1% for most cases, except for cases that phoretic and Coulomb repulsive forces are so strong that collision is almost impossible and it is difficult to reduce uncertainty by increasing the number of trials.

The simulated results of trajectory model are complex as many effects are involved, and the computational times are of order a day for each simulation. It is necessary to parameterize the results for use in cloud models, and Tinsley and Leddin [2013] made an initial parameterization, and Tinsley and Zhou [2015] use an improved approach to parameterize results for  $A = 3 \mu\text{m}, 6 \mu\text{m},$  and  $15 \mu\text{m}$  but only for  $RH = 100\%$ . In this Chapter we simulate and parameterize results for  $A = 3 \mu\text{m}$  and  $RH = 95\%, 98\%, 99\%, 100\%,$  and  $101\%$  to investigate the effect of phoretic forces, taking into account ‘wif’ effects for the larger particles. Also, some empirical formulas are given that roughly estimate the rate coefficients for some cases.

We first evaluate the part of the base level  $N_{0,0,RH}$  which applies to  $Q = 0e$  and  $q = 0e$ , which includes phoretic effects, but in the absence of ‘wif’ effects, and can be calculated by equation (2.32), then we fit the departure of the simulated results  $R_{0,0,RH}$  (which now includes the ‘wif’ effects) from  $N_{0,0,RH}$  to be a function of particle radius and relative humidity. Second, we get the departure of  $R_{0,q,RH}$  from  $R_{0,0,RH}$ , which represents the effect of the image charge induced by the particle charge, and then fit the departure to be a function of particle charge, particle radius and relative humidity. Similarly, we can fit the departure of  $R_{Q,0,RH}$  from  $R_{0,0,RH}$ , which represents the effect of image charge induced by the droplet charge. Finally, if the droplet charge  $Q$  is of opposite sign to the particle charge  $q$ , we fit  $R_{Q,q,RH} - (R_{0,q,RH} + R_{Q,0,RH} - R_{0,0,RH})$  to a function of  $Q, q, a, RH$ ; if they are same sign, we fit  $\log_{10}(R_{Q,q,RH}) - \log_{10}(R_{0,q,RH} + R_{Q,0,RH} - R_{0,0,RH})$  to a function of  $Q, q, a, RH$ . For all the above fitting processes, we separate the particles radius into two ranges,  $0.01 \mu\text{m} \leq a \leq 0.2 \mu\text{m}$  and  $0.2 \mu\text{m} \leq a \leq 2.5 \mu\text{m}$ , as the predominant factors are different for small particles and for large particles.

## 4.2 Results and parameterization of collision rate coefficients.

### 4.2.1 Parameterization of $R_{0,0,RH}$ (base level) rates for varying relative humidity

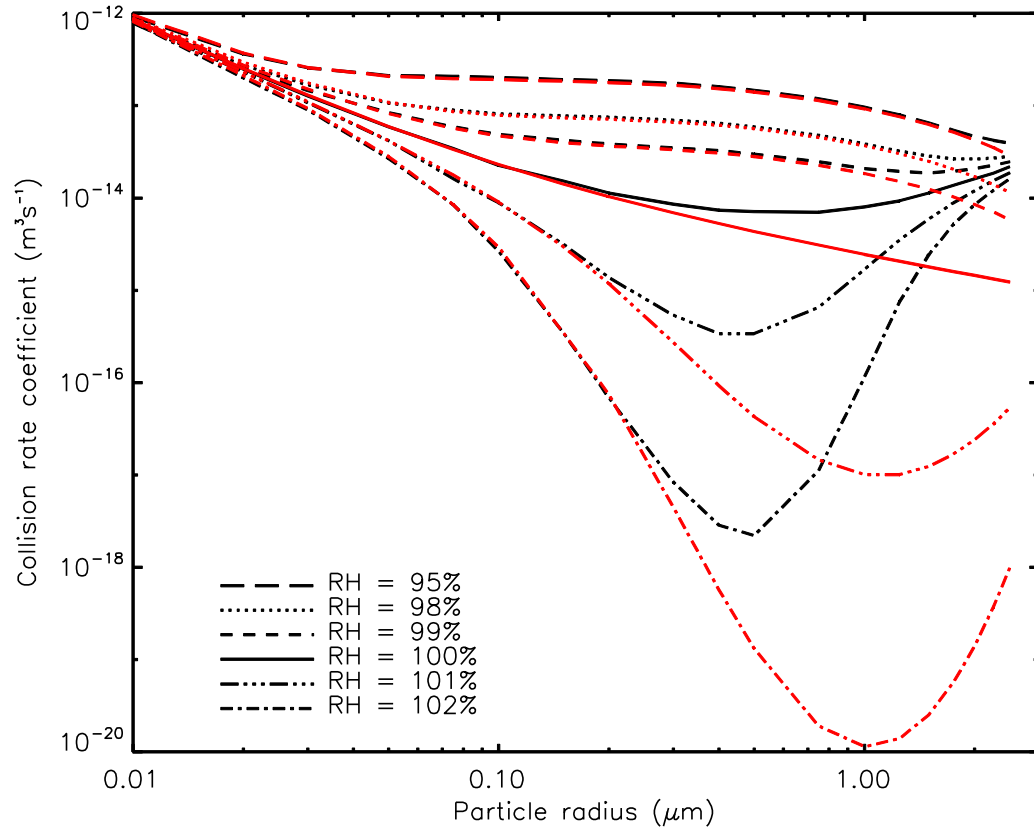


Figure 4.1. Simulated collision rate coefficients (black lines) for phoretic with ‘wif’ ( $R_{0,0,RH}$ ), and analytic collision rate coefficients (red lines) without ‘wif’ ( $N_{0,0,RH}$ ) for Relative Humidity  $RH = 95\%$ ,  $98\%$ ,  $99\%$ ,  $100\%$ ,  $101\%$ ,  $102\%$ .

In Figure 4.1 simulated results of rate coefficients  $R_{0,0,RH}$  (for zero charges and varying relative humidity) are shown by black lines, and analytic results of rate coefficients  $N_{0,0,RH}$  calculated by equation (2.32) are shown by red lines. Equation (2.32) for zero charges reflects diffusive and phoretic effects only, which minimize near  $a = 1.0 \mu\text{m}$  or greater, depending on relative humidity. For the range of particle radii  $0.01 \mu\text{m} \leq a \leq 0.2 \mu\text{m}$ , the simulated results are

coincident with the analytic value, while for the range of particle radius  $0.2 \mu\text{m} \leq a \leq 2.5 \mu\text{m}$ , the simulated results are much greater than analytic results. This is because the ‘wif’ effects are not included in the analytic solution and they are negligible for small particles but become considerable for large particles.

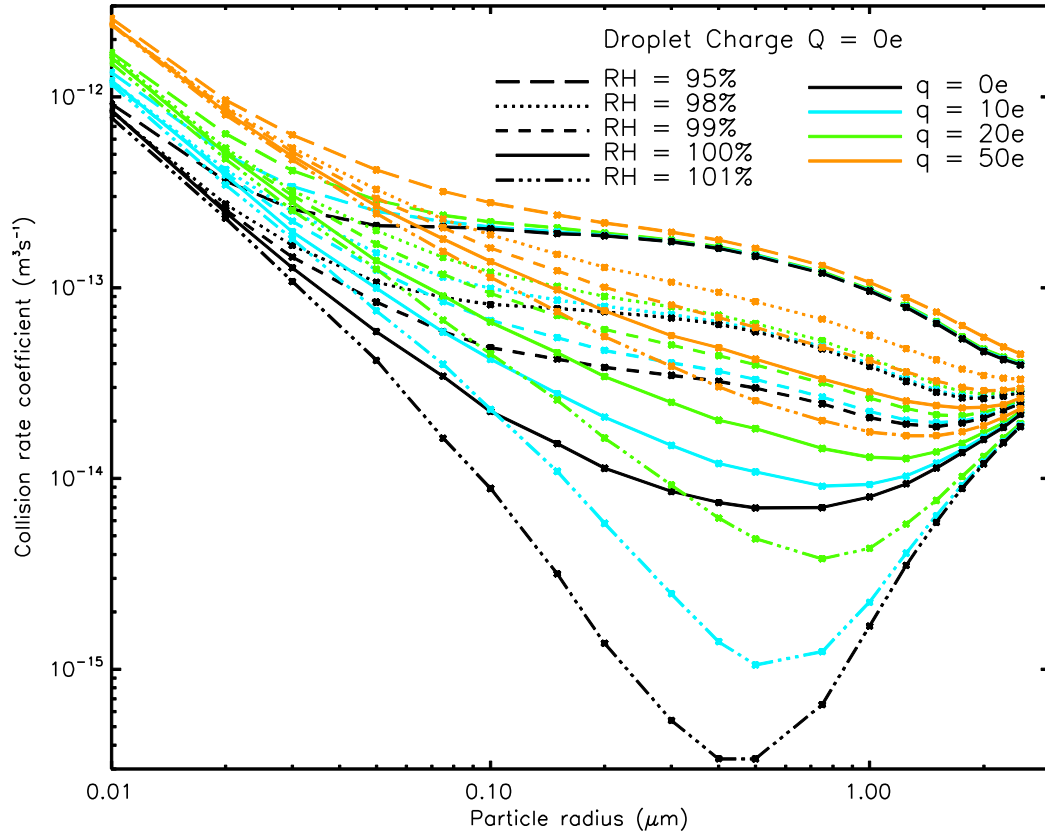


Figure 4.2. Simulated rate coefficients ( $R_{0,q,RH}$ ) with droplet charges  $Q = 0e$ , particle charge  $q = 0e, 10e, 20e, 50e$ , and relative humidity  $RH = 95\%, 98\%, 99\%, 100\%, 101\%$ .

#### 4.2.1.1 Results of $R_{0,0,RH}$ for $0.01 \mu\text{m} \leq a \leq 0.2 \mu\text{m}$

As can be seen in Figure 4.1, for particle radii  $0.01 \mu\text{m} \leq a \leq 0.2 \mu\text{m}$ , the value of the rate coefficient is same as the analytic solution, as the ‘wif’ effects can be neglected.

$$R_{0,0,RH} = N_{0,0,RH}. \quad (4.1)$$

#### 4.2.1.2 Results of $R_{0,0,RH}$ for $0.2 \mu\text{m} \leq a \leq 2.5 \mu\text{m}$

For the range  $0.2 \mu\text{m} \leq a \leq 2.5 \mu\text{m}$ , the ‘wif’ effects become important, and the rate coefficient  $R_{0,0,RH}$  is higher than  $N_{0,0,RH}$ . The differences between  $R_{0,0,RH}$  and  $N_{0,0,RH}$  are given by,

$$\log_{10}(R_{0,0,RH} - N_{0,0,RH}) = A_0 + A_1 \log_{10} a. \quad (4.2)$$

The expressions of  $A_0$ ,  $A_1$  are given as a function of  $s$ ,

$$A_0 = -14.25 - 0.41s + 0.030s^2, RH \leq 100\%, \quad (4.3)$$

$$A_0 = -14.25 + 0.47s - 0.005s^2, RH \geq 100\%, \quad (4.4)$$

$$A_1 = 1.37 + 1.01s - 0.1s^2, RH \leq 100\%, \quad (4.5)$$

$$A_1 = 1.37 - 1.35s - 0.1s^2, RH \geq 100\%. \quad (4.6)$$

#### 4.2.2 Parameterization of collision rate coefficients $R_{0,q,RH}$ for zero droplet charge.

For zero droplet charge ( $Q = 0e$ ), the simulated result of rate coefficients  $R_{0,q,RH}$  for  $q = 0e, 10e, 20e, 50e$  and  $RH = 95\%, 98\%, 99\%, 100\%, 101\%$  are shown in Figure 4.2. For a given particle charge  $q$ , the rate coefficients converge at very small particle radius and very large particle radius, and the effect of relative humidity is most obvious for about  $1.0 \mu\text{m}$  particle radius. At very small particle radii the net phoretic forces (the difference between larger attractive thermophoretic and smaller repulsive diffusiophoretic forces) are small compared to diffusion. At increasingly large particle radii the decreasing thermophoretic force tends towards cancellation by the diffusiophoretic force and the net force becomes small compared to the ‘wif’ effects. The image forces are attractive and short-range, and their values vary roughly as  $q^2$  and depend strongly on the distance between the surface of droplet and the particle center. The centers of smaller particles approach closer to the droplet surface before colliding, hence the effect of the image force is more

significant for small particles, which is evident in Figure 4.2 from the separation of the curves for different  $q$  at  $a = 0.1 \text{ } \mu\text{m}$ .

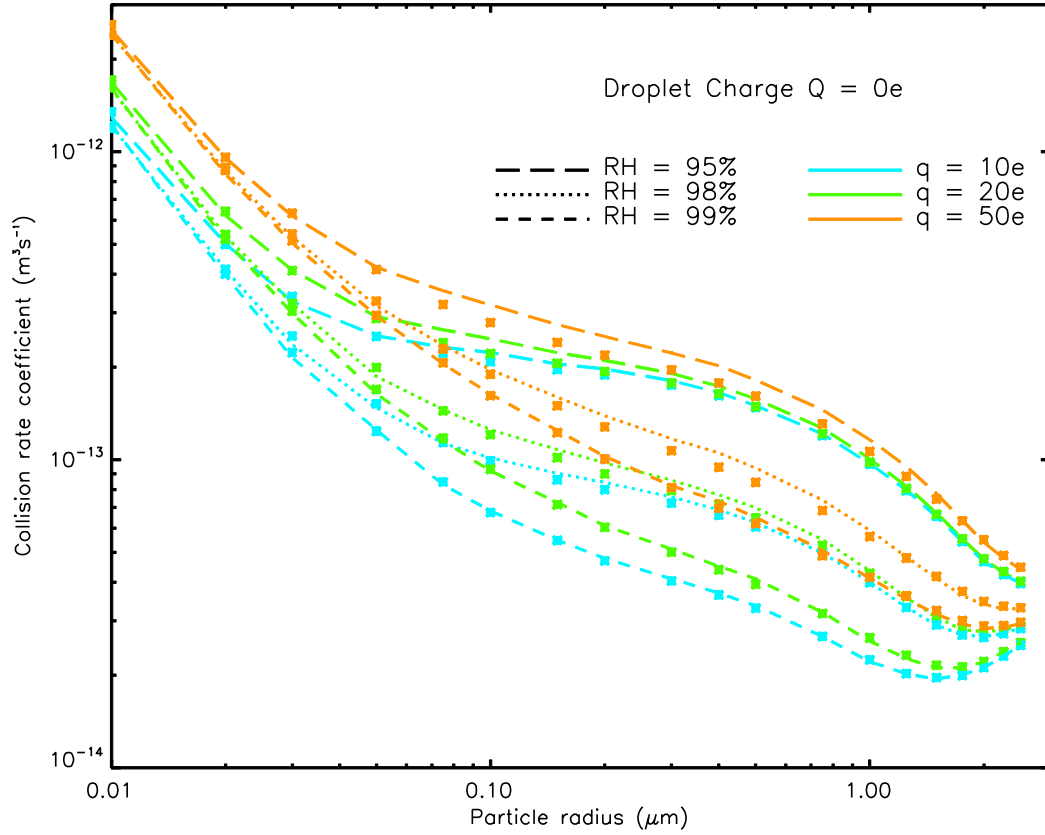


Figure 4.3. Points are the simulated results of rate coefficients  $R_{0,q,RH}$ ; Lines are the results of  $R_{0,0,RH} + R_{0,q,100\%} - R_{0,0,100\%}$ ; for  $RH = 95\%, 98\%, 99\%$  and  $q = 10e, 20e, \text{ and } 50e$ .

#### 4.2.2.1 Results for $R_{0,q,100\%}$

When  $RH = 100\%$  with  $Q = 0$  and  $q \neq 0$ , the difference of the rate coefficient from the basic rate depends only on the image force due to the square of the particle charge  $q$ . The image force is attractive and its effect is to increase rate coefficient, and we fit  $R_{0,q,100\%} - R_{0,0,100\%}$  to get the increment of rate coefficient due to image forces.

For the range  $0.01 \text{ } \mu\text{m} \leq a \leq 0.2 \text{ } \mu\text{m}$ , a rough fit is,

$$R_{0,q,100\%} - R_{0,0,100\%} = q * 10^{-15.26 - 2.51 \log_{10} a - 0.33 (\log_{10} a)^2}. \quad (4.7)$$

This makes the approximation that for small particles the effect of the image force on the rate coefficient is roughly linear with particle charge  $q$ . A more precise expression is given by the polynomials of  $\log_{10} a$  and  $\log_{10} q$ ,

$$\begin{aligned} \log_{10} (R_{0,q,100\%} - R_{0,0,100\%}) = & -15.859 - 0.715 \log_{10} a + 0.328 (\log_{10} a)^2 \\ & + (-1.41 - 0.308 \log_{10} a - 0.003 (\log_{10} a)^2) \log_{10} q. \end{aligned} \quad (4.8)$$

For the range  $0.2 \text{ } \mu\text{m} \leq a \leq 2.5 \text{ } \mu\text{m}$ , the fitting is also precise with the polynomial of  $\log_{10} a$  and  $\log_{10} q$ ,

$$\begin{aligned} \log_{10} (R_{0,q,100\%} - R_{0,0,100\%}) = & -16.575 - 2.536 \log_{10} a + 0.193 (\log_{10} a)^2 + 1.456 (\log_{10} a)^3 \\ & + (-1.709 + 0.878 (\log_{10} a) - 0.827 (\log_{10} a)^2 - 1.456 (\log_{10} a)^3) \log_{10} q. \end{aligned} \quad (4.9)$$

For large particles, the ‘wif’ effects become important, so we have to fit to third order of  $\log_{10} a$ . When  $q = 1e$ , the right side of equation (4.8) and (4.9) will be very small, approximately -16 to -17, thus as  $q$  approach  $0e$ ,  $R_{0,q,100\%}$  will converge to  $R_{0,0,100\%}$ , which ensures that the fitting expressions of equations (4.8) and (4.9) are self-consistent.

#### 4.2.2.2 Results for $R_{0,q,RH \neq 100\%}$

The value of  $R_{0,q,RH} - R_{0,0,RH}$  roughly represents the effect of image forces for different relative humidities, and it changes little with relative humidity for  $a \leq 0.1 \text{ } \mu\text{m}$  and  $a \geq 1.5 \text{ } \mu\text{m}$ , as where the effect of relative humidity is weak, so the effect of the image forces and relative humidity have little influence on each other. On the assumption that the two effects work independently,

$$R_{0,q,RH} \approx R_{0,0,RH} + R_{0,q,100\%} - R_{0,0,100\%}. \quad (4.10)$$

Obviously the equation (4.10) holds for  $RH = 100\%$  or  $q = 0$ . Figure 4.3 compares the two sides of equation (4.10) for  $RH = 95\%, 98\%, 99\%, 101\%$  and  $q = 10e, 20e, 50e$ , with points corresponding to the simulated results of  $R_{0,q,RH}$ , and lines representing the value of  $R_{0,0,RH} + R_{0,q,100\%} - R_{0,0,100\%}$ . For  $RH < 100\%$ , equation (4.10) holds very well except for the case of  $RH = 95\%, q = 50e, 0.05 \mu m \leq a \leq 1.5 \mu m$ , as the two effects are both strong and they will not be independent, the value of  $R_{0,0,RH} + R_{0,q,100\%} - R_{0,0,100\%}$  will be higher than  $R_{0,q,RH}$  by about 10%. For  $RH = 101\%$ , equation (4.10) holds well for small particles, while it does not hold for the range of  $0.1 \mu m \leq a \leq 1.0 \mu m$ , as the effect of repulsive phoretic forces are not linear, the value of  $R_{0,q,RH}$  could not be simply estimated by the sum of the two effects.

In order to get a more accurate rate coefficient  $R_{0,q,RH}$ , we fit it by polynomials in terms of saturation  $s$ , the logarithm of particle radius and the logarithm of particle charge. For  $0.01 \mu m \leq a \leq 0.2 \mu m$ ,

$$\log_{10}(R_{0,q,RH} - R_{0,0,RH}) = \sum_{i,j,k} B_{i,j,k} s^i (\log_{10} a)^j (\log_{10} q)^k, \quad (4.11)$$

where  $i = 0, 1, 2; j = 0, 1, 2; k = 0, 1$ . The coefficients  $B_{i,j,k}$  are given in the file of 'parameter1.txt' in the Appendix for  $s < 0$  and  $s \geq 0$  separately. For  $0.2 \mu m \leq a \leq 2.5 \mu m$ ,

$$\log_{10}(R_{0,q,RH} - R_{0,0,RH}) = \sum_{i,j,k} C_{i,j,k} s^i (\log_{10} a)^j (\log_{10} q)^k, \quad (4.12)$$

where  $i = 0, 1, 2; j = 0, 1, 2, 3; k = 0, 1, 2$ . The coefficients  $C_{i,j,k}$  are given in the file of 'parameter1.txt' in the Appendix for  $s < 0$  and  $s \geq 0$  separately.



### 4.2.3 Parameterization of collision rate coefficients $R_{Q,0,RH}$ for zero particle charge.

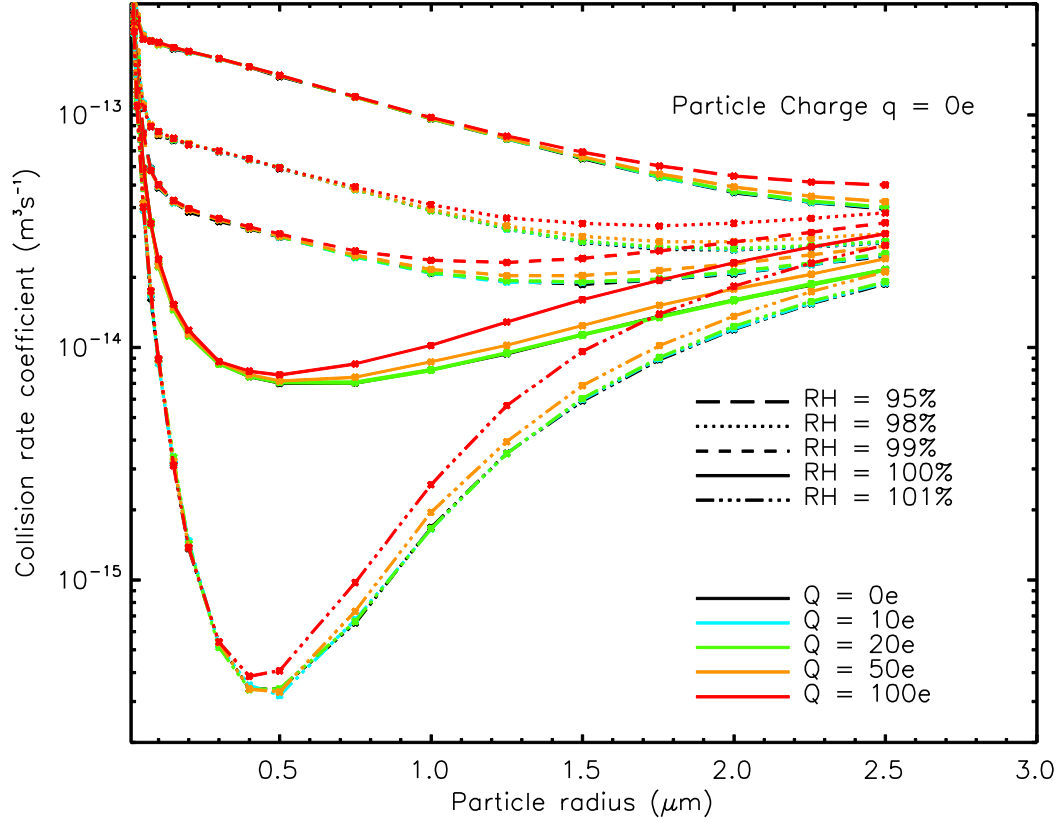


Figure 4.4. Simulated results of rate coefficients  $R_{Q,0,RH}$  for particle charge  $q = 0e$ , droplet charge  $Q = 0e, 10e, 20e, 50e, 100e$ , relative humidity  $RH = 95\%, 98\%, 99\%, 100\%, 101\%$ .

Generally, the induced image force induced by large charged droplets on small particles is very weak, however, our present work focuses on smaller charged droplets with radii of 3 μm, and so when the size of the particle is comparable to that of droplet, the image force due to the droplet charge will also enhance the collision rate coefficient. The simulated results of  $R_{Q,0,RH}$  for  $Q = 10, 20, 50, 100e$  and  $RH = 95\%, 98\%, 99\%, 100\%, 101\%$  are shown in Figure 4.4. For small particles,  $a < 0.5$  μm, the departure of  $R_{Q,0,RH}$  from  $R_{0,0,RH}$  can be neglected, as the image

charge force on small particles is very weak, so that we apply a linear scale for the X-axis to better reveal the image force on large particles. For large particles, the value of  $R_{Q,0,RH} - R_{0,0,RH}$  is approximately linearly dependent on  $Q^2$ , so for  $Q \leq 20e$  the effect of image force is very weak, and the curves for  $Q = 0e$  and  $Q = 10e$  are overlaid by that of  $Q = 20$ , while for  $Q = 50e$  and  $Q = 100e$  the effect is significant.

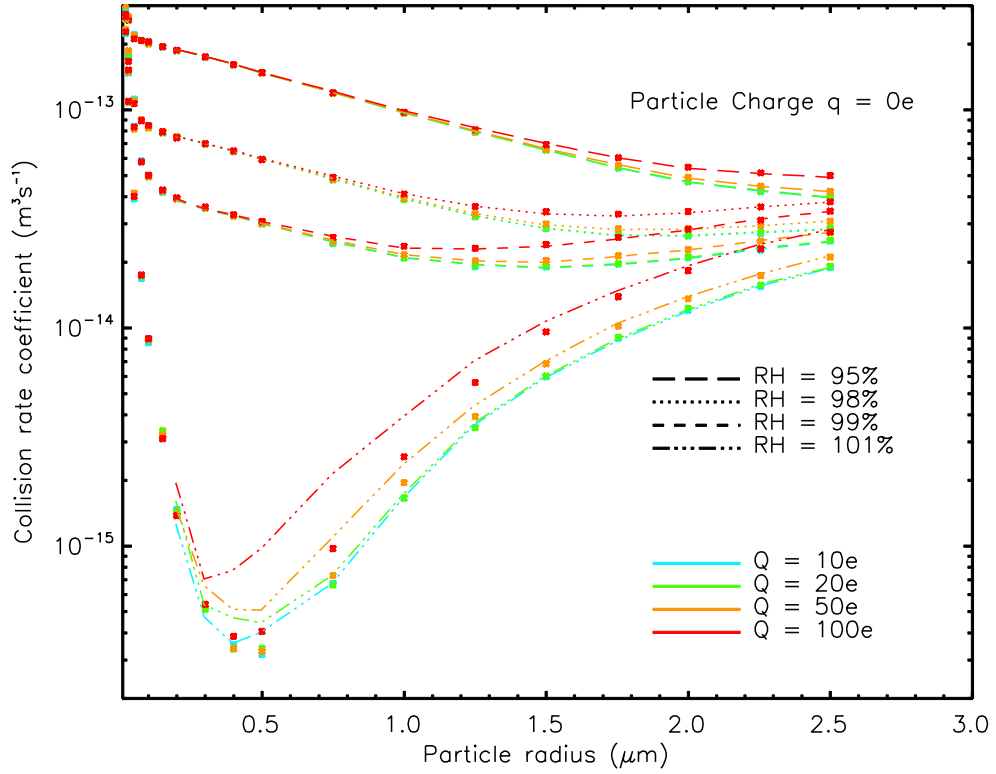


Figure 4.5. Points are the simulated results of rate coefficients  $R_{Q,0,RH}$ , lines are the results of  $R_{0,0,RH} + R_{Q,0,100\%} - R_{0,0,100\%}$  for  $RH = 95\%, 98\%, 99\%, 101\%$  and  $Q = 10e, 20e, 50e, 100e$ .

For  $RH = 100\%$ , if  $a < 0.5 \mu m$ , then  $R_{Q,0,100\%} = R_{0,0,100\%}$ ; if  $a \geq 0.5 \mu m$ , the effect of image charge is roughly linear with particle size  $a$ , and strongly depends on  $Q^2$ , we fit  $R_{Q,0,100\%} - R_{0,0,100\%}$  in the form of,

$$R_{Q,0,100} - R_{0,0,100\%} = (-5.571 \times 10^{-19} - 2.953 \times 10^{-18} a)Q + (-1.974 \times 10^{-19} + 4.797 \times 10^{-18} a)Q^2. \quad (4.13)$$

As with processing the case of zero droplet charge, assuming the effect of the image force induced by the droplet is independent of the effect of relative humidity, we can roughly estimate  $R_{Q,0,RH}$  to be the sum of two effects in the form of,

$$R_{Q,0,RH} \approx R_{0,0,RH} + R_{Q,0,100\%} - R_{0,0,100\%}. \quad (4.14)$$

Obviously equation (4.14) holds for  $RH = 100\%$  or  $Q = 0$ . The lines in Figure 4.5 show the right side of equation (4.14), and the points represent the simulated results of  $R_{Q,0,RH}$  for  $RH = 95\%$ ,  $98\%$ ,  $99\%$ ,  $101\%$  and  $Q = 10e$ ,  $20e$ ,  $50e$ ,  $100e$ . Equation (4.14) can be used to estimate reasonably well the cases of  $RH < 100\%$ , as for medium particle size the effect of relative humidity is strong while the effect of the image force is weak, and for large particle size the effect of the image force is strong while the effect of relative humidity is weak, hence the two effects are roughly independent. For  $RH = 101\%$ , equation (4.14) holds for large particles as the effect of humidity is weak, but does not hold for the range of  $0.5 \mu m \leq a \leq 1.5 \mu m$  due to the effect of strong and repulsive phoretic forces, and besides, the standard deviation of  $R_{Q,0,100\%} - R_{0,0,100\%}$  is comparable to the values of  $R_{Q,0,101\%}$ . Thus for medium particles equation (4.14) does not hold for  $RH > 100\%$ .

For better fitting to the value of  $R_{Q,0,RH}$ , we use a function of the polynomial of saturation ( $s$ ), particle radius ( $a$ ) and droplet charge ( $Q$ ),

$$R_{Q,0,RH} - R_{0,0,RH} = \sum_{i,j,k} D_{i,j,k} s^i a^j Q^k, \quad a \geq 0.5 \mu m, \quad (4.15)$$

where  $i = 0, 1, 2, 3, j = 0, 1, 2, 3, k = 1, 2, 3$ , the value of  $D_{i,j,k}$  is given in the file of 'parameter1.txt' in the Appendix. For small particles with  $a < 0.5 \mu\text{m}$ , the effect of the image force is very weak and hence  $R_{Q,0,RH} = R_{0,0,RH}$ .

#### 4.2.4 Parameterization of collision rate coefficients $R_{Q,q,RH}$ for opposite-sign droplet charge and particle charge.

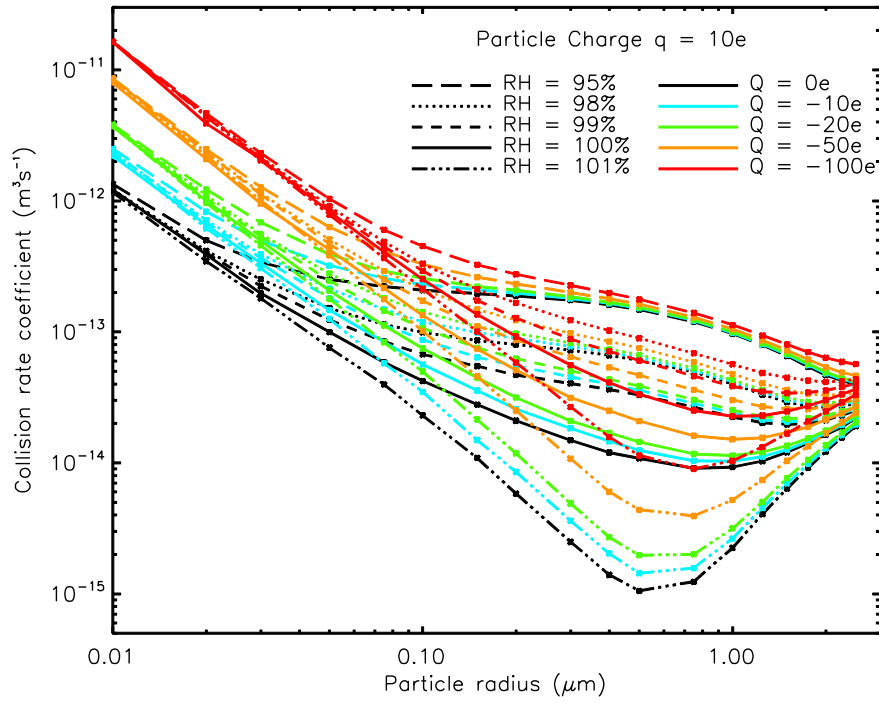


Figure 4.6. Simulated results of rate coefficients  $R_{Q,q,RH}$  for particle charge  $q = 10\text{e}$ , droplet charge  $Q = 0\text{e}, -10\text{e}, -20\text{e}, -50\text{e}, -100\text{e}$ , relative humidity  $RH = 95\%, 98\%, 99\%, 100\%, 101\%$ .

When droplets and particles are charged with opposite-sign charges, the Coulomb forces are attractive, which enhances collision rates.. Simulated results of rate coefficientss $R_{Q q RH}$  for particle charge  $q = 10\text{e}$ , droplet charge  $Q = 0\text{e}, -10\text{e}, -20\text{e}, -50\text{e}, -100\text{e}$ , relative humidity  $RH =$

95%, 98%, 99%, 100%, 101%. have been obtained and are shown in Figure 4.6. As mentioned above, the electric forces dominate rate coefficients for small particles and the phoretic forces are dominant for large particles.

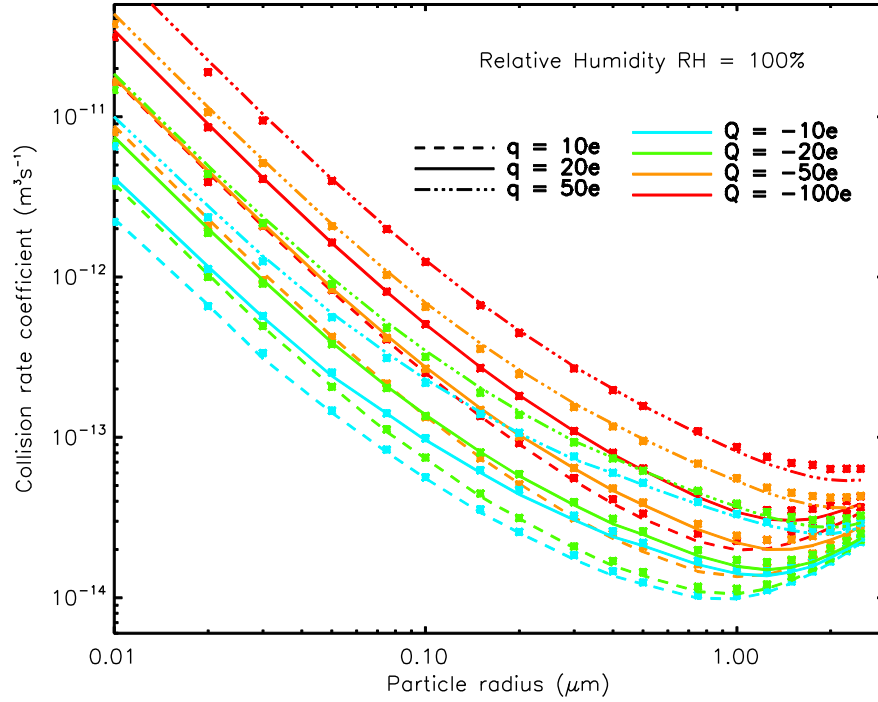


Figure 4.7. Points are the simulated results of rate coefficients  $R_{Q,q,RH}$ , lines are the right side of equation (4.16),  $N_{Q,q,RH} + (R_{0,q,RH} - R_{0,0,RH}) + (R_{Q,0,RH} - R_{0,0,RH}) + (R_{0,0,RH} - N_{0,0,RH})$ , with relative humidity  $RH = 100\%$ , droplet charge  $Q = -10e, -20e, -50e, -100e$  and particle charge  $q = 10e, 20e, 50e$ .

If effects of humidity and charge are independent, then we can estimate the collision rate coefficient  $R_{Q,q,RH}$  by the following formula,

$$R_{Q,q,RH} \approx N_{Q,q,RH} + (R_{0,q,RH} - R_{0,0,RH}) + (R_{Q,0,RH} - R_{0,0,RH}) + (R_{0,0,RH} - N_{0,0,RH}). \quad (4.16)$$

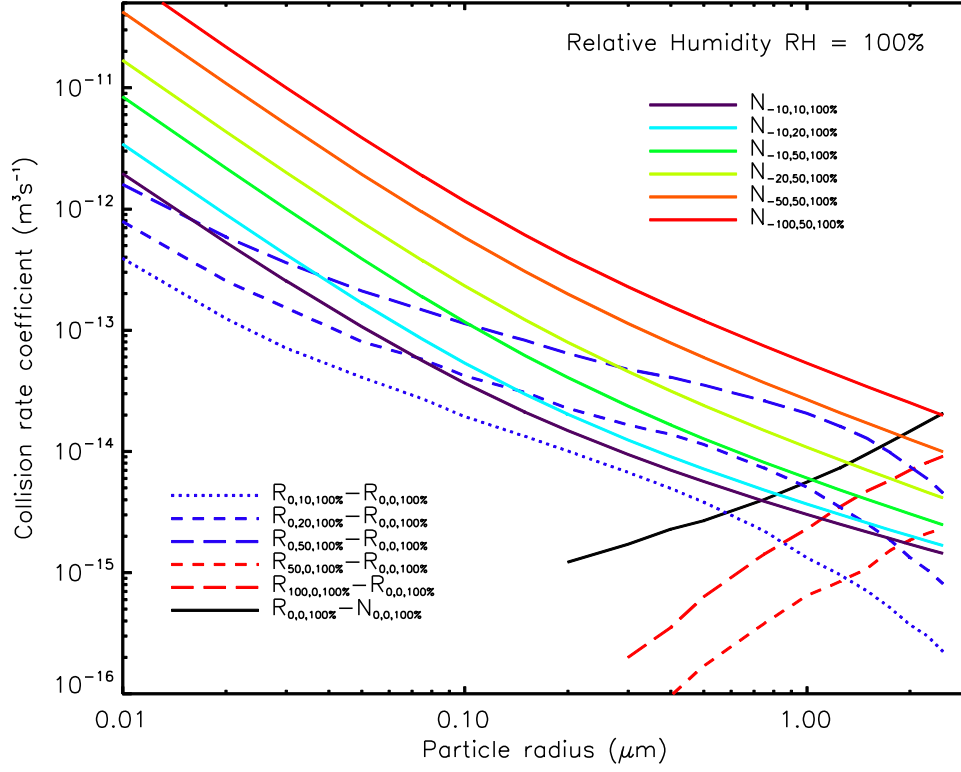


Figure 4.8. Contributions to rate coefficients by each of the four terms in the right side of equation (4.16) for  $RH = 100\%$ ; the terms are  $N_{Q,q,RH}$ ,  $R_{0,q,RH} - R_{0,0,RH}$ ,  $R_{Q,0,RH} - R_{0,0,RH}$ , and  $R_{0,0,RH} - N_{0,0,RH}$ .

The first term in the right side is the effect of the Coulomb force and phoretic forces and diffusion which can be obtained from equation (5), the second term is the effect of the image force induced by the particle charge, the third term is the effect of the image force induced by the droplet charge, the last term is the large particle ‘wif’ effect. Figure 4.7 shows the case of  $RH = 100\%$ , in which points represent the simulated results of  $R_{Q,q,RH}$  for  $Q = -10e, -20e, -50e, -100e$  and  $q = 10e, 20e, 50e$ , and lines represent the right side of equation (4.16). Figure 4.7 shows that equation (4.16) works quite well for  $RH = 100\%$ . For  $RH < 100\%$ , equation (4.16) also works well for particle radii  $a \leq 1.5 \mu m$  (not shown) while for larger particles, equation (4.16) is found to

underestimate the rate coefficient by about 20%, due to the non-independence of the effect of the image force acting with the other forces along the trajectory. For larger particles, which collide with droplet at a distance of ' $A+a$ ' rather than ' $A$ ' in equation (2.33), we can reduce the underestimate by modifying the ' $A$ ' in equation (2.33) to be ' $A+a$ '.

For  $RH = 101\%$ , equation (4.16) only holds for  $a \leq 0.2 \text{ } \mu\text{m}$  because for larger particles there is non-independence of the effect of the repulsive phoretic force with the 'wif' effects and the attractive electrical forces, and the result for the whole trajectory is far from the sum of the separate effects in equation (4.16).

We show the contributions to rate coefficients by each of the four terms of the right side of equation (4.16) in Figure 4.8 for six combinations of  $Q$  and  $q$ , for  $RH = 100\%$ , utilizing  $q = 10e, 20e, 50e$ , and  $Q = -10e, -20e, -50e, -100e$ . For particle radii  $a \leq 0.2 \text{ } \mu\text{m}$  only the Coulomb force and image charge force induced by the particle contribute to the rate coefficient, the third and last terms can be ignored. As particle radius decreases, the two terms both increase with the increasing particle mobility, while the effect of Coulomb force increases faster. Also, the Coulomb force also increases with droplet charge. So if the particle radius is very small and droplet charge is quite large the collision rate coefficient is dominated by the Coulomb force, otherwise the contribution of the image force induced by particle charges must be considered. For particles of radii  $0.2 \text{ } \mu\text{m} \leq a \leq 2.5 \text{ } \mu\text{m}$ , the former two effects continue to decrease, the 'wif' effects appear, and the effect of image charge induced by the droplet also appears; the four terms are comparable and should all be considered when using this approximation for  $R_{Q,q,RH}$ .

#### 4.2.4.1 Results of $0.01 \text{ } \mu\text{m} \leq a \leq 0.2 \text{ } \mu\text{m}$

Equation (4.16) using the algebraic sums can be used to estimate the collision rate coefficient  $R_{Q,q,RH}$  for particles in the range of  $0.01 \text{ } \mu\text{m} \leq a \leq 0.2 \text{ } \mu\text{m}$ . However, a better fit is obtained by using

$$\log_{10} (R_{Q,q,RH} - R_{0,q,RH}) = E_0 + E_1 \log_{10}(|Q|) + E_2 \log_{10}(q) + E_3 \log_{10}(|Q|) \log_{10}(q). \quad (4.17)$$

The parameters  $E_0, E_1, E_2, E_3$  are fitted by,

$$E_i = \sum_{j,k} F_{i,j,k} (\log_{10} a)^j s^k, \quad (4.18)$$

where  $i = 0, 1, 2, 3; j = 0, 1, 2, 3; k = 0, 1, 2, 3$ , and  $F_{i,j,k}$  are given in the file of ‘parameter1.txt’ in the Appendix.

#### 4.2.4.2 Results of $0.2 \text{ } \mu\text{m} \leq a \leq 2.5 \text{ } \mu\text{m}$

For large particles, equation (4.16) gives a poor estimate of the collision rate coefficient for  $RH > 100\%$ , We can fit  $R_{Q,q,RH}$  by,

$$\begin{aligned} \log_{10} (R_{Q,q,RH} - R_{0,q,RH} - R_{Q,0,RH} + R_{0,0,RH}) = \\ G_0 + G_1 \log_{10}(|Q|) + G_2 \log_{10}(q) + G_3 \log_{10}(|Q|) \log_{10}(q). \end{aligned} \quad (4.19)$$

The parameters  $G_0, G_1, G_2, G_3$  are fitted by,

$$G_i = \sum_{j,k} H_{i,j,k} (\log_{10} a)^j s^k, \quad (4.20)$$

where  $i = 0, 1, 2, 3; j = 0, 1, 2, 3; k = 0, 1, 2, 3$ , and the  $H_{i,j,k}$  are given in the file of ‘parameter1.txt’ in the Appendix.



#### 4.2.5 Parameterization of rate coefficients for same-sign droplet charge and particle charge.

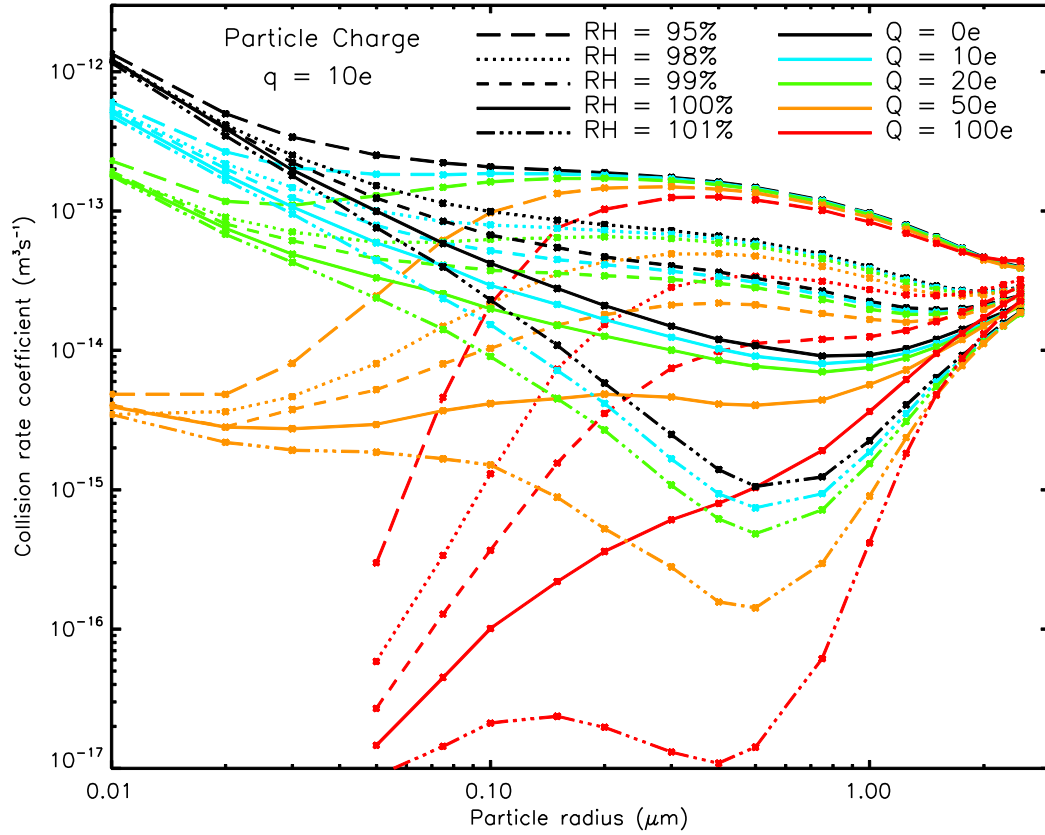


Figure 4.9. Simulated results of rate coefficients for particle charge  $q = 10e$ , droplet charge  $Q = 0e, 10e, 20e, 50e, 100e$ , relative humidity  $RH = 95\%, 98\%, 99\%, 100\%, 101\%$ .

Figure 4.9 shows the simulated results of particle charge  $q = 10e$ , droplet charge  $Q = 0e, 10e, 20e, 50e, 100e$ , and relative humidity  $RH = 95\%, 98\%, 99\%, 100\%, 101\%$ . Unlike the cases of opposite-sign charges, the same-sign charges provide a repulsive Coulomb force which can reduce the rate coefficient to very small value. With  $RH > 100\%$  the repulsive phoretic force has the same effect. For small particles, the combination of the Coulomb force, phoretic forces, diffusion and the image

force induced by particle need to be considered, but the collision rate coefficient could not be estimated simply by the sum of these factors, as they are non-linear.

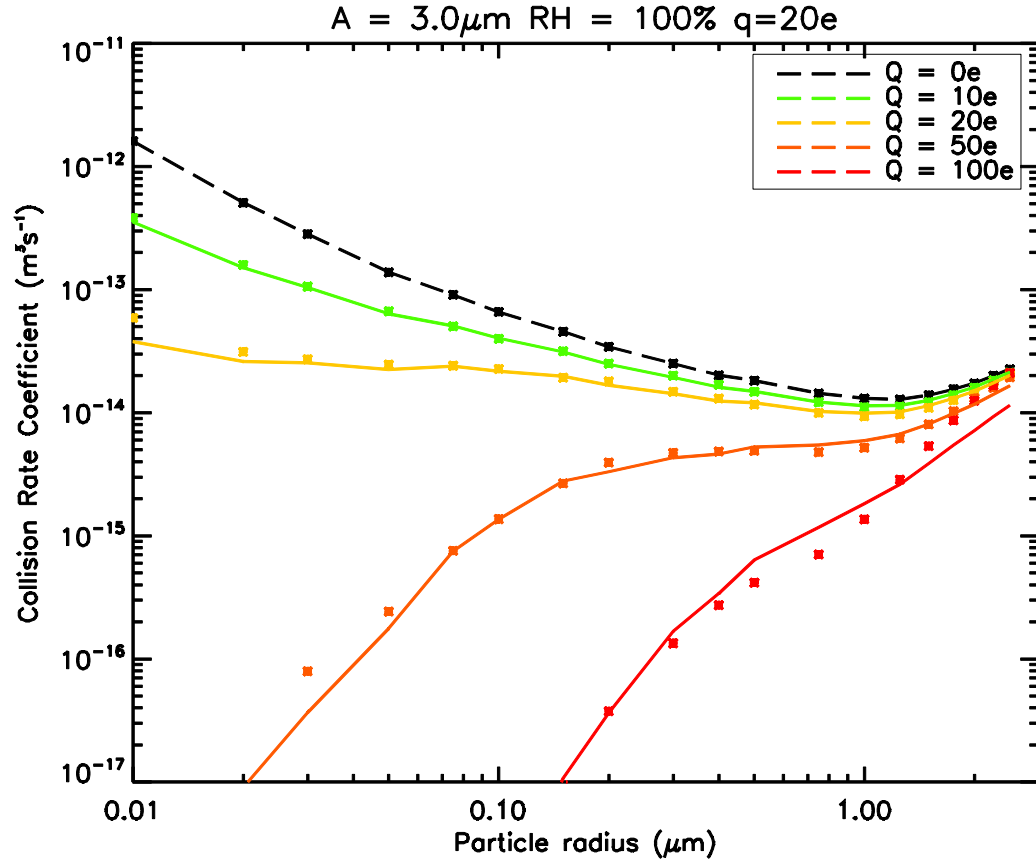


Figure 4.10. Points are the simulated results of collision rate coefficient for same-sign charged droplet and particles, and lines are the results of approximately empirical formula given in equations (4.21) and (4.22).

For small particles, the ‘wif’ effects are negligible, and if the effect of image force could also be neglected, the rate coefficient would be the value of  $N_{Q,q,RH}$  in equation (2.35). But due to the existence of the attractive image force, the rate coefficient  $R_{Q,q,RH}$  is much larger than  $N_{Q,q,RH}$ . We could roughly estimate the rate coefficient by modifying equation (2.35) to be,

$$R_{Q,q,RH} \approx N_B \frac{x}{e^{x/y} - 1}, \quad (4.21)$$

where,

$$y = 1 + e^{-x/(5+0.5q)} \left( \frac{R_{0,q,100\%}}{N_B} - 1 \right). \quad (4.22)$$

Here  $yA$  is the modified contact radius due to the short-range image force, and we assume when the separation between droplet and particle is less than  $yA$  then they will collide due to the strong short-range image force. If the image force is weak, that is,  $R_{0,q,100\%}$  approaches  $N_B$ , then the value of  $y$  in equation (4.22) will approach 1, equation (4.21) will reduce to equation (2.35), in which the effect of inverse square forces is dominant. As shown in Figure 4.10 the results of approximate empirical formula (4.21) match well with the simulated results of collision rate coefficients. The equation (4.21) is a good estimate for collision rate coefficient of small particles with radius a less than 0.5  $\mu\text{m}$ , but a poor estimate for larger particles. In order to get a better result of collision rate coefficient for same-sign charges, we must do the fitting as in the following sections.

#### 4.2.5.1 Results for $0.01 \mu\text{m} \leq a \leq 0.2 \mu\text{m}$

As the particle sizes are small and the induced image charge on particles by the droplet charge are negligible,  $R_{Q,0,RH} = R_{0,0,RH}$ , so we fit  $R_{Q,q,RH}$  from  $R_{0,q,RH}$ , and

$$\log_{10} R_{0,q,RH} - \log_{10} R_{Q,q,RH} = L_1 qQ + L_2 q^2 Q + L_3 qQ^2. \quad (4.23)$$

The parameters  $L_1$ ,  $L_2$ ,  $L_3$  are fitted by saturation  $s$ , where  $s = RH - 100\%$ , and particle radius  $a$  as follows,

$$L_i = \sum_{j,k} M_{i,j,k} (\log_{10} a)^j s^k, \quad (4.24)$$

where  $i = 0, 1, 2, 3; j = 0, 1, 2, 3; k = 0, 1, 2, 3$ , and  $M_{i,j,k}$  are given in the file of ‘parameter1.txt’ in the Appendix.

#### 4.2.5.2 Results for $0.2 \mu\text{m} \leq a \leq 2.5 \mu\text{m}$

For large particles, the image force induced by droplet also needs to be considered, so that we fit  $R_{Q,q,RH}$  by

$$\log_{10} (R_{0,q,RH} + R_{Q,0,RH} - R_{0,0,RH}) - \log_{10} R_{Q,q,RH} = U_1 qQ + U_2 q^2 Q + U_3 qQ^2. \quad (4.25)$$

For either  $Q = 0$  or  $q = 0$ , both sides of equation (4.25) are equal to zero. We have fitted  $U_1, U_2, U_3$  in terms of saturation  $s$ , and particle radius  $a$  as,

$$U_i = \sum_{j,k} V_{i,j,k} (\log_{10} a)^j s^k, \quad (4.26)$$

where  $i = 1, 2, 3; j = 0, 1, 2, 3; k = 0, 1, 2, 3$ , and  $V_{i,j,k}$  are given in the file of ‘parameter1.txt’ in the Appendix. Normally the rate coefficient  $R_{Q,q,RH}$  is less than  $R_{0,q,RH}$  due to the repulsive Coulomb force, while as seen in Figure 4.9 for large particles and large droplet charge  $Q$ , the value of  $R_{Q,q,RH}$  could be greater than  $R_{0,q,RH}$  due to the strong image force induced by the droplet charge. Thus for large particles the term  $\log_{10}(R_{0,q,RH}) - \log_{10} R_{Q,q,RH}$  in equation (4.23) could be either positive or negative which is difficult to be fitted, and so that we fit the collision rate coefficient in the form of  $\log_{10}(R_{0,q,RH} + R_{Q,0,RH} - R_{0,0,RH}) - \log_{10} R_{Q,q,RH}$  in equation (4.25) in order to keep its value to be positive and make the fitting easier.

### 4.3 Discussion

For small particles, Coulomb forces and diffusion are important, with image forces and phoretic forces relatively weak. If the droplet and particle have opposite-sign charges, the Coulomb force is attractive, and the total rate coefficient can be roughly estimated by the sum of these four effects. If the particle is small enough and the droplet charge is large enough, then the effect of Coulomb force is predominant over other effects, and we can apply the analytic solution in equation (2.35) directly. If the droplet and particle have same-sign charges, the Coulomb force is repulsive and the analytic value of the rate coefficient tends to be exponential for the small particles. The simulated rate coefficient is greater than the analytic value only due to the short-range image forces. Given that the image electric force is short-range, and on the assumption that particles moving into that range must be captured by the droplet, a modified analytic solution for small particles can be used to roughly estimate the order of magnitude of the rate coefficient. To get better results, parameterizations are given for both opposite-sign and same-sign cases, which give good fits to the simulated results.

For large particles, a series of effects are involved in the rate coefficient. The effect of phoretic forces increases with particle radius and reaches a maximum at about  $1.0 \mu\text{m}$ . The ‘wif’ effects become important for large particles. The image force induced by the droplet contributes increasingly with increasing particle size, and the contribution is roughly proportional to  $Q^2$ , thus when the droplet has a large charge, its image effect may be comparable to that of the Coulomb force and may be greater than the effect of the image force induced by the particle. If the Coulomb force and phoretic forces are both attractive, it is still possible to estimate the rate coefficient by the sum of each factor. If there are repulsive forces, then it is difficult to estimate the rate coefficient by

simply adding all factors; we must apply the parameterization to get the rate coefficient. Besides, there is a significant peak for the phoretic forces at about  $1.0 \mu\text{m}$  particle radius as shown in Figure 4.1. Near  $1.0 \mu\text{m}$  particle radius, if the relative humidity is very low, for example,  $RH \leq 80\%$ , the effect of attractive phoretic forces will dominate over effects of the other factors, and the analytic value in equation (2.35) is a good estimate for collision rate coefficient.

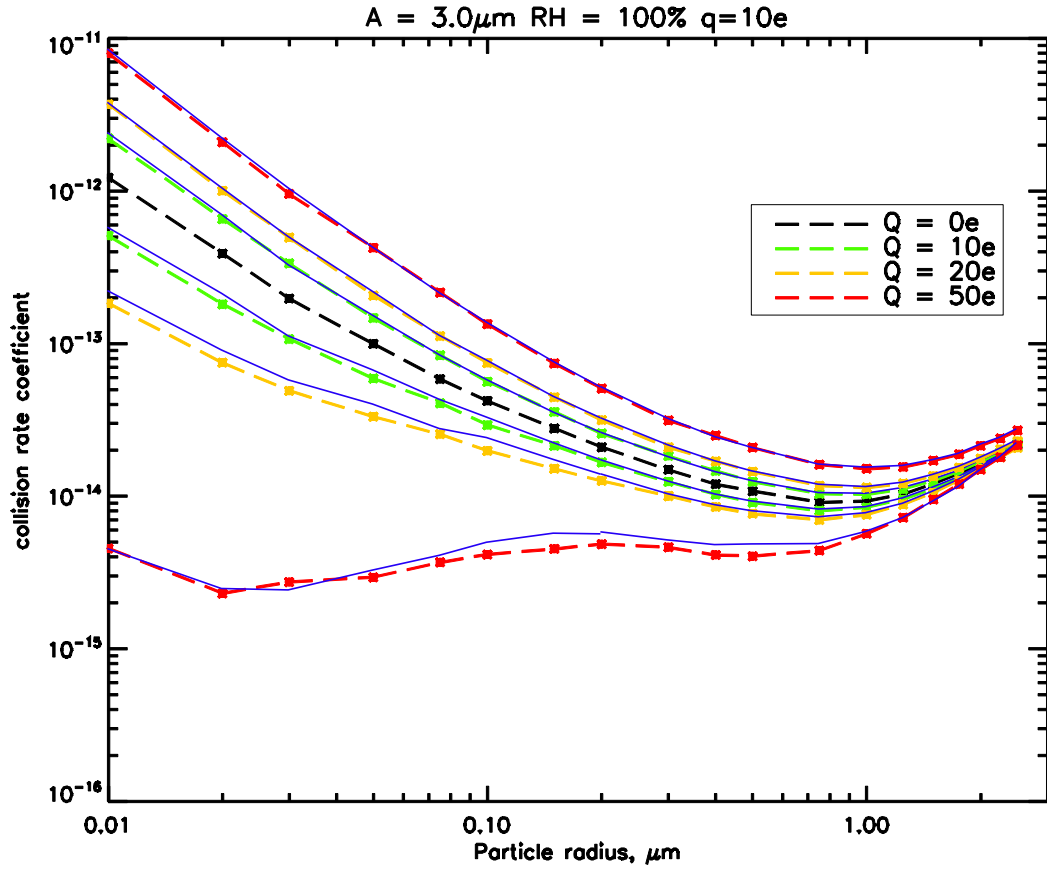


Figure 4.11. The fitted results of collision rate coefficient (blue solid line) comparing with the simulated results with particle charge  $q$  of  $10e$ , droplet charge  $Q$  of  $0e, \pm 10e, \pm 20e, \pm 50e$ , relative humidity  $RH$  of  $100\%$ .

In short, to get the rate coefficient of  $R_{Q,q,RH}$ , the first step is to get the analytic value of  $N_{0,0,RH}$  and the  $R_{0,0,RH}$  by equations (2.35), (4.1), and (4.2). Next, we need to get the rate

coefficient due to image forces  $R_{0,q,RH}$  and  $R_{Q,0,RH}$  by equations (4.11), (4.12), and (4.15). Finally, if the droplet and particle charge are opposite-sign, then we can get  $R_{Q,q,RH}$  by equations (4.17), and (4.19), or else if they are same-sign, then we can get  $R_{Q,q,RH}$  by equations (4.23), and (4.25). The rate coefficient  $R_{Q,q,RH}$  obtained by our parameterization is quite close to the simulated results if inputs lie in the ranges of  $Q \leq 100e$ ,  $q \leq 50e$ ,  $95\% \leq RH \leq 101\%$ ,  $0.01 \mu m \leq a \leq 2.5 \mu m$ ; If the inputs exceed these ranges, the empirical formula of equation (4.7), (4.10), (4.13), (4.14), (4.16), (4.21) can be used to roughly estimate the value of the collision rate coefficients.

Figure 4.11 compares the simulated results of collision rate coefficient (dashed lines) with the fitted results (solid lines) according to the above parameterizations, for particle charge  $q$  of  $10e$ , droplet charge  $Q$  of  $0e, \pm 10e, \pm 20e, \pm 50e$ , relative humidity  $RH$  of  $100\%$ . We fit the same-sign and opposite sign charged droplet and particles separately, and fit the small particles and large particles separately. The two groups of lines match well with each other, which means that our parameterizations can describe the collision rate coefficients simply and well.

#### 4.4 Summary

Parameterization of the modulation of aerosol scavenging by electric charges on particles and droplets under different values of relative humidity has been made for  $3 \mu m$  radius droplets and a wide range of particle radii. When charged particles encounter an uncharged droplet, the image force due to the particle charge is induced for all particle radii and it will increase the scavenging rates. When uncharged particles encounter a charged droplet, the image force is induced only for large particles. For droplets and particles that are charged with opposite-sign charges, the attractive

Coulomb force will further increase the rate coefficients. When they are charged with same-sign charges, the repulsive Coulomb force tends to decrease rate the coefficient; in this case the short-range attractive image force is quite important. The phoretic forces, like the Coulomb force, act as inverse square forces. The effect of Coulomb forces tend to dominant for small particles and that of phoretic forces tends to dominant for large particles. There is an analytic flux expression for rate coefficients for inverse square forces; However due to the image forces and 'wif' effects, the simulated results for large particles usually depart far from the analytic solution. We give parameterizations which fit the simulated results closely.



## CHAPTER 5

### PARAMETERIZATION OF AEROSOL SCAVENGING DUE TO ATMOSPHERIC IONIZATION UNDER VARYING PARTICLE DENSITY

#### 5.1 Approach to Simulation and Parameterization

In Chapter 4 the collision rate coefficients obtained with the trajectory model are designated as  $R_{Q,q,A,a,RH}$ , (where,  $Q$  is the droplet charge,  $q$  is the particle charge,  $A$  is the droplet radius,  $a$  is the particles radius,  $RH$  is the relative humidity). For convenience, in Chapter 4 the collision rate coefficient is abbreviated as  $R_{Q,q,RH}$ , as the particle density was fixed at  $500 \text{ kg} \cdot \text{m}^{-3}$ . In this Chapter we evaluate the collision rate coefficient for an extended range of particle density, and the collision rate coefficients are designated as  $R_{Q,q,A,a,RH,\rho}$  and abbreviated as  $R_{Q,q,RH,\rho}$ . The particle density values  $\rho$ , were 1, 500, 1000, 1500, 2000  $\text{kg} \cdot \text{m}^{-3}$ . The value of  $A$  used was  $3 \text{ } \mu\text{m}$ , while the values of  $a$  used were 0.2, 0.3, 0.4, 0.5, 0.75, 1.0, 1.25, 1.5, 1.7543, 2.0, 2.2556,  $2.5 \text{ } \mu\text{m}$  for particle density less equal than  $1000 \text{ kg} \cdot \text{m}^{-3}$ , while the maximum radii were 2.3076 and  $2.0 \text{ } \mu\text{m}$  for particle density of 1500 and  $2000 \text{ kg} \cdot \text{m}^{-3}$  respectively. For particle radius  $a < 0.2 \text{ } \mu\text{m}$ , the results are the same as Chapter 4 for particle density of  $500 \text{ kg} \cdot \text{m}^{-3}$ , as the weight effect can be neglected for small particles. The particle charges  $q$  were 0, 10, 20 and 50e, and the droplet charges  $Q$  were 0e,  $\pm 10\text{e}$ ,  $\pm 20\text{e}$ ,  $\pm 50\text{e}$ ,  $\pm 100\text{e}$ . The values of relative humidity  $RH$  were 95%, 98%, 99%, 100%, 101%. The atmospheric pressure and temperature were still 540 hPa, and 256.15 K respectively. The computational uncertainties of the collision rate coefficient in present simulations are less than 1% for most cases, except for cases

of high particle density and strong repulsive force in which collision rate coefficient is quite low and it is hard to further reduce uncertainty by increasing the number of trials.

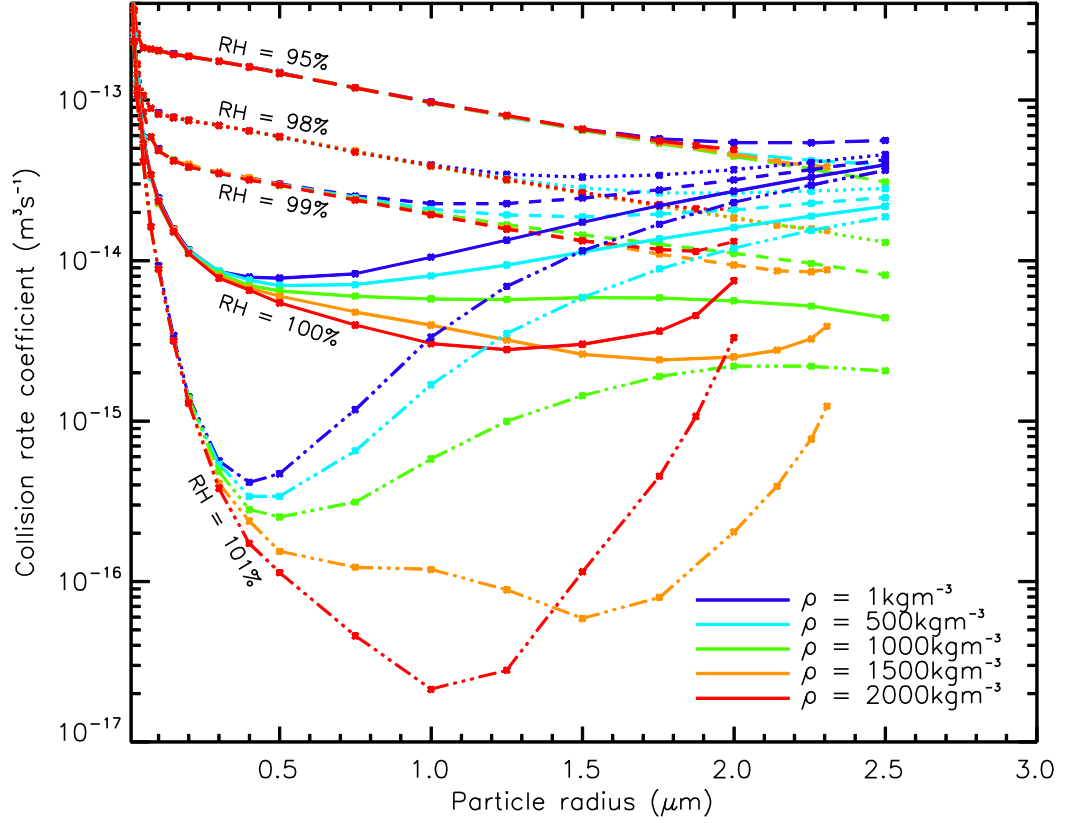


Figure 5.1. Simulated collision rate coefficients ( $RH_{0,0,RH,\rho}$ ) with droplet charges  $Q = 0$ , particle charge  $q = 0$ , relative humidity  $RH = 95\%, 98\%, 99\%, 100\%, 101\%$  and particle density  $\rho = 1, 500, 1000, 1500, 2000 \text{ kg} \cdot \text{m}^{-3}$ .

To parameterize the collision rate coefficient, we first fit the simulated results of the collision rate coefficient  $R_{0,0,3,a,RH,\rho}$  for zero droplet charge and zero particle charge as a function of  $a$ ,  $RH$  and  $\rho$ . Using this base level, we then fit  $R_{0,q,RH,\rho}$  and  $R_{Q,0,RH,\rho}$ , which represent the effect of image electric forces induced by particles and droplet charges respectively. The collision rate coefficients vary differently for attractive and repulsive Coulomb forces, so we fitted  $R_{Q,q,RH,\rho}$  for

opposite sign and same sign charges respectively. For the above fitting processes, we separate the particle density into two range,  $\rho \leq 1000 \text{ kg} \cdot \text{m}^{-3}$  and  $\rho > 1000 \text{ kg} \cdot \text{m}^{-3}$ , due to the weight effects are different for low and high particle density as shown in Figure 3.7.

## 5.2 Results and parameterizations of collision rate coefficients.

### 5.2.1 Parameterization of collision rate coefficients $R_{0,0,RH,\rho}$ for zero-charged droplet and particle.

Figure 5.1 shows the simulated results of collision rate coefficients  $R_{0,0,RH,\rho}$  for zero charged droplet and particles, with relative humidity  $RH = 95\%, 98\%, 99\%, 100\%, 101\%$  and particle density  $\rho = 1, 500, 1000, 1500, 2000 \text{ kg} \cdot \text{m}^{-3}$ . It is evident that for small particles with radius  $a < 0.2 \text{ } \mu\text{m}$  the collision rate coefficient is same for different particle densities due to the gravitational force being negligible comparing with other forces. When droplet and particles are charged, the weight effect is still negligible for small particles, so that in this Chapter we only deal with particles with radius  $a \geq 0.2 \text{ } \mu\text{m}$ .

The simulated results show that the difference between collision rate coefficients for particles with density of  $\rho$  and that for particles with density of  $500 \text{ kg} \cdot \text{m}^{-3}$  is roughly the same amount for different relative humidities, that is,

$$R_{0,0,RH,\rho} - R_{0,0,RH,500} \approx R_{0,0,100\%,\rho} - R_{0,0,100\%,500}. \quad (5.1)$$

This means the effects of weight and phoretic forces on collision rate coefficient are roughly independent. The lower the relative humidity, the stronger the effect of phoretic forces, therefore the weight effect is relatively weaker for lower relative humidity. As shown in Figure 5.1 which has a logarithmic scale, for  $RH = 95\%$  the weight effect is negligible for particle radius less than

1.5  $\mu\text{m}$ . We have shown in Figure 2.1 and Figure 4.1 that the phoretic forces reach maximum at the particle radius of about 1.0  $\mu\text{m}$ , then for larger particles the phoretic forces decreases and the gravitational force increases and they become comparable, so that the weight effect needs to be considered for large particles even if the relative humidity is very low.

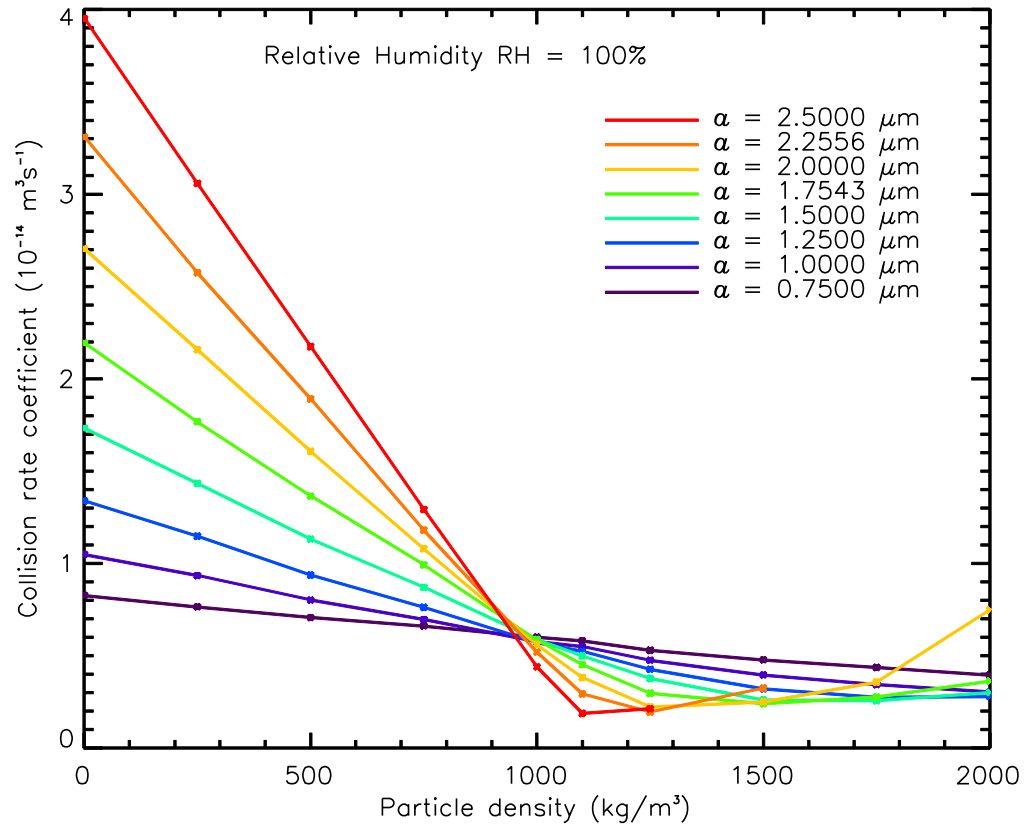


Figure 5.2. Simulated collision rate coefficients ( $RH_{0,0,RH,\rho}$ ) with droplet charges  $Q = 0$ , particle charge  $q = 0$ , relative humidity  $RH = 100\%$ , and a wide range of particle density  $\rho$  and particle radius  $a$ .

For the simulated results of  $RH = 100\%$ , as shown by the solid lines in Figure 5.1, the weight effect starts to take effect for particle radius  $a \geq 0.2 \mu\text{m}$  and tends to decrease collision rate coefficients at the beginning, however, for particles with density  $\rho = 1500$  and  $2000 \text{ kg} \cdot$

$\text{m}^{-3}$ , the weight effect turns to increase the collision rate coefficient when the particle radius is large enough to make the fall speed of particle relative to undisturbed air approach to that of droplet. This is because for a large particle with density greater than droplet density the collisions occur at the back side of droplet and the process is strongly non-linear, as shown in Figure 3.7, and also because when the fall speed of particle relative to undisturbed air approaches that of the droplet there is a longer time of random movement of particles for them to traverse flow lines and move close to the droplet surface.

Figure 5.2 shows the simulated results of collision rate coefficients for relative humidity  $RH = 100\%$ , and it is obvious that the results vary approximately linearly with particle density when  $\rho \leq 1000 \text{ kg} \cdot \text{m}^{-3}$ , and become non-linear for particle density  $\rho > 1000 \text{ kg} \cdot \text{m}^{-3}$ . Also, this linear pattern for particle density  $\rho \leq 1000 \text{ kg} \cdot \text{m}^{-3}$  still holds for relative humidities  $RH \neq 100\%$  which are not shown. Figure 5.2 indicates the collision rate coefficient varying with particle density in different ways for low and high particle density, so that we fit collision rate coefficients for particle density less and greater than  $1000 \text{ kg} \cdot \text{m}^{-3}$  separately.

The collision rate coefficient  $R_{0,0,RH,\rho}$  is the base level for the further fitting of  $R_{Q,q,RH,\rho}$ , and in order to fit  $R_{0,0,RH,\rho}$  with high accuracy we have calculated the collision rate coefficient for particle density  $\rho = 250, 750, 1100, 1250, 1750 \text{ kg} \cdot \text{m}^{-3}$ . First, for  $\rho \leq 1000 \text{ kg} \cdot \text{m}^{-3}$ , based on the results of  $R_{0,0,RH,500}$  which has already been calculated and fitted in Chapter 4, the collision rate coefficient  $R_{0,0,RH,\rho}$  is given in the following expression,

$$R_{0,0,RH,\rho} - R_{0,0,RH,500} = \sum_{i,j,k} A_{i,j,k} (\rho - 500)^i s^j a^k, \quad (5.2)$$

where  $i = 1, 2$ ,  $j = 0, 1, 2, 3$ ,  $k = 0, 1, 2$ ,  $s = RH - 100$  is the saturation, and value of  $A_{i,j,k}$  are given in the file of 'parameter2.txt' in the Appendix.

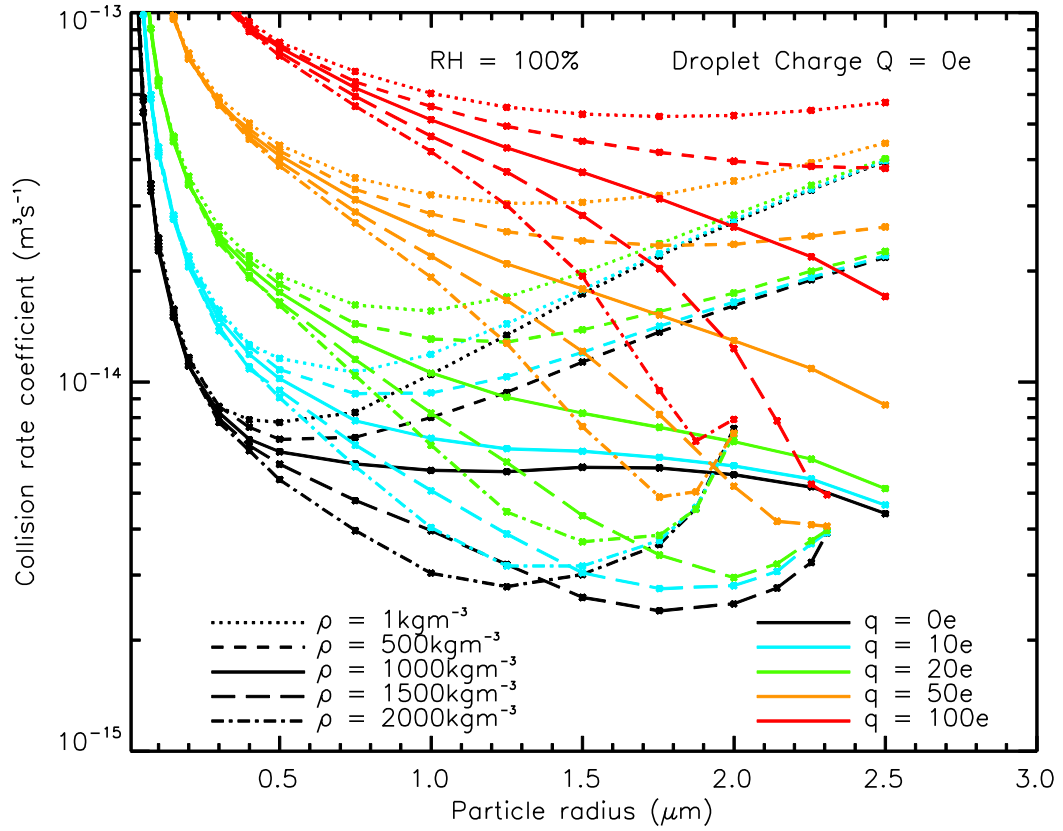


Figure 5.3. Simulated collision rate coefficients ( $R_{0,q,RH,\rho}$ ) with droplet charge  $Q = 0$ , particle charge  $q = 0e, 10e, 20e, 50e$ , relative humidity  $RH = 100\%$ , and particle density  $\rho = 1, 500, 1000, 1500, 2000 \text{ kg} \cdot \text{m}^{-3}$ .

Secondly, for particle density  $\rho > 1000 \text{ kg} \cdot \text{m}^{-3}$ , the collision rate coefficients  $R_{0,0,RH,\rho}$  are non-linear and fitted in the form of,

$$\log_{10} R_{0,0,RH,\rho} - \log_{10} R_{0,0,RH,500} = \sum_{i,j,k} B_{i,j,k} (\rho - 500)^i s^j a^k, \quad (5.3)$$

where  $i = 1, 2, 3, 4, 5$ ,  $j = 0, 1, 2, 3, 4$ ,  $k = 0, 1, 2, 3, 4$ , and values of  $B_{i,j,k}$  are given in the file of 'parameter2.txt' in the Appendix.

If the relative humidity  $RH < 95\%$ , and the saturation  $s$  has a large negative value, then the expressions in equation (5.2) and (5.3) that are given in the form of the polynomial of saturation  $s$  may diverge, so that they could not be used to estimate the collision rate coefficient for very low relative humidity. If relative humidity  $RH < 95\%$ , the value of  $R_{0,0,RH,\rho}$  could be better estimated by  $R_{0,0,RH,500} + (R_{0,0,100\%,\rho} - R_{0,0,100\%,500})$  according to equation (5.1), and it is obvious that if  $RH$  is very low and the weight effect is negligible then we have  $R_{0,0,RH,\rho} \approx R_{0,0,RH,500}$ .

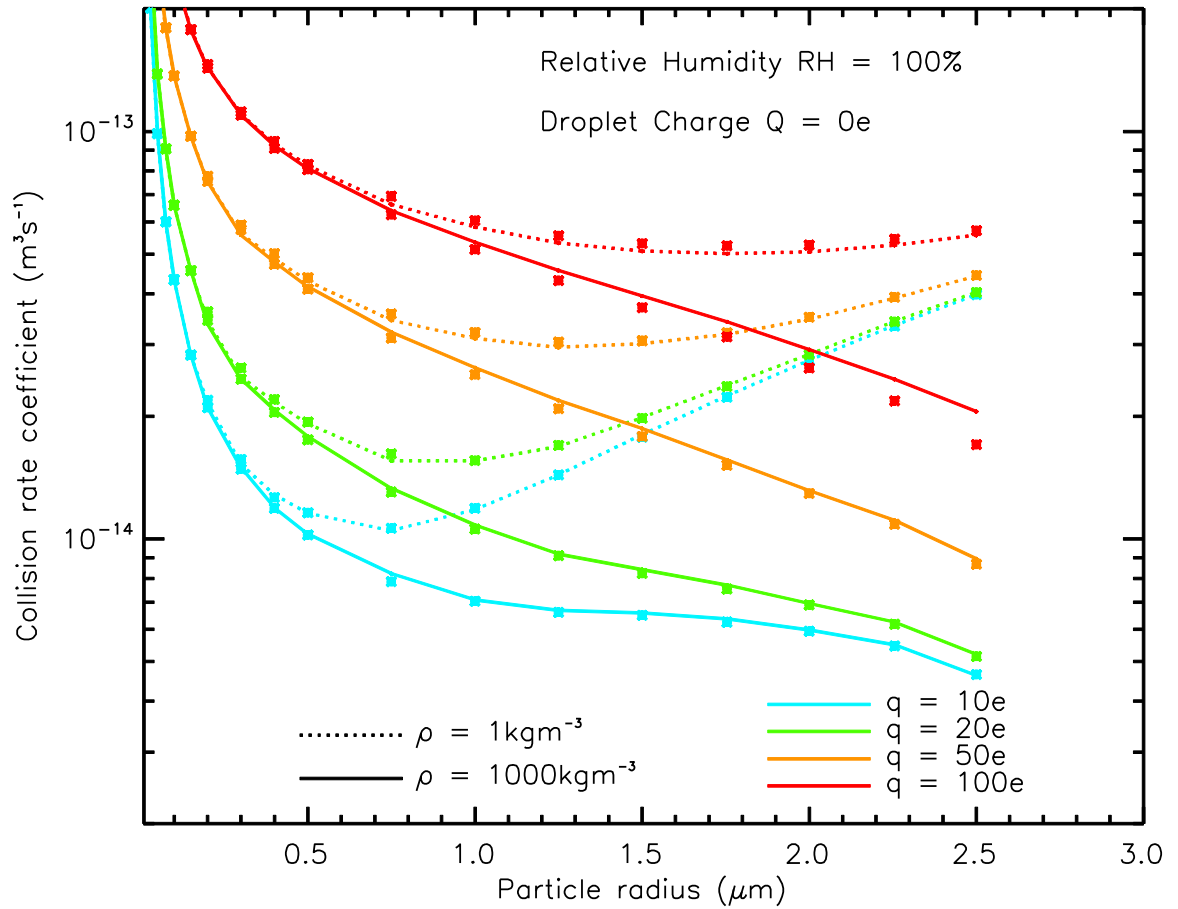


Figure 5.4. Points are simulated results of the collision rate coefficient  $R_{0,q,RH,\rho}$ ; Lines are the results of  $R_{0,0,RH,\rho} + R_{0,q,RH,500} - R_{0,q,RH,500}$ ; for  $RH = 100\%$ ,  $q = 10e, 20e, 50e, 100e$ , and  $\rho = 1, 1000 \text{ kg} \cdot \text{m}^{-3}$ .

### 5.2.2 Parameterization of collision rate coefficients $R_{0,q,RH,\rho}$ for charged particles.

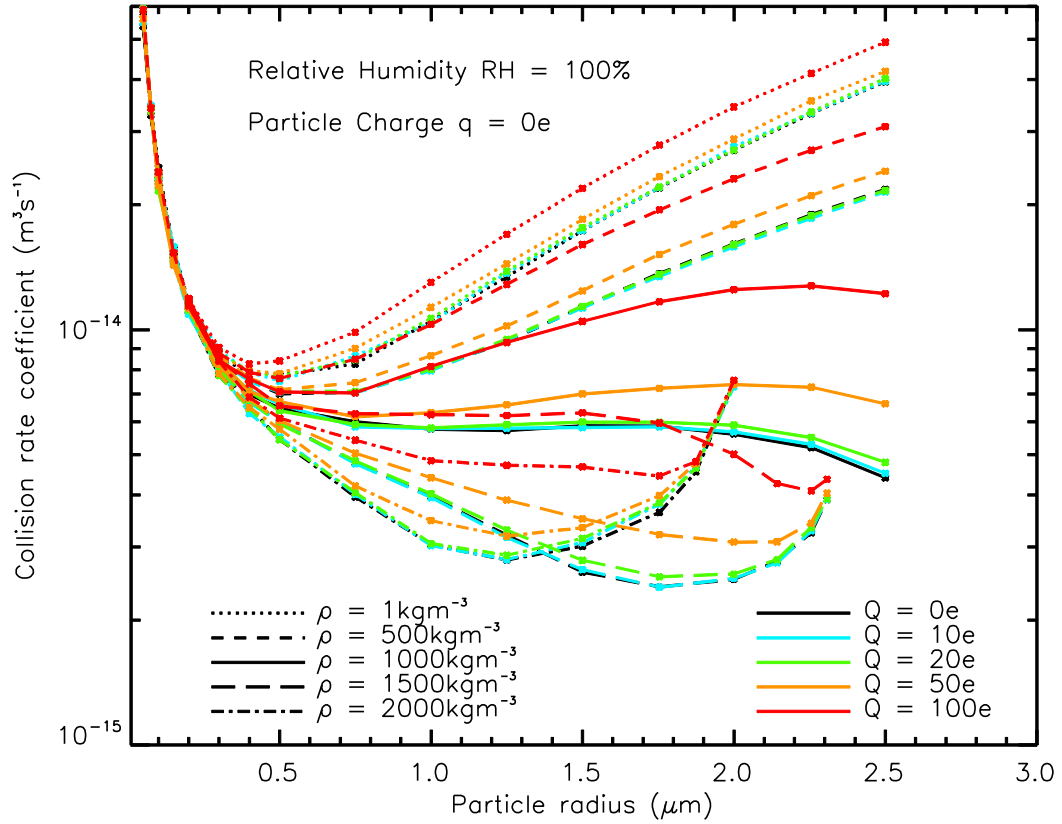


Figure 5.5. Simulated results of collision rate coefficient  $R_{Q,0,RH,\rho}$  for particle charge  $q = 0$ , droplet charge  $Q = 0e, 10e, 20e, 50e, 100e$ , relative humidity  $RH = 100\%$ , and  $\rho = 1, 500, 1000, 1500, 2000 \text{ kg} \cdot m^{-3}$ .

With particle charge  $q \neq 0$ , the image electric force induced by the particle tends to increase the collision rate coefficient, and the effect of the image force is more significant for small particles due to their high mobility. Figure 5.3 shows the collision rate coefficient  $R_{0,q,RH,\rho}$  for relative humidity  $RH = 100\%$ , droplet charge  $Q = 0e$ , particle charge  $q = 0, 10, 20, 50, 100e$ , and particle density  $\rho = 1, 500, 1000, 1500, 2000 \text{ kg} \cdot m^{-3}$ . It is clear that the effect of the image electric



force dominates for small particle, while the intercept effect and weight effect become significant for large particles.

For particle density  $\rho > 1000 \text{ kg} \cdot \text{m}^{-3}$ , the effect of the image electric force decreases quickly for large particles and vanishes at the particle radius where the fall speed relative to quiet air  $U_{a,\infty}$  of particle is equal to  $U_{A,\infty}$  of droplet. This is because the stagnation region discussed in section 3.4 prevents particles from moving close to the droplet, which means the short-range image electric force is limited and hence its effect on the collision rate coefficient for heavy particles is weak and tends to vanish. In fact, the effects of all the forces are weakened by the stagnation region when the fall speed relative to quiet air  $U_{a,\infty}$  of the particle approaches that of the droplet because it is difficult for the particle to approach the droplet, however, unlike image electric forces which do not become effective, the effects of long-range inverse-square forces remain, which will be shown in section 5.2.4 and 5.2.5.

For particle density  $\rho \leq 1000 \text{ kg} \cdot \text{m}^{-3}$ , the collision rate coefficient can be approximately estimate by,

$$R_{0,q,RH,\rho} \approx R_{0,q,RH,500} + R_{0,0,RH,\rho} - R_{0,0,RH,500}. \quad (5.4)$$

Figure 5.4 compares the two sides of equation (5.4) for relative humidity  $RH = 100\%$ , with the points being the simulated results of collision rate coefficient  $R_{0,q,RH,\rho}$  and the lines being the results of  $R_{0,0,RH,\rho} + R_{0,q,RH,500} - R_{0,0,RH,500}$ , and it is obvious that the two sides of equation (5.4) match well. For the case of particle charge  $q = 100e$  and droplet density  $\rho = 1000 \text{ kg} \cdot \text{m}^{-3}$ , the collision rate coefficients are over estimated by about 10% as shown in Figure 5.4, and this is because the effect of the image electric force and weight are both strong, and the collision rate coefficient could not be accurately estimated by the sum of the two effects. In addition, for the

cases of relative humidity  $RH \neq 100\%$  which are not shown, the equation (5.4) still holds well. In the right side of equation (5.4) the term  $R_{0,0,RH,\rho} - R_{0,0,RH,500}$  changes roughly linearly with particle density for  $\rho \leq 1000 \text{ kg} \cdot \text{m}^{-3}$  as shown in Figure 5.3, therefore the collision rate coefficients  $R_{0,q,RH,\rho}$  are also approximately linear with particle density for  $\rho \leq 1000 \text{ kg} \cdot \text{m}^{-3}$ .

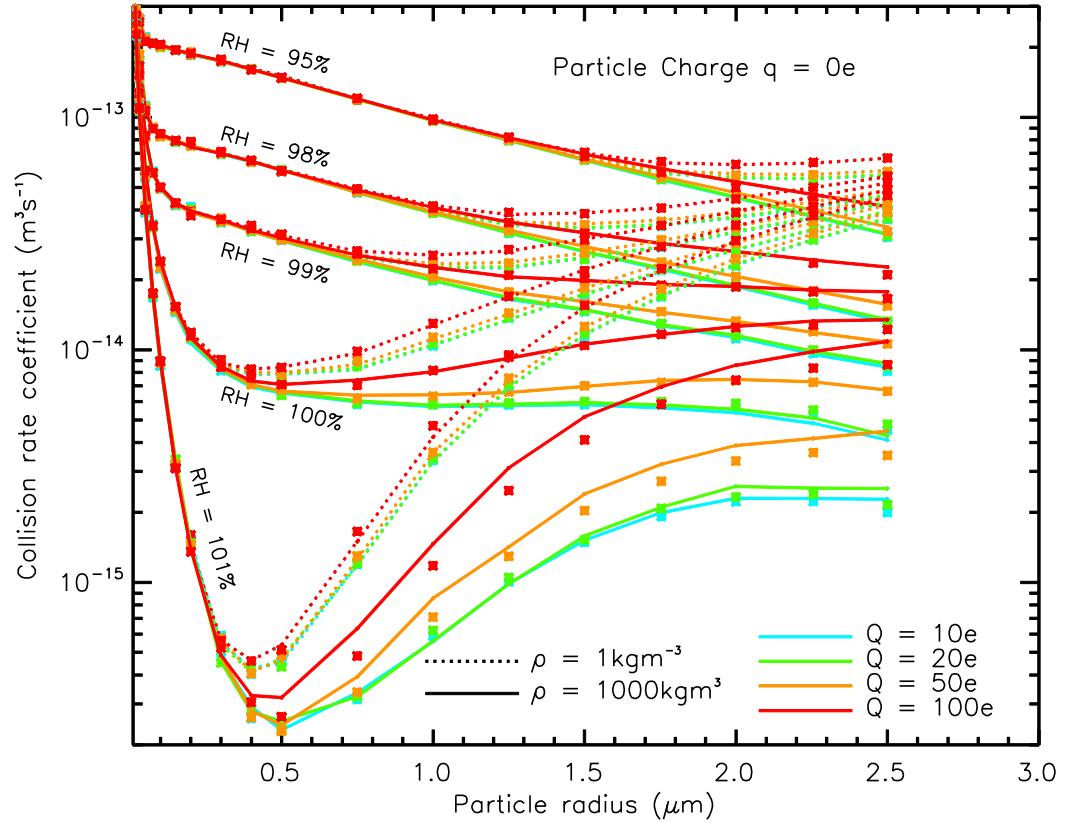


Figure 5.6. Points are the simulated results of collision rate coefficient  $R_{Q,0,RH,\rho}$ ; Lines are the results of  $R_{0,0,RH,\rho} + R_{Q,0,RH,500} - R_{0,0,RH,500}$ , for  $RH = 95\%, 98\%, 99\%, 100\%, 101\%$ ,  $Q = 10e, 20e, 50e, 100e$ , and  $\rho = 1, 1000 \text{ kg} \cdot \text{m}^{-3}$ .

For particle density  $\rho \leq 1000 \text{ kg} \cdot \text{m}^{-3}$ , we fit  $R_{0,q,RH,\rho}$  in the form of

$$R_{0,q,RH,\rho} - R_{0,q,RH,500} - R_{0,0,RH,\rho} + R_{0,0,RH,500} = \sum_{i,j,k} C_{i,j,k,r} (\rho - 500)^i q^j s^k a^r, \quad (5.5)$$

where  $i = 1, 2; j = 1, 2; k = 0, 1, 2, 3; r = 0, 1, 2, 3$  and  $C_{i,j,k,r}$  are given in the file of ‘parameter2.txt’ in the Appendix. As the left side in equation (5.5) is equal to zero if  $\rho = 500$  or  $q = 0$ , the value of ‘ $i$ ’ and ‘ $j$ ’ start from 1 rather than from 0. When the relative humidity  $RH < 95\%$  or the particle charge  $q > 100e$ , we can apply equation (5.4) to estimate the collision rate coefficient.

For particle density  $\rho > 1000 \text{ kg} \cdot \text{m}^{-3}$ , we fit  $R_{0,q,RH,\rho}$  in the form of

$$\begin{aligned} & \log_{10} R_{0,q,RH,\rho} - \log_{10} R_{0,q,RH,500} - \log_{10} R_{0,0,RH,\rho} + \log_{10} R_{0,0,RH,500} \\ &= \sum_{i,j,k,r} D_{i,j,k,r} (\rho - 500)^i q^j s^k a^r, \end{aligned} \quad (5.6)$$

where  $i = 1, 2, 3; j = 1, 2, 3; k = 0, 1, 2, 3, 4; r = 0, 1, 2, 3, 4$  and  $D_{i,j,k,r}$  are given in the file of ‘parameter2.txt’ in the Appendix. When the relative humidity  $RH < 95\%$ , the attractive phoretic forces are strong and the collision rate coefficient can be estimated as  $R_{0,q,RH,\rho} \approx R_{0,q,RH,1000}$ , for which the value of  $R_{0,q,RH,1000}$  can be calculated by equation (5.4).

### 5.2.3 Parameterization of collision rate coefficients $R_{Q,0,RH,\rho}$ for charged droplets.

When the droplet charge  $Q \neq 0$  and the particle charge  $q = 0$ , the droplet charge can induce the image electric force on large particles. Figure 5.5 shows the collision rate coefficient  $R_{Q,0,RH,\rho}$  for relative humidity  $RH = 100\%$ , particle charge  $Q = 0, 10, 20, 50, 100e$ , and particle density  $\rho = 1, 500, 1000, 1500, 2000 \text{ kg} \cdot \text{m}^{-3}$ , in which the effect of the image electric force is negligible for small particles and significant for large droplet charge.

For particle density  $\rho \leq 1000 \text{ kg} \cdot \text{m}^{-3}$ , the collision rate coefficient can be approximately estimated by

$$R_{Q,0,RH,\rho} \approx R_{0,0,RH,\rho} + R_{Q,0,RH,500} - R_{0,0,RH,500} \quad (5.7)$$

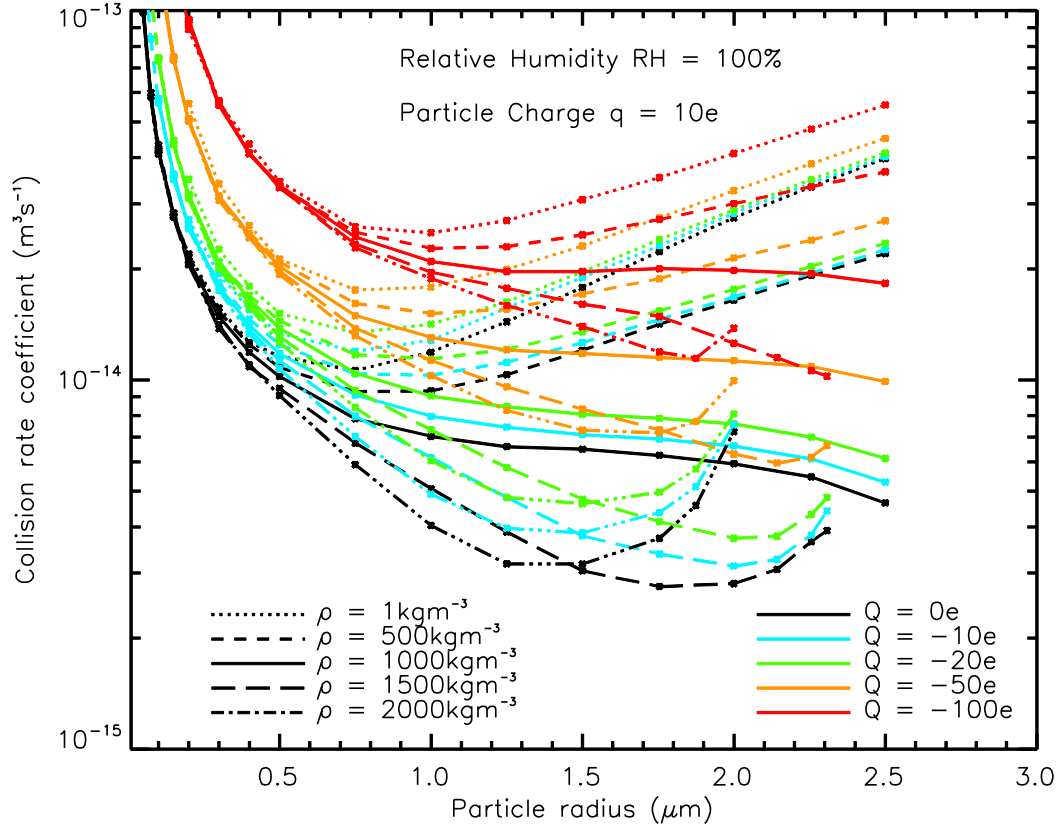


Figure 5.7. Simulated results of collision rate coefficient  $R_{Q,q,RH,\rho}$  for particle charge  $q = 10e$ , droplet charge  $Q = 0e, -10e, -20e, -50e, -100e$ , relative humidity  $RH = 100\%$  and particle density  $\rho = 1, 500, 1000, 1500, 2000 \text{ kg} \cdot \text{m}^{-3}$ .

Figure 5.6 compares the two sides of equation (5.7), with the points being the simulated results of  $R_{Q,0,RH,\rho}$  and the lines being the results of  $R_{0,0,RH,\rho} + R_{Q,0,RH,500} - R_{0,0,RH,500}$ , and it is apparent that equation (5.7) is a good approximation for the collision rate coefficients. However, for relative humidity  $RH = 101\%$  the approximation overestimates the collision rate coefficient a little for droplet charge  $Q = 50e, 100e$  and particle density  $\rho = 1000 \text{ kg} \cdot \text{m}^{-3}$ , as the total effect of

attractive image force, repulsive phoretic forces and gravitational force can not be accurately estimated by the sum of each effect.

For particle density  $\rho > 1000 \text{ kg} \cdot \text{m}^{-3}$ , the effect of image electric force induced by the droplet becomes smaller for large particles. In Figure 5.5 the collision rate coefficients  $R_{Q,0,RH,\rho}$  for different droplet charges converge for particle density  $\rho = 1500, 2000 \text{ kg} \cdot \text{m}^{-3}$ , just like the collision rate coefficient  $R_{0,q,RH,\rho}$  in Figure 5.3. The reason is also that the stagnation region diminishes the effect of the short-range image electric forces so that their effect on the collision rate coefficient is negligible when the fall speed of the particle in quiet air approaches that of the droplet.

For particle density  $\rho \leq 1000 \text{ kg} \cdot \text{m}^{-3}$ , we fit  $R_{Q,0,RH,\rho}$  in the form of

$$R_{Q,0,RH,\rho} - R_{Q,0,RH,500} - R_{0,0,RH,\rho} + R_{0,0,RH,500} = \sum_{i,j,k,r} E_{i,j,k,r} (\rho - 500)^i Q^j s^k a^r, \quad (5.8)$$

where  $i = 1, 2; j = 1, 2; k = 0, 1, 2, 3; r = 0, 1, 2, 3$  and  $E_{i,j,k,r}$  are given in the file of ‘parameter2.txt’ in the Appendix. As the left side in equation (5.8) is equal to zero if  $\rho = 500$  or  $q = 0$ , the value of ‘ $i$ ’ and ‘ $j$ ’ in the right side start from 1 rather than 0. When the relative humidity  $RH < 95\%$  or particle charge  $q > 50e$  the polynomial  $q^j s^k$  in equation (5.8) may diverge, and then equation (5.7) is a good alternative to estimate the collision rate coefficient.

For particle density  $\rho > 1000 \text{ kg} \cdot \text{m}^{-3}$ , we fit  $R_{Q,0,RH,\rho}$  in the form of

$$\begin{aligned} & \log_{10} R_{Q,0,RH,\rho} - \log_{10} R_{Q,0,RH,500} - \log_{10} R_{0,0,RH,\rho} + \log_{10} R_{0,0,RH,500} \\ &= \sum_{i,j,k,r} F_{i,j,k,r} (\rho - 500)^i Q^j s^k a^r, \end{aligned} \quad (5.9)$$

where  $i = 0, 1; j = 0, 1; k = 0, 1; r = 0, 1, 2, 3$  and  $F_{i,j,k,r}$  are given in the file of ‘parameter2.txt’ in the Appendix. When the relative humidity  $RH < 95\%$ , the attractive phoretic forces are strong

and the collision rate coefficient can be estimated as  $R_{Q,0,RH,\rho} \approx R_{Q,0,RH,1000}$ , for which the value of  $R_{Q,0,RH,1000}$  can be calculated by equation (5.7).

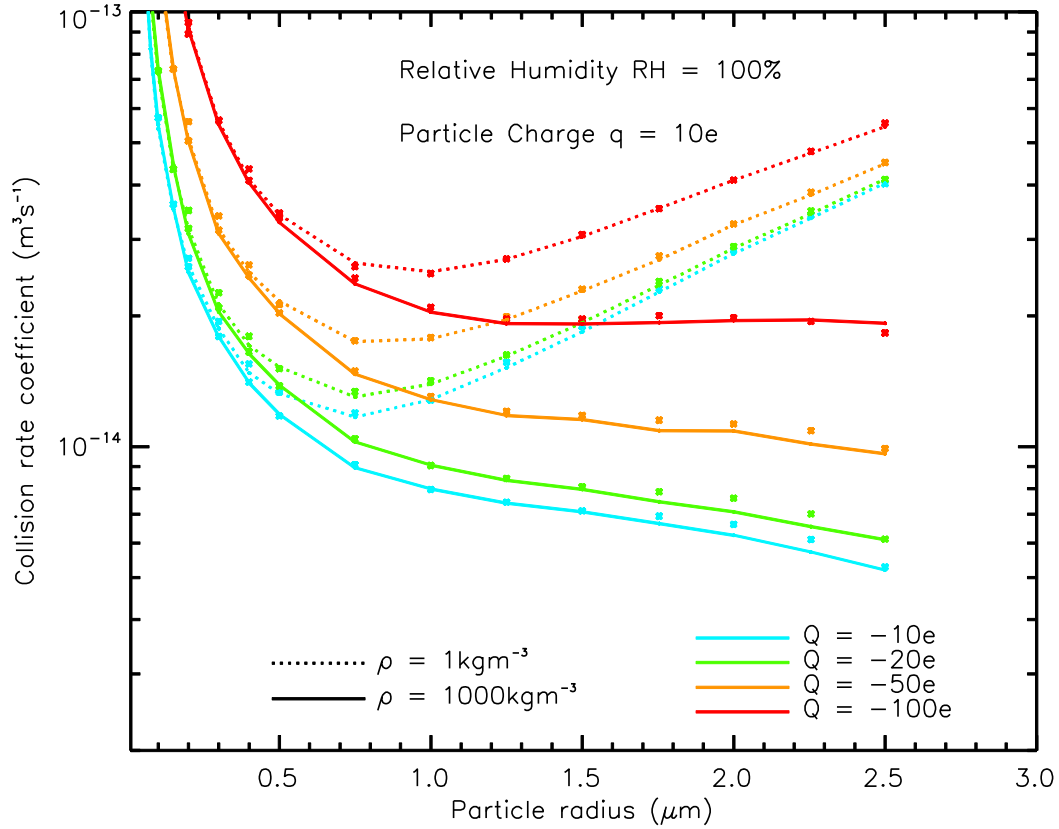


Figure 5.8. Points are the simulated result of collision rate coefficient  $R_{Q,q,RH,\rho}$ ; Lines are the results of  $R_{0,q,RH,\rho} + R_{Q,q,RH,500} - R_{0,q,RH,500}$ ; for particle charge  $q = 10e$ , relative humidity  $RH = 100\%$ , droplet charge  $Q = -10e, -20e, -50e, -100e$ , particle density  $\rho = 1, 1000 \text{ kg} \cdot \text{m}^{-3}$ .

#### 5.2.4 Parameterization of collision rate coefficients $R_{Q,q,RH}$ for opposite-sign droplet charge and particle charge.

Figure 5.7 shows the collision rate coefficients for  $RH = 100\%$ , particle charge  $q = 10e$ , droplet charge  $Q = 0, -10, -20, -50, -100e$ , and particle density  $\rho = 1, 500, 1000, 1500, 2000 \text{ kg} \cdot \text{m}^{-3}$ . Unlike Figure 5.3 and Figure 5.5, in which the collision rate coefficients of  $\rho > 1000 \text{ kg} \cdot \text{m}^{-3}$ .

$\text{m}^{-3}$  for different charges tend to converge at the particle radius where the fall speed of particles in quiet air equals that of the droplet, the collision rate coefficients in Figure 5.7 do not converge at large particle radius. This is because the effect of the Coulomb force is not strongly influenced by the presence of the stagnation region near the droplet as the Coulomb force acts at long range.

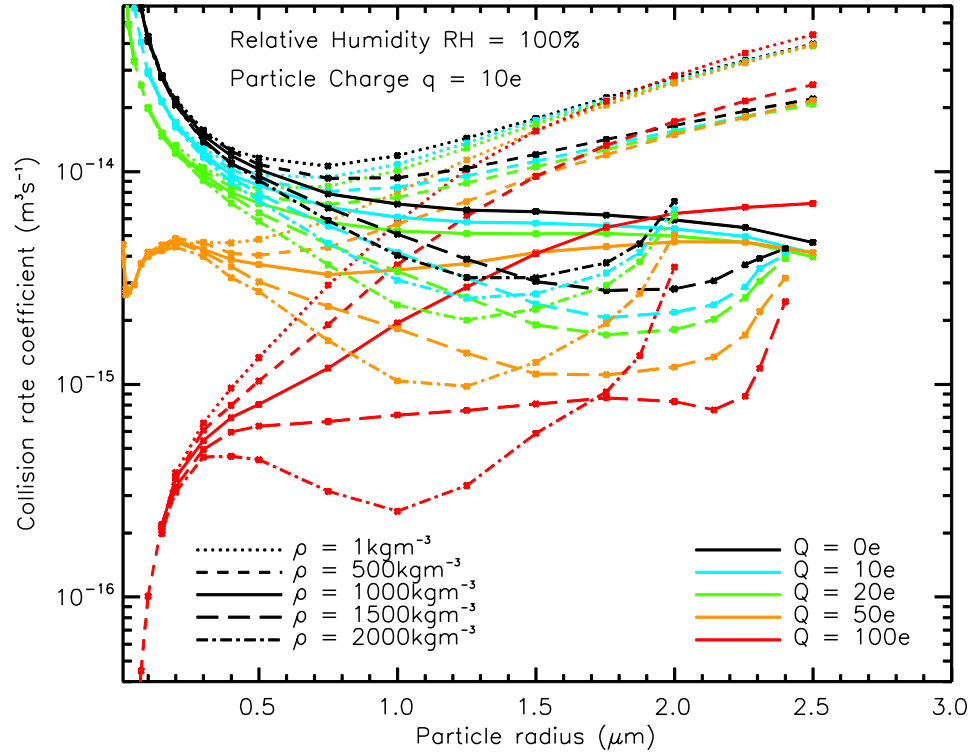


Figure 5.9. Simulated results of collision rate coefficient  $R_{Q,q,RH,\rho}$  for particle charge  $q = 10e$ , droplet charge  $Q = 0, 10e, 20e, 50e, 100e$ , relative humidity  $RH = 100\%$ , and particle density  $\rho = 1, 500, 1000, 1500, 2000 \text{ kg} \cdot \text{m}^{-3}$ .

For particle density  $\rho \leq 1000 \text{ kg} \cdot \text{m}^{-3}$ , the effects of Coulomb forces for opposite-sign droplet and particle charges are approximately independent with the weight effect, and a good estimation of collision rate coefficient is given as,

$$R_{Q,q,RH,\rho} \approx R_{0,q,RH,\rho} + R_{Q,q,RH,500} - R_{0,q,RH,500} \quad (5.10)$$

Figure 5.8 compares the two sides of equation (5.10) for relative humidity  $RH = 100\%$ ,  $q = 10e$ , and particle density  $\rho = 1, 1000 \text{ kg} \cdot \text{m}^{-3}$ , with the points representing the simulated results of collision rate coefficient and the lines representing the result of  $R_{0,q,RH,\rho} + R_{Q,q,RH,500} - R_{0,q,RH,500}$ , and it is evident that equation (5.10) holds well. In fact, for relative humidity  $RH = 95\%, 98\%, 99\%, 101\%$  and particle charge  $q = 20e, 50e$ , (not shown) equation (5.10) is also quite valid. For particle density  $\rho > 1000 \text{ kg} \cdot \text{m}^{-3}$ , equation (5.10) is still applicable for small particles but can only poorly estimate the collision rate coefficient for large particles.

For particle density  $\rho \leq 1000 \text{ kg} \cdot \text{m}^{-3}$ , according to equation (5.10) we fit the collision rate coefficient as,

$$\begin{aligned} & \left( R_{Q,q,RH,\rho} - R_{Q,0,RH,\rho} - R_{0,q,RH,\rho} + R_{0,0,RH,\rho} \right) - \left( R_{Q,q,RH,500} - R_{Q,0,RH,500} - R_{0,q,RH,500} + R_{0,0,RH,500} \right) \\ &= \sum_{i,j,k,r} G_{i,j,k,r} (\rho - 500)^i Q^j q^k s^r a^t, \end{aligned} \quad (5.11)$$

where  $i = 1, 2; j = 1, 2; k = 1, 2; r = 0, 1, 2, 3; t = 0, 1, 2, 3$  and  $G_{i,j,k,r,t}$  are given in the file of ‘parameter2.txt’ in the Appendix. When  $Q = 0$  or  $q = 0$  or  $\rho = 500$ , the left side is equal to zero, so that  $i, j, k$  start from 1 rather than 0.

For particle density  $\rho > 1000 \text{ kg} \cdot \text{m}^{-3}$ , the collision rate coefficients are quite different from that of particle density  $\rho = 500 \text{ kg} \cdot \text{m}^{-3}$ , so that we fit the collision rate coefficient in the following way,

$$\begin{aligned} & \log_{10} \left( R_{Q,q,RH,\rho} - R_{0,q,RH,\rho} \right) - \log_{10} \left( R_{Q,q,RH,500} - R_{0,q,RH,500} \right) \\ &= \sum_{i,j,k,r,t} H_{i,j,k,r,t} (\rho - 500)^i Q^j q^k s^r a^t, \end{aligned} \quad (5.12)$$

where  $i = 1, 2, 3; j = 0, 1, 2; k = 0, 1, 2; r = 0, 1, 2, 3; t = 0, 1, 2, 3, 4$  and  $H_{i,j,k,r,t}$  are given in the file of ‘parameter2.txt’ in the Appendix.



### 5.2.5 Parameterization of collision rate coefficients $R_{Q,q,RH,\rho}$ for same-sign droplet charge and particle charge.

Figure 5.9 shows the collision rate coefficient  $R_{Q,q,RH,\rho}$  for  $RH = 100\%$ , particle charge  $q = 10e$ , particle charge  $Q = 0, 10, 20, 50, 100e$ , and particle density  $\rho = 1, 500, 1000, 1500, 2000 \text{ kg} \cdot \text{m}^{-3}$ . The collision rate coefficients for large particle radii are strongly affected by particle density, and for particle charge  $q = 20e$  and  $50e$  the effects of particle density are relatively greater. For relative humidity  $RH \leq 95\%$ , the weight effect is small or even negligible for opposite-sign charged droplet and particle in accordance of equation (5.10), however, when droplet and particle charges are same-sign, the weight effect is still considerable even for relative humidity  $RH \leq 95\%$ .

In Figure 5.9 for particle density  $\rho \leq 1000 \text{ kg} \cdot \text{m}^{-3}$ , in most cases the collision rate coefficient  $R_{Q,q,RH,\rho}$  for large droplet charges is smaller than that for small droplet charges, but in some cases it can be greater than that for small droplet charges, for example  $R_{100,10,100\%,1000} > R_{10,10,100\%,1000}$  when particle radius  $a \geq 2.0 \text{ } \mu\text{m}$ , which is because the image electric force induced by droplet charges becomes considerable on large particles. This phenomenon disappears for particle density  $\rho > 1000 \text{ kg} \cdot \text{m}^{-3}$ , because the long-range Coulomb force dominates over the short-range image electric force, as particles are less able to enter the stagnation region near the droplet and the image forces are not effective.

When the droplet and particle charges are same-sign, the range of the collision rate coefficients is very wide, so that they are fitted in the logarithmic scale in the following way,

$$\begin{aligned} & \log_{10} R_{Q,q,RH,\rho} - \log_{10} R_{0,q,RH,\rho} - \log_{10} R_{Q,q,RH,500} + \log_{10} R_{0,q,RH,500} \\ &= \sum_{i,j,k,r,t} U_{i,j,k,r,t} (\rho - 500)^i Q^j q^k s^r a^t, \end{aligned} \quad (5.13)$$

where  $i = 1, 2, 3, 4; j = 1, 2; k = 0, 1, 2; r = 0, 1, 2, 3, 4; t = 0, 1, 2, 3, 4, 5$  and  $U_{i,j,k,r,t}$  are given in the file of ‘parameter2.txt’ in the Appendix.

### 5.3 Discussion and Conclusion.

Simulations and parameterization of collision rate coefficient for 3  $\mu\text{m}$ -droplets have been extended to a wide range of particle densities. For small particle with radius less than 0.2  $\mu\text{m}$ , the gravitational force is much smaller than the other forces, so that the weight effect can be neglected for small particles, while it becomes significant for larger particles. In this Chapter, we only calculate and parameterize the collision rate coefficient for particle radius  $a \geq 0.2 \mu\text{m}$  to investigate the weight effect.

For particle density  $\rho \leq 1000 \text{ kg} \cdot \text{m}^{-3}$ , the weight of particles tends to pull particles away from the droplet and thus reduce the value of the collision rate coefficient. The collision rate coefficients vary approximately linearly with particle density in the absence of phoretic forces and electric forces for particle density  $\rho \leq 1000 \text{ kg} \cdot \text{m}^{-3}$ . Besides, the weight effect is roughly independent with the effects of other forces, except for strong repulsive forces, and the collision rate coefficients can be obtained simply by the sum of each effect. If the relative humidity is very low, the effect of phoretic forces can predominate over the weight effect, then the weight effect can be neglected.

For particle density  $\rho > 1000 \text{ kg} \cdot \text{m}^{-3}$ , the particle’s weight in the stagnation region results in complex effects. First, the stagnation region prevents the collision occurring at the front side of

droplet, while it makes collisions at the back side of droplet possible. When the fall speed of the particle in quiet air approaches that of the droplet, more time is needed for particles released below the droplet to pass over it and thus the diffusion can transport more particles to the upside of stagnation region through which particles can easily collide with the back side of droplet, therefore in this condition the weight effect tends to increase rather than decrease the collision rate coefficient. Secondly, the stagnation region prevents the short-range image electric forces acting while it has little influence on long-range Coulomb forces. Thus when the fall speed of particle relative to undisturbed air approaches that of the droplet, the effect of short-range image electric forces are negligible. For particle with density  $\rho \leq 1000 \text{ kg} \cdot \text{m}^{-3}$ , the image electric forces can be more significant than Coulomb force and enhance the process of scavenging even if droplet and particles are same-sign charged, which we call ‘electro-scavenging’. However, for large particles with density  $\rho > 1000 \text{ kg} \cdot \text{m}^{-3}$  and same-sign charged as droplet, the effects of image electric forces are reduced and the corresponding electro-scavenging disappears, then the repulsive Coulomb force is predominant, which can be called ‘electro-anti-scavenging’.

In brief, the collision rate coefficients are quite complex including the weight effect, in conjunction with diffusion, electric forces, phoretic forces, intercept effect and flow around the particle. We have parameterized the simulated results of collision rate coefficients to make it easy for them to be applied in cloud models. Also, we also provide several approximate empirical equations which could be applied as alternatives if the inputs exceed the ranges of parameters in our simulation and the parameterizations are inaccurate. Up until the present we have obtained the value of collision rate coefficient  $R_{Q,q,A,a,RH,\rho}$  for  $A = 3 \text{ } \mu\text{m}$  and for sets of droplet charge  $Q$ , particle charge  $q$ , particle radius  $a$ , relative humidity  $RH$  and particle density  $\rho$  that are realistic

for clouds. It is planned to calculate and parameterize a range of densities for greater droplet radii in future work, and then the collision rate coefficients  $R_{Q,q,A,a,RH,\rho}$  could be obtained for all inputs and applied in cloud models.

## CHAPTER 6

### CONCLUSION AND IDEA FOR FUTURE WORK

#### 6.1 Conclusion

For 3.0  $\mu\text{m}$  radii droplets we have extensively calculated and parameterized the collision rate coefficient  $R_{Q,q,A,a,RH,\rho}$  for droplet charge  $Q$  of 0e,  $\pm 10\text{e}$ ,  $\pm 20\text{e}$ ,  $\pm 50\text{e}$ ,  $\pm 100\text{e}$ , for particle charge  $q$  of 0e, 10e, 20e, 50e, for relative humidity of 95%, 98%, 99%, 100%, 101%, for particle radius  $a$  ranging between 0.01  $\mu\text{m}$  to 2.5  $\mu\text{m}$ , and for particle density of 1, 500, 1000, 1500 and 2000  $\text{kg} \cdot \text{m}^{-3}$ . The image electric force induced by particles can enhance the collision rate coefficients of small particles by several times as shown in Figure 4.2; the image force induced by the droplet can increase the collision rate coefficient of large particles as shown in Figure 4.4; the Coulomb force can increase or decrease the collision rate coefficient by up to several orders of magnitude compared to uncharged rates as shown in Figure 4.6 and Figure 4.9. In short, the charging of aerosol particles and droplets in electrified cloud boundary region can significantly influence the scavenging process, and provides a possible mechanism to magnify the small inputs of the solar wind. This would account for the observed changes in weather and climate correlated with the changes in the current density flowing through clouds, as discussed in Chapter 1. We can use our results of parameterization to obtain the collision rate coefficient when the parameters lie in the ranges given above, and in the Appendix we have provided the parameters and code written in IDL to calculate the collision rate coefficient. When some parameters exceed these ranges we can also get the collision rate coefficient by the approximately empirical formulas we provided.

## 6.2 Idea for future work

We have calculated and parameterized the collision rate coefficient  $R_{Q,q,A,a,RH,\rho}$  for a fixed droplet radius of  $3.0 \mu\text{m}$ , so that the future work is to complete the simulations to include phoretic and density variations for droplet radii of 6, 9, 12, 15  $\mu\text{m}$ .

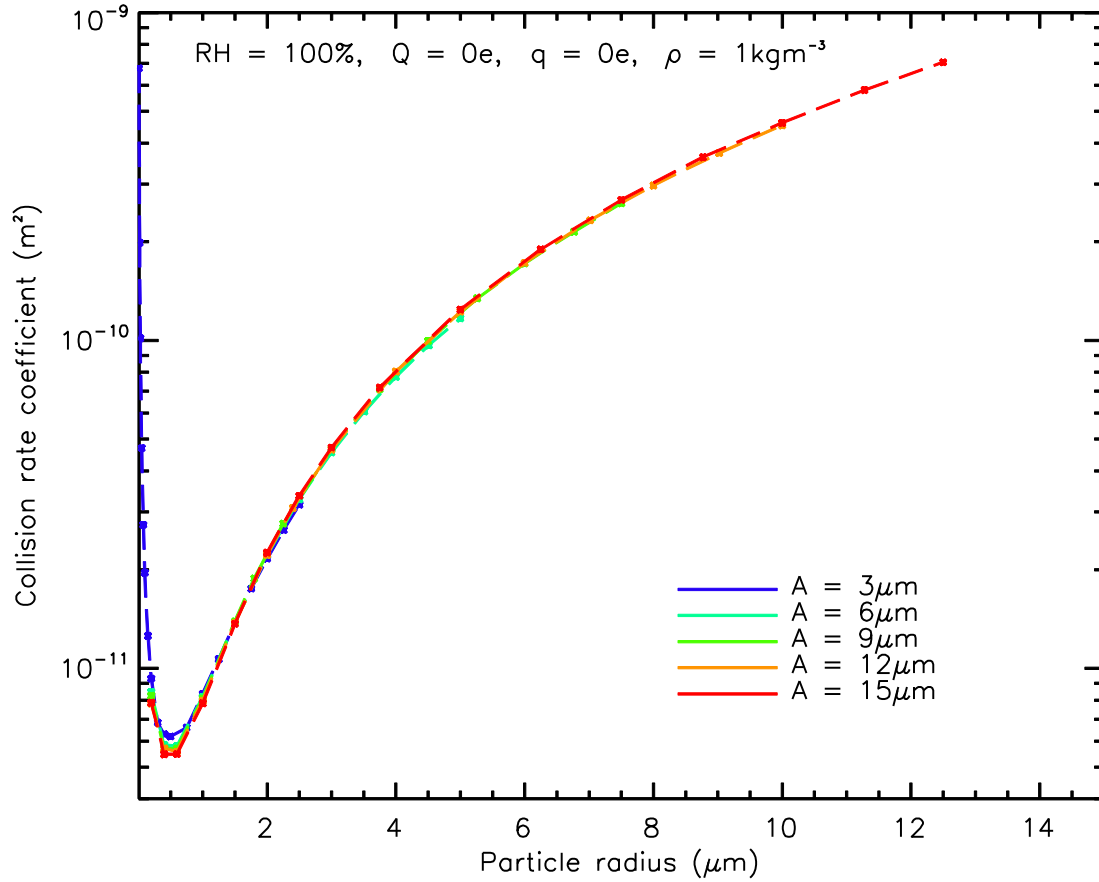


Figure 6.1. The results of collision rate coefficient divided by the fall speed of the droplet, with droplet radius of 3, 6, 9, 12, 15  $\mu\text{m}$ , particle density of  $1 \text{ kg} \cdot \text{m}^{-3}$ , droplet charge of  $0e$ , particle charge of  $0e$ , relative humidity of 100%.

Similarly to the results for the  $3 \mu\text{m}$  droplets, for the collision rate coefficient of larger droplets with small particles of radius less than  $0.2 \mu\text{m}$ , the intercept effect, weight effect, ‘fap’ effect and the image electric force induced by droplet charge all can be neglected, the analytic

solution in flux model can be applied if the image electric force induced by particle charges can be neglected. In consideration of the image electric force induced by particle charges, we have shown in equation (4.16) that if the Coulomb forces are attractive then the contribution of image force can be linearly added. That is,

$$R_{Q,q,A,a,RH,\rho} \approx N_{Q,q,A,a,RH} + (R_{0,q,A,a,RH} - N_{0,0,A,a,RH}), \quad (6.1)$$

where  $N_{Q,q,A,a,RH}$  is the easily obtained analytic solution which considers the purely inverse square Coulomb force and phoretic forces. The right side of equation (6.1) does not include particle density as the weight effect can be neglected for small particles. So that for small particles with opposite-charged droplet and particles, we only need to calculate the value of  $R_{0,q,A,a,RH}$  and then get the collision rate coefficient by equation (6.1), which will greatly reduce the workload for computing time. If the droplet and particles are same-sign charged, similar as equation (4.21), we can also fit a similar approximate empirical formula to illustrate the effect of image electric forces by assuming that the short-range image force plays a role by increase the radius of the contact sphere.

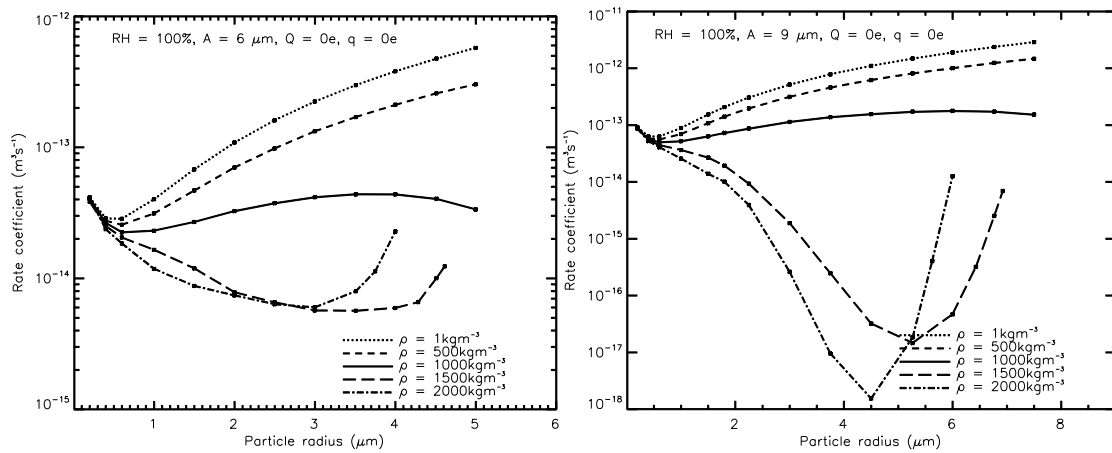


Figure 6.2. Collision rate coefficient for droplet radius of 6  $\mu\text{m}$  (left) and 9  $\mu\text{m}$  (right), with particle density of 1, 500, 1000, 1500, 2000  $\text{kg} \cdot \text{m}^{-3}$  respectively.

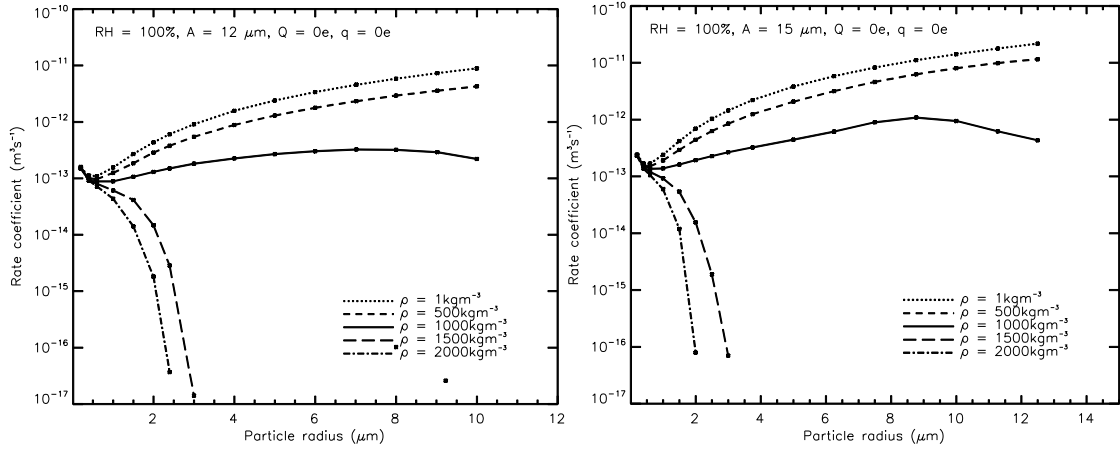


Figure 6.3. Collision rate coefficient for droplet radius of 12  $\mu\text{m}$  (left) and 15  $\mu\text{m}$  (right), with particle density of 1, 500, 1000, 1500, 2000  $\text{kg} \cdot \text{m}^{-3}$  respectively.

For the collision rate coefficient of larger droplets with large particles of radius greater than 0.2  $\mu\text{m}$ , the intercept effect, weight effect, ‘fap’ effect and the image electric force induced by droplet charge should not be neglected. Our preliminary results show that for  $\rho = 1 \text{ kg} \cdot \text{m}^{-3}$  in which only the intercept effect is important the collision rate coefficient is roughly proportional to the square of droplet radius. As shown in Figure 6.1, the results of collision rate coefficient divided by the fall speed of the droplet for particle density of  $1 \text{ kg} \cdot \text{m}^{-3}$  is very similar for different sizes of droplet, especially for particle radius greater than 1  $\mu\text{m}$ . The results only include the intercept effect and the results for different droplet radii coincide with each other very well, and for particle radius less than 1  $\mu\text{m}$  the results also include the effect of diffusion. Thus there is little difference in the results for different droplet sizes. Then for particles density less than  $1000 \text{ kg} \cdot \text{m}^{-3}$ , the collision rate coefficient is roughly linearly dependent on particle density, as shown in Figure 5.2, so that we could also easily fit the collision rate coefficient for particle density less than  $1000 \text{ kg} \cdot \text{m}^{-3}$ .



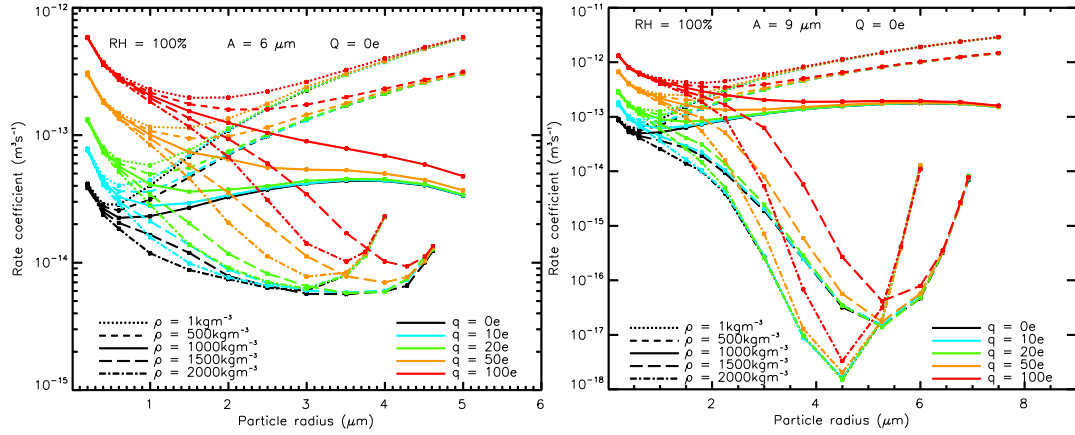


Figure 6.4. Collision rate coefficient for droplet radius of 6  $\mu\text{m}$  (left) and 9  $\mu\text{m}$  (right), with relative humidity  $RH = 100\%$ , particle density of 1, 500, 1000, 1500, 2000  $\text{kg} \cdot \text{m}^{-3}$  respectively, droplet charge  $Q = 0e$ , particle charges  $q = 0e, 10e, 20e, 50e, 100e$  respectively.

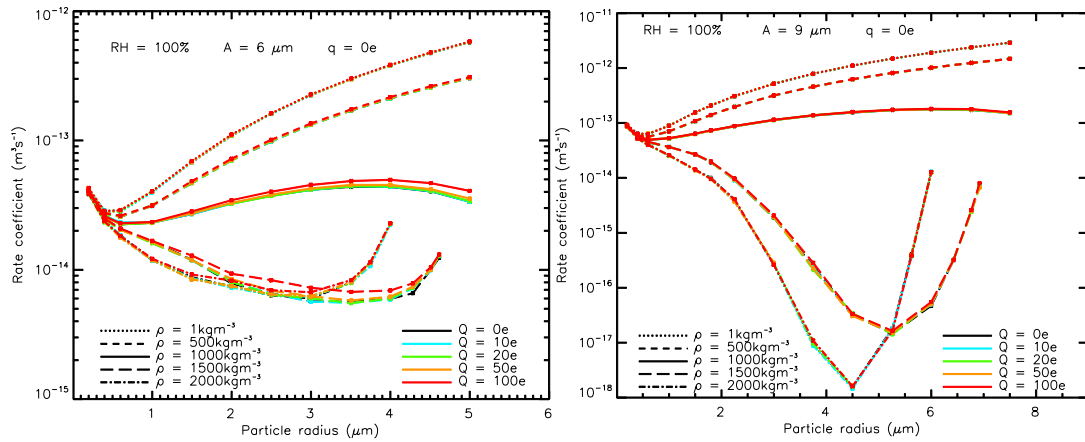


Figure 6.5. Collision rate coefficient for droplet radius of 6  $\mu\text{m}$  (left) and 9  $\mu\text{m}$  (right), with relative humidity  $RH = 100\%$ , particle density of 1, 500, 1000, 1500, 2000  $\text{kg} \cdot \text{m}^{-3}$  respectively, droplet charge  $Q = 0e, 10e, 20e, 50e, 100e$  respectively, particle charges  $q = 0e$ .

For particle density greater than that of the droplet the results become more complex. Figure 6.2 shows the collision rate coefficient of 6  $\mu\text{m}$  and 9  $\mu\text{m}$  droplets in which we can still see the similar character of back-side collisions as previously shown in Figure 5.3; while Figure 6.3 shows the collision rate coefficient of 12  $\mu\text{m}$  and 15  $\mu\text{m}$  droplets in which the back-side

collision is weak, because the mobility of large particles is small and because the fall speed of the droplet increases by the square of droplet radius thus the time for particles to over pass the droplet is shorter, therefore particles can't move close to the low flow region at the back side of the droplet by diffusion.

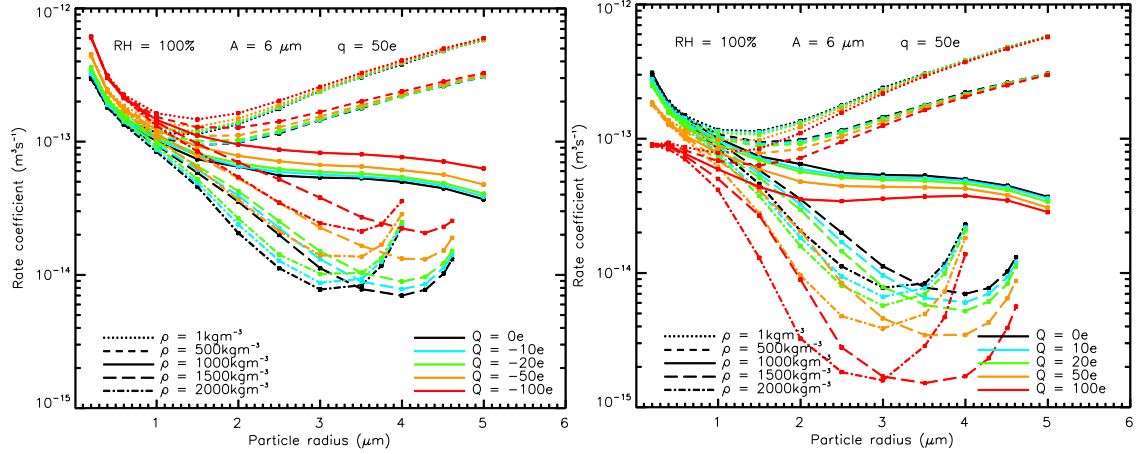


Figure 6.6. Collision rate coefficient for 6  $\mu\text{m}$  droplet radius of opposite-sign charges (left) and same-sign charges (right), with relative humidity  $RH = 100\%$ , particle density of 1, 500, 1000, 1500, 2000  $\text{kg} \cdot \text{m}^{-3}$  respectively, particle charges  $q = 50e$  and droplet charge  $Q = 0e, \pm 10e, \pm 20e, \pm 50e, \pm 100e$  respectively.

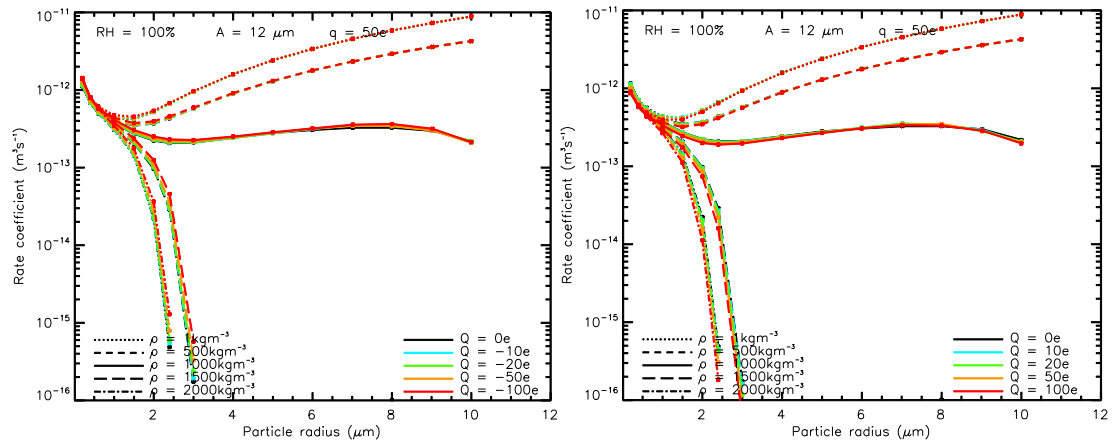


Figure 6.7. Collision rate coefficient for 12  $\mu\text{m}$  droplet radius of opposite-sign charges (left) and same-sign charges (right), with relative humidity  $RH = 100\%$ , particle density of 1, 500, 1000, 1500, 2000  $\text{kg} \cdot \text{m}^{-3}$  respectively, particle charges  $q = 50e$  and droplet charge  $Q = 0e, \pm 10e, \pm 20e, \pm 50e, \pm 100e$  respectively.

For large droplets and large particles, the image electric force induced by the particles is still significant, as shown in Figure 6.4 for 6  $\mu\text{m}$  and 9  $\mu\text{m}$  droplets, and for 12  $\mu\text{m}$  and 15  $\mu\text{m}$  droplets the results are similar while not shown here, this is because the image force depends on the small particle radius rather than the large droplet radius. However, the image electric force induced by the droplet is negligible, as shown in Figure 6.5 of 6  $\mu\text{m}$  and 9  $\mu\text{m}$  droplets. This is because the image force induced by the droplet takes effect only when the radius of the particle is comparable with that of the droplet, thus in Figure 6.5 for the smaller droplet of 6  $\mu\text{m}$  we can still see the effect, while for the large droplet of 9  $\mu\text{m}$  the effect disappears, and for 12  $\mu\text{m}$  and 15  $\mu\text{m}$  droplets the results are similar as that of 9  $\mu\text{m}$  droplet (not shown). In short, for large droplets, the effect of the image electric force induced by the particle still contributes to the collision rate coefficient while the effect of the image electric force induced by the droplet is very small.

For large droplets and large particles, the effect of the Coulomb electric force becomes weak due to the distance between their centers being large, so the contribution of the Coulomb force is small and roughly linear. Figure 6.6 shows the results of 6  $\mu\text{m}$  for opposite-sign charges and same-sign charges separately, in which the effect of Coulomb electric force is still important especially for particles with density higher than that of droplet. Figure 6.7 is similar to Figure 6.6, with the radius of droplet increased to 12  $\mu\text{m}$ . The effect of the Coulomb electric forces is very weak no matter whether the charges are of opposite-sign or same-sign. In brief, the effect of the Coulomb force decreases for large droplets and it is negligible, for the charges considered, if the droplet radius is large enough. Besides, the phoretic forces caused by relative humidity are also inverse-squaredly dependent on the separation between droplet and particle centers as for the

Coulomb force, so that their effects should also decrease for larger droplets. We have calculated some cases of different relative humidity for large droplets, while this is still not complete for all cases, we are calculating the remaining cases and will provide the fitted parameters and the code in future work.

In a word, the work for calculation and parameterization the collision rate coefficient for large droplets is ongoing, and after we have completed this work we can obtain the collision rate coefficient for any given droplet radius, droplet charge, particle radius, particle charge, particle density, and relative humidity. Then cloud models can be improved to better describe microphysical processes by applying the results of our parameterization.

## REFERENCES

- Baumgaertner A., et al., 2013, Toward a comprehensive global electric circuit model: Atmospheric conductivity and its variability in CESM1 (WACCM) model simulations, *J. Geophys. Res.*, *118*, 9221-9232, doi: 10.1002/jgrd.50725.
- Beard, K., T. H. Ochs III, and C. H. Twohy, 2004, Aircraft measurements of high average charges on cloud drops in layer clouds, *Geophys. Res. Lett.*, *31*, L14111, doi:10.1029/2004GL020465.
- Burns, G. B., Tinsley, B.A., French, W.J.R., Troshichev, O.A. and Frank - Kamenetsky, A.V., 2008. Atmospheric circuit influences on ground - level pressure in the Antarctic and Arctic. *Journal of Geophysical Research: Atmospheres*, *113*(D15).
- Charlson, R. J, and S. E. Schwartz, 1992, Climate forcing by anthropogenic aerosols, *Science*, *255*, 423.
- Davis, M. H., 1964a, Two Charged Spherical conductors in a Uniform Electric Field: Forces and Field Strength, RM-3860-PR, The Rand Corp., Santa Monica, Calif.
- Davis, M. H., 1964b, Two Charged Spherical Conductors in a Uniform Electric Field: Forces and Field Strength, *Q. J. Mech. Appl. Math.*, *17*, 499-511.
- DeMott, Paul J, A. J. Prenni, X. Liu, S. M. Kreidenweis, M. D. Petters, C. H. Twohy, M. S. Richardson, T. Eidhammer, and D. C. Rogers, 2010, Predicting global atmospheric ice nuclei distributions and their impacts on climate, *Proceedings of the National Academy of Sciences*, *107*, 11217-11222.
- Fang X., et al., 2008, Electron impact ionization: A new parameterization for 100eV to 1 MeV electrons, *J. Geophys. Res.*, *113*, A09311, doi:10.1029/2008JA013384.
- Fullekrug M., 2004, The contribution of intense lightning discharges to the global atmospheric electric circuit during April 1998, *J. Atmos. Terr. Phys.* *66*, 1115-1119.
- Gray, L.J., J. Beer, M. Geller, J. D. Haigh, M. Lockwood, K. Matthes, U. Cubasch, D. Fleitmann, G. Harrison, L. Hood, J. Luterbacher, G. A. Meehl, D. Shindell, B. van Geel, and W. White, 2010, Solar influence on climate, *Rev. Geophys.* *48*, DOI: 10.1029/2009RG000282.
- Hand, J. L, and S. M. Kreidenweis, 2002, A new method for retrieving particle refractive index and effective density from aerosol size distribution data, *Aerosol Sc. & Tech.*, *36*, 1012-1026.

- Heymsfield, A. J., and L. M. Miloshevich, 1995, Relative humidity and temperature influences on cirrus formation and evolution: Observations from wave clouds and FIRE II, *J. Atmos. Sci.*, **52**, 4302-4326.
- Kniveton, D. R., 2004, Precipitation, cloud cover and Forbush decreases in galactic cosmic rays, *J. Atmos. Solar-Terr. Phys.* **66**, 1135-1142.
- Kulmala, M., Vehkamäki, H., Petäjä, T., Dal Maso, M., Lauri, A., Kerminen, V.M., Birmili, W. and McMurry, P.H., 2004. Formation and growth rates of ultrafine atmospheric particles: a review of observations. *Journal of Aerosol Science*, **35**(2), pp.143-176.
- Lam, M. M., Chisham, G. and Freeman, M.P., 2013. The interplanetary magnetic field influences mid-latitude surface atmospheric pressure. *Environmental Research Letters*, **8**(4), p.045001.
- Lam M. M. and B. A. Tinsley, 2015, Solar wind - atmospheric electricity - cloud microphysics connections to weather and climate, *J. Atmos. Solar-Terr. Phys.* **149**, 277-290.
- Novakov, T., and Penner, J. E., 1993, Large contribution of organic aerosols to cloud-condensation-nuclei concentrations, *Nature*, **365**, 823 – 826.
- Oseen, C. W., 1910, *Ark. F. Math. Astron. Og. Fys.* **6**(29).
- Oseen, C. W., 1913, *Ark. F. Math. Astron. Og. Fys.* **9**(16).
- Proudman, I., and J. R. A. Pearson, 1957, Expansions at small Reynolds numbers for the flow past a sphere and a circular cylinder, *J. Fluid Mech.* **2**, 237-262.
- Pruppacher, H. R., and J. D. Klett, 1997, *Microphysics of Clouds and Precipitation*, 2<sup>nd</sup> rev. ed., Kluwer, Dordrecht, Netherland.
- Rosenfeld, D., Y. Kaufman, and I. Koren, 2006, Switching cloud cover and dynamical regimes from open to closed Benard cells in response to the suppression of precipitation by aerosols, *Atmos. Chem. Phys.*, **6**, 2503-2511.
- Rosenfeld, D., U. Lohmann, G. B. Raga, C. O'Dowd, M. Kulmala, S. Fuzzi, A. Reissell, and O. Meinrat, 2008, Flood or drought: how do aerosols affect precipitation?, *Science*, **321**, 1309-1313
- Spracklen, D. V, K. S. Carslaw, M. Kulmala, V-M. Kerminen, S. L. Sihto, I. Riipinen, J. Merikanto, G. W. Mann, M. Chipperfield, A. Wiedensohler, W. Birmili, and H. Lihavainen, 2008, Contribution of particle formation to global cloud condensation nuclei concentrations, *Geophys. Res. Lett.* **35**, L06808.

- Szyrmer, W., and I. Zawadzki, 1997, Biogenic and anthropogenic sources of ice-forming nuclei: A review, *Bull. Am. Meteorol. Soc.* 78, 209-228
- Tripathi S. N., and R. G. Harrison, 2002, Enhancement of contact nucleation by scavenging of charged aerosol particles, *Atmos. Res.* 62, 57-70.
- Tinsley, B. A., 2000, Influence of solar wind on the global electric circuit, and inferred effects on cloud microphysics, temperature, and dynamics in the troposphere, *Space Science Reviews* 94: 231-258.
- Tinsley, B. A., 2004, Scavenging of condensation nuclei in clouds: dependence of sign of electroscavenging effect on droplet and CCN sizes, Proc. 14<sup>th</sup> Int. Conf. on Clouds and Precipitation, ICCP, 18-23 July 2004, Bologna, Italy
- Tinsley, B. A., 2008, The global atmospheric electric circuit and its effects on cloud microphysics, *Rep. Prog. Phys.* 71, 066801 (31pp).
- Tinsley, B. A., 2010, Electric charge modulation of aerosol scavenging in clouds: Rate coefficients with Monte Carlo simulation of diffusion, *J. Geophys. Res.*, 115, D23211, doi:10.1029/2010JD014580.
- Tinsley, B. A., 2012, A working hypothesis for connections between electrically-induced changes in cloud microphysics and storm vorticity, with possible effects on circulation, *Adv. Space Res.*, 50, 791-805.
- Tinsley, B. A. and F. Yu, 2004, Atmospheric ionization and clouds as links between solar activity and climate, *Solar Variability and its Effects on Climate*, Geophysical Monograph # 41, pp. 321-339, AGU Press., Washington, DC, 2004.
- Tinsley, B. A. and D. B. Leddon, 2013, Charge modulation of scavenging in clouds: Extension of Monte Carlo simulations and initial parameterization, *J. Geophys. Res.: Atmos.*, 118, 8612-8624.
- Tinsley, B. A., and L. Zhou, 2014. Comments on “Effect of electric charge on collisions between cloud droplets”, *J. Appl. Meteor. Climatol.* 53, 1317-1320.
- Tinsley, B. A. and L. Zhou, 2015, Parameterization of aerosol scavenging due to atmospheric ionization, *J. Geophys. Res.: Atmos.*, 120, doi: 10.1002/2014JD023016.
- Tinsley, B. A., J. T. Hoeksema, D. N. Baker, 1994, Stratospheric volcanic aerosols and changes in air - earth current density at solar wind magnetic sector boundaries as conditions for the Wilcox tropospheric vorticity effect, *J. Geophys. Res.: Atmosph.* 99, 16805-16813

- Tinsley, B. A., R. P. Rohrbaugh, M. Hei, K. V. Beard, 2000, Effects of image charges on the scavenging of aerosol particles by cloud Droplets and on droplet charging and possible ice nucleation processes, *J. Atmos. Sci.*, *57*, 2118-2134
- Tinsley, B. A., Rohrbaugh, R. P., Hei, M., 2001, Electroscavenging in clouds with broad droplet size distributions and weak electrification, *Atmospheric Research*, *59-60*, 115-135
- Tinsley, B. A., L. Zhou and A. Plemmons, 2006, Changes in scavenging of particles by droplets due to weak electrification in clouds, *Atmos. Res.* *79*, 266-295.
- Tsyganenko N. A., 2002, A model of the near magnetosphere with a dawn-dusk asymmetry, *J. Geophys. Res.*, *107*(A8), 1170, doi: 10.1029/2001JA000219
- Wilson, C. T. R., 1920. Investigations on lightning discharges and on the electric field of thunderstorms. *Philos. Trans. Roy. Soc. Lond.*, *A221*, 73-115.
- Yin, Y., Z. Levin, T. G. Reisin, S. Tzivion, 2000, The effects of giant cloud condensation nuclei on the development of precipitation in convective clouds - a numerical study, *Atmos. Res.*, *53*, 91-116
- Yu, S., 2000, Role of organic acids (formic, acetic, pyruvic and oxalic) in the formation of cloud condensation nuclei (CCN): a review, *Atmos. Res.*, *53*, 185-217
- Zhang, L., and B. A. Tinsley, 2017, Parameterization of Aerosol Scavenging due to Atmospheric Ionization under Varying Relative Humidity. *J. Geophys. Res.: Atmos.*, *122*, doi:10.1002/2016JD026255.
- Zhou L. and B. A. Tinsley, 2007, Production of space charge at the boundaries of layer clouds, *J. Geophys. Res.: Atmosph.* *112*, D11203.
- Zhou L., B. A. Tinsley and A. Plemmons, 2009, Scavenging in weakly electrified saturated and subsaturated clouds, treating aerosol particles and droplets as conducting spheres, *J. Geophys. Res.*, *114*, D18201, doi: 10.1029/2008JD011527.
- Zhou L., B.A. Tinsley, Wang L. and Burns G., 2017, The zonal-mean and regional tropospheric pressure responses to changes in ionospheric potential, in press, *Journal of Atmospheric and Solar-Terrestrial Physics*



## APPENDIX

‘parameter1.txt’

B1 3 3 2 ; Parameter name and number of elements in each dimension

-1.548082e+001 1.123827e+000 4.968335e-002  
-2.708921e-001 1.668906e+000 1.354767e-001  
4.098891e-001 5.619178e-001 5.811007e-002

1.200133e+000 -5.973762e-001 -3.634411e-002  
6.630110e-002 -8.813166e-001 -8.213144e-002  
-4.556703e-002 -2.954579e-001 -3.339021e-002

B2 3 3 2  
-1.560758e+001 -6.553335e-001 -1.363709e+000  
-4.372264e-001 -6.917685e-001 -1.769542e+000  
3.612958e-001 -2.029903e-001 -5.437491e-001

1.265005e+000 3.303216e-001 7.457038e-001  
1.519866e-001 3.324334e-001 9.793446e-001  
-2.079219e-002 9.337345e-002 3.043391e-001

C1 3 4 2  
-1.648387e+001 6.531489e-003 -2.328666e-002  
-2.624748e+000 -6.192688e-001 -2.569448e-002  
2.597352e-002 2.164069e+000 4.771477e-001  
1.414579e+000 3.758195e+000 7.565323e-001

1.659731e+000 5.449442e-004 9.632045e-003  
9.239975e-001 2.527803e-001 8.801243e-003  
-7.573323e-001 -1.349919e+000 -3.130041e-001  
-1.451957e+000 -2.099512e+000 -4.775302e-001

C2 3 4 2  
-1.650466e+001 -4.038239e-001 -4.374275e-001  
-2.560154e+000 -1.066718e-002 2.424263e+000  
-2.846985e-001 2.683388e+000 -1.831225e+000  
8.760949e-001 3.838866e+000 -8.031823e+000

1.668992e+000 2.102557e-001 2.220296e-001  
8.929524e-001 1.294392e-002 -1.356643e+000  
-5.520749e-001 -1.569475e+000 1.226378e+000  
-1.113715e+000 -2.313721e+000 4.755531e+000

D    4    4    3  
 -2.332108e-017 -3.068830e-017 6.568525e-017 1.092383e-017  
 5.568076e-017 6.252351e-017 -1.475836e-016 -2.551189e-017  
 -4.720279e-017 -4.080983e-017 1.050931e-016 1.858012e-017  
 9.491831e-018 8.829763e-018 -2.127640e-017 -3.823045e-018  
  
 7.373591e-019 8.511501e-019 -1.801678e-018 -3.107351e-019  
 -1.732539e-018 -1.765272e-018 3.831004e-018 6.842180e-019  
 1.793189e-018 1.013494e-018 -2.712227e-018 -4.887223e-019  
 -3.638710e-019 -1.956203e-019 5.490071e-019 9.950679e-020  
  
 -4.952926e-021 -4.452837e-021 1.191129e-020 2.000867e-021  
 1.162451e-020 7.954149e-021 -2.600916e-020 -4.474679e-021  
 -1.018636e-020 -4.086584e-021 1.854350e-020 3.219989e-021  
 2.078601e-021 7.521941e-022 -3.773883e-021 -6.591309e-022  
  
 F    4    4    4  
 -1.941430e+001 2.108360e+000 3.407004e+000 -1.180542e+000  
 -5.742598e+000 2.267883e+000 5.688291e+000 -2.844459e+000  
 -3.368552e+000 1.837878e+000 4.584893e+000 -2.292329e+000  
 -9.381477e-001 4.834376e-001 1.192799e+000 -5.916518e-001  
  
 -2.133917e+000 6.236601e-001 1.115380e+000 -3.083317e-001  
 -2.754604e+000 6.205576e-001 1.427949e+000 -2.877285e-001  
 -1.179209e+000 1.547866e-001 6.081698e-001 -5.956081e-002  
 -1.739030e-001 3.392854e-003 9.109941e-002 1.181488e-003  
  
 -1.359788e+000 6.678728e-001 6.750156e-001 -3.289316e-001  
 -3.031605e+000 1.634271e+000 1.572899e+000 -8.578234e-001  
 -2.339030e+000 1.343948e+000 1.269822e+000 -7.430504e-001  
 -5.924025e-001 3.522541e-001 3.334585e-001 -2.019347e-001  
  
 -1.961365e-001 1.100117e-001 9.477132e-002 -5.385021e-002  
 -4.933793e-001 2.938531e-001 2.553989e-001 -1.550705e-001  
 -4.084789e-001 2.513163e-001 2.224282e-001 -1.393708e-001  
 -1.072078e-001 6.682991e-002 6.040937e-002 -3.824947e-002  
  
 H    4    4    4  
 -1.722609e+001 1.125932e+000 1.117345e+000 -5.091606e-002  
 -5.538772e-001 -9.090397e-002 -1.917776e-002 -3.631044e-002  
 1.055374e+000 -4.692705e-001 -1.695198e-001 1.586706e-001  
 1.429694e+000 -1.005214e+000 -8.028995e-001 5.649458e-001  
  
 -7.114344e-001 2.100397e-001 3.574854e-001 -1.009574e-001

1.940327e+000 -6.119718e-001 -1.120176e+000 3.487877e-001  
4.408560e-001 1.818603e-002 -1.510493e-001 -4.068732e-002  
-3.713138e+000 1.307213e+000 2.237019e+000 -7.737119e-001

-2.642854e-001 7.562283e-002 1.357359e-001 -3.503689e-002  
1.351104e+000 -4.567159e-001 -8.235060e-001 2.809265e-001  
-2.045924e-001 1.348475e-001 9.183469e-002 -6.045161e-002  
-3.814595e+000 1.414803e+000 2.288366e+000 -8.469607e-001

-2.610795e-002 6.632946e-003 1.307900e-002 -2.729091e-003  
1.900049e-001 -6.546364e-002 -1.177093e-001 4.109965e-002  
-6.121718e-002 2.857722e-002 2.784644e-002 -1.239755e-002  
-5.894172e-001 2.185697e-001 3.555254e-001 -1.321400e-001

M 3 4 4  
3.170259e-003 -6.207653e-005 3.943912e-005  
7.015363e-003 -1.328874e-004 1.092439e-004  
6.649510e-003 -1.200834e-004 1.153876e-004  
1.572872e-003 -3.316887e-005 3.064895e-005

6.122200e-004 -2.387929e-005 1.598011e-005  
-1.321810e-004 -2.799668e-005 3.264807e-005  
-5.114886e-004 -1.174330e-005 2.095580e-005  
-1.473341e-004 -1.627124e-006 4.219386e-006

3.038084e-005 4.185663e-006 -2.011907e-005  
7.080345e-004 2.700120e-006 -6.750078e-005  
1.106348e-003 -6.025109e-006 -6.591980e-005  
4.019260e-004 -3.538625e-006 -1.925768e-005

-3.463828e-005 1.800885e-006 -4.475086e-006  
7.448718e-005 2.272269e-006 -1.439225e-005  
1.794150e-004 -1.054362e-007 -1.366954e-005  
7.103233e-005 -4.761409e-007 -3.921898e-006

V 3 4 4  
3.872137e-004 -5.492226e-006 2.124541e-006  
-7.100673e-004 1.839350e-005 -7.733089e-006  
-2.421117e-004 7.414333e-008 4.956273e-006  
-5.179213e-004 -6.029486e-006 3.548723e-006

2.115426e-004 -4.149530e-006 1.397198e-006  
-1.053630e-003 2.150892e-005 -2.728357e-006  
5.621125e-004 -9.877771e-006 -4.006257e-006

2.030685e-003 -4.227433e-005 2.115708e-007  
5.497399e-005 -1.187590e-006 4.203374e-007  
-5.351762e-004 9.027821e-006 1.410779e-006  
4.172375e-004 -4.998391e-006 -4.360879e-006  
1.883913e-003 -2.945071e-005 -1.048608e-005  
5.165528e-006 -1.152406e-007 4.355967e-008  
-6.990692e-005 1.082502e-006 3.213878e-007  
5.863626e-005 -6.194553e-007 -6.736684e-007  
2.853292e-004 -4.161413e-006 -1.976765e-006

'parameter2.txt'

A 2 4 3 ; Parameter name and number of elements in each dimension  
-9.496913e-019 1.430493e-022  
2.779895e-019 -1.436315e-021  
-5.003616e-019 2.333488e-022  
-5.213201e-020 6.960137e-023

3.348858e-018 1.414516e-021  
-5.695032e-019 1.616864e-021  
2.638384e-018 -1.369606e-022  
4.040137e-019 -3.235897e-023

-6.804319e-018 -4.573591e-022  
1.675280e-019 -4.867689e-022  
-9.650655e-019 2.674070e-022  
-1.623094e-019 3.403526e-023

B 5 5 5  
-6.337690e-003 2.733711e-005 -4.168372e-008 2.693383e-011 -6.283185e-015  
-7.819812e-003 3.432212e-005 -5.256804e-008 3.379164e-011 -7.792296e-015  
-2.016562e-003 9.760017e-006 -1.494479e-008 9.336426e-012 -2.071210e-015  
5.270381e-004 -1.884691e-006 3.048889e-009 -2.203625e-012 5.709187e-016  
1.330289e-004 -5.340571e-007 8.503966e-010 -5.850185e-013 1.443392e-016

2.638921e-002 -1.110061e-004 1.644148e-007 -1.028683e-010 2.322635e-014  
3.564242e-002 -1.522150e-004 2.262161e-007 -1.406692e-010 3.137897e-014  
1.258008e-002 -5.763501e-005 8.563682e-008 -5.200323e-011 1.123908e-014  
-1.948795e-004 -9.926565e-007 8.144426e-010 5.828745e-013 -4.081262e-016  
-2.956106e-004 1.051819e-006 -1.694348e-009 1.222614e-012 -3.143154e-016

-3.603375e-002 1.457562e-004 -2.079835e-007 1.247517e-010 -2.695448e-014  
-4.791184e-002 1.934858e-004 -2.744623e-007 1.618293e-010 -3.415786e-014  
-1.545374e-002 6.353122e-005 -8.418620e-008 4.336094e-011 -7.543833e-015  
1.080368e-003 -4.493725e-006 1.108200e-008 -1.101014e-011 3.446562e-015  
5.027541e-004 -2.101467e-006 3.686087e-009 -2.819660e-012 7.559779e-016

1.721851e-002 -6.621072e-005 8.767938e-008 -4.810026e-011 9.380290e-015  
2.216751e-002 -8.244663e-005 1.057988e-007 -5.513174e-011 1.004805e-014  
5.079705e-003 -1.547410e-005 1.010713e-008 3.252512e-012 -2.857226e-015  
-1.856593e-003 9.469723e-006 -1.899837e-008 1.576603e-011 -4.433848e-015  
-4.216931e-004 1.947516e-006 -3.481226e-009 2.648923e-012 -7.048808e-016

-2.234232e-003 7.482578e-006 -7.903139e-009 2.949443e-012 -2.313871e-016

-2.809699e-003 8.738477e-006 -8.289071e-009 2.271898e-012 8.893622e-017  
-1.001833e-004 -1.477892e-006 5.734680e-009 -6.002566e-012 1.864770e-015  
6.180066e-004 -3.180128e-006 6.043559e-009 -4.746416e-012 1.282481e-015  
1.082232e-004 -5.173260e-007 9.235572e-010 -6.945850e-013 1.827672e-016

C 2 2 4 4  
-1.884988e-020 4.257035e-023  
1.983419e-022 2.693443e-024

4.101177e-020 -3.209227e-023  
-1.096834e-021 9.269495e-025

-2.814552e-020 1.495240e-022  
1.429015e-021 -4.912177e-024

-7.279740e-021 2.949445e-023  
3.281944e-022 -9.450935e-025

-1.904399e-020 -1.432298e-022  
-1.884406e-021 -4.709489e-024

-8.582658e-020 1.013798e-023  
2.273796e-021 -1.655681e-024

-1.407760e-021 -3.359955e-022  
-2.790308e-021 1.127283e-023

1.363441e-021 -5.546605e-023  
-6.330106e-022 1.981367e-024

3.877905e-020 9.376732e-023  
1.244205e-021 3.082563e-024

4.360784e-020 5.225135e-024  
-1.425819e-021 1.142898e-024

1.269374e-020 2.402759e-022  
1.579894e-021 -8.448498e-024

2.669762e-021 3.678950e-023  
3.711486e-022 -1.447992e-024

-1.103093e-020 -1.953589e-023  
-2.261325e-022 -6.220964e-025

-6.063868e-021 -2.951719e-024  
2.516600e-022 -2.455882e-025

-2.739935e-021 -5.245833e-023  
-2.971697e-022 1.905258e-024

-7.500156e-022 -7.788897e-024  
-7.146737e-023 3.267559e-025

D 3 3 5 5  
3.840565e-005 -9.588794e-008 4.641316e-011  
-2.821810e-006 8.125148e-009 -4.233057e-012  
3.880348e-008 -1.155807e-010 6.138819e-014

1.927087e-005 -4.939156e-008 2.353784e-011  
-2.586386e-006 7.017233e-009 -3.730166e-012  
3.732508e-008 -1.016590e-010 5.522064e-014

-4.461998e-005 1.065580e-007 -5.117870e-011  
1.839214e-006 -5.605663e-009 2.732226e-012  
-2.714790e-008 8.715968e-011 -4.278768e-014

-2.926707e-005 6.945486e-008 -3.303747e-011  
1.619798e-006 -4.711106e-009 2.353753e-012  
-2.408107e-008 7.277437e-011 -3.678581e-014

-3.964947e-006 9.367665e-009 -4.438320e-012  
2.334539e-007 -6.734979e-010 3.378263e-013  
-3.483156e-009 1.042143e-011 -5.294365e-015

-1.594471e-004 4.169617e-007 -2.109071e-010  
1.340690e-005 -3.986070e-008 2.143243e-011  
-1.878952e-007 5.761019e-010 -3.158286e-013

-8.386718e-005 2.429562e-007 -1.215452e-010  
1.290782e-005 -3.673895e-008 1.992085e-011  
-1.867487e-007 5.297693e-010 -2.940882e-013

1.684936e-004 -4.097937e-007 2.094086e-010

-5.767447e-006 1.964415e-008 -1.031030e-011  
9.131109e-008 -3.275712e-010 1.705794e-013

1.105218e-004 -2.738206e-007 1.390889e-010  
-5.923156e-006 1.865504e-008 -9.936799e-012  
9.183225e-008 -2.991303e-010 1.597865e-013

1.489761e-005 -3.701636e-008 1.877605e-011  
-8.682915e-007 2.708840e-009 -1.447379e-012  
1.346473e-008 -4.331559e-011 2.325039e-014

2.376244e-004 -6.380290e-007 3.390831e-010  
-2.052992e-005 6.361937e-008 -3.503400e-011  
2.891546e-007 -9.282792e-010 5.204795e-013

1.083488e-004 -3.382203e-007 1.782076e-010  
-1.731571e-005 5.579754e-008 -3.063956e-011  
2.490617e-007 -8.103079e-010 4.560256e-013

-2.654235e-004 6.791211e-007 -3.705274e-010  
9.612662e-006 -3.079879e-008 1.781312e-011  
-1.504554e-007 5.038421e-010 -2.846362e-013

-1.680747e-004 4.432065e-007 -2.418253e-010  
8.775104e-006 -2.853067e-008 1.629602e-011  
-1.351579e-007 4.524098e-010 -2.567398e-013

-2.247219e-005 5.975870e-008 -3.265616e-011  
1.261341e-006 -4.125422e-009 2.356360e-012  
-1.942923e-008 6.526397e-011 -3.712577e-014

-1.450577e-004 3.930942e-007 -2.160973e-010  
1.238396e-005 -3.831519e-008 2.135527e-011  
-1.752207e-007 5.627376e-010 -3.188047e-013

-6.134499e-005 1.970707e-007 -1.088042e-010  
8.947937e-006 -3.113037e-008 1.729616e-011  
-1.284768e-007 4.569410e-010 -2.601456e-013

1.673378e-004 -4.408412e-007 2.483993e-010  
-6.745801e-006 2.049043e-008 -1.236800e-011  
1.017348e-007 -3.206259e-010 1.891678e-013



1.044625e-004 -2.851741e-007 1.616728e-010  
-5.410840e-006 1.765470e-008 -1.049129e-011  
8.129360e-008 -2.729880e-010 1.608758e-013

1.393782e-005 -3.848051e-008 2.189293e-011  
-7.598381e-007 2.524095e-009 -1.499991e-012  
1.142778e-008 -3.901849e-011 2.304391e-014

2.927867e-005 -7.960989e-008 4.493865e-011  
-2.440074e-006 7.482959e-009 -4.223482e-012  
3.484757e-008 -1.107989e-010 6.340742e-014

1.195663e-005 -3.864423e-008 2.222004e-011  
-1.550010e-006 5.661954e-009 -3.195417e-012  
2.237119e-008 -8.417147e-011 4.860844e-014

-3.448056e-005 9.226961e-008 -5.302612e-011  
1.514871e-006 -4.477826e-009 2.756912e-012  
-2.223777e-008 6.776850e-011 -4.096260e-014

-2.137855e-005 5.939211e-008 -3.451452e-011  
1.111548e-006 -3.615268e-009 2.204415e-012  
-1.635907e-008 5.478491e-011 -3.314880e-014

-2.850377e-006 8.018360e-009 -4.683128e-012  
1.532901e-007 -5.111994e-010 3.121555e-013  
-2.259231e-009 7.756983e-012 -4.708250e-015

E 2 2 4 4  
-4.135322e-020 1.288706e-022  
5.195788e-022 -1.889399e-024

3.629813e-020 -2.304354e-023  
-4.223414e-022 1.319552e-025

2.251329e-020 -8.650477e-023  
-2.435558e-022 1.510617e-024

4.082892e-021 -1.878381e-023  
-4.230325e-023 3.200872e-025

1.284951e-019 -3.358810e-022  
-1.753165e-021 5.178742e-024

-1.135550e-019 9.624485e-023  
1.353744e-021 -8.615359e-025

-7.583870e-020 1.966195e-022  
9.048031e-022 -3.708369e-024

-1.411289e-020 4.612241e-023  
1.568774e-022 -8.093937e-025

-1.092805e-019 2.811757e-022  
1.548118e-021 -4.252276e-024

8.894841e-020 -8.723014e-023  
-1.129966e-021 8.479150e-025

6.934175e-020 -1.507630e-022  
-8.829177e-022 2.784878e-024

1.301230e-020 -3.580793e-023  
-1.523109e-022 6.103948e-025

2.606660e-020 -6.222096e-023  
-3.850391e-022 9.321229e-025

-1.998541e-020 1.894293e-023  
2.602853e-022 -1.932090e-025

-1.740839e-020 2.931820e-023  
2.245510e-022 -5.665734e-025

-3.271913e-021 7.354800e-024  
3.887577e-023 -1.267686e-025

F 3 3 5 5  
2.900880e-005 -4.721980e-008 1.962625e-011  
-9.658077e-007 1.726615e-009 -7.513660e-013  
6.542727e-009 -1.170538e-011 5.107668e-015

2.353739e-005 -2.476629e-008 7.508391e-012  
-8.551642e-007 1.282722e-009 -5.236169e-013  
6.127636e-009 -9.309439e-012 3.868805e-015

-2.982866e-005 4.085724e-008 -1.584233e-011  
1.066574e-006 -1.457014e-009 5.505985e-013  
-8.079051e-009 1.145429e-011 -4.362783e-015

-2.392539e-005 2.761816e-008 -9.417229e-012  
9.010927e-007 -1.193294e-009 4.452899e-013  
-6.944547e-009 9.662066e-012 -3.686929e-015

-3.459040e-006 3.791174e-009 -1.233509e-012  
1.325849e-007 -1.737333e-010 6.448169e-014  
-1.029489e-009 1.424485e-012 -5.431478e-016

-1.063116e-004 1.830026e-007 -7.912242e-011  
3.621747e-006 -7.061018e-009 3.206886e-012  
-2.437191e-008 4.789221e-011 -2.189593e-014

-1.107527e-004 1.437898e-007 -5.271561e-011  
4.087280e-006 -7.287178e-009 3.242441e-012  
-2.971865e-008 5.397368e-011 -2.447083e-014

9.135442e-005 -1.301988e-007 5.360199e-011  
-3.150726e-006 4.141345e-009 -1.541897e-012  
2.395117e-008 -3.278898e-011 1.206118e-014

8.452131e-005 -1.050282e-007 3.887357e-011  
-3.144606e-006 4.412501e-009 -1.723176e-012  
2.441484e-008 -3.598580e-011 1.421642e-014

1.258350e-005 -1.507252e-008 5.402518e-012  
-4.777492e-007 6.743872e-010 -2.644359e-013  
3.738579e-009 -5.562206e-012 2.216068e-015

1.260422e-004 -2.311826e-007 1.037729e-010  
-4.405897e-006 9.235109e-009 -4.320011e-012  
2.959682e-008 -6.278093e-011 2.969109e-014

1.468606e-004 -2.177990e-007 8.813845e-011  
-5.549885e-006 1.109746e-008 -5.196551e-012

4.062849e-008 -8.252224e-011 3.938710e-014  
 -1.065133e-004 1.792968e-007 -7.980595e-011  
 3.413637e-006 -4.925425e-009 1.908474e-012  
 -2.564644e-008 3.782123e-011 -1.404993e-014  
 -1.046447e-004 1.568017e-007 -6.495387e-011  
 3.758045e-006 -6.040137e-009 2.526126e-012  
 -2.903666e-008 4.816138e-011 -2.007601e-014  
 -1.577426e-005 2.302134e-008 -9.363228e-012  
 5.804782e-007 -9.439041e-010 3.976828e-013  
 -4.523165e-009 7.607710e-012 -3.209630e-015  
 -5.922032e-005 1.145296e-007 -5.266405e-011  
 2.065822e-006 -4.524962e-009 2.144916e-012  
 -1.387875e-008 3.105662e-011 -1.498005e-014  
 -7.563660e-005 1.234150e-007 -5.281945e-011  
 2.848153e-006 -6.072462e-009 2.915121e-012  
 -2.101785e-008 4.564049e-011 -2.238036e-014  
 5.335339e-005 -1.017879e-007 4.705330e-011  
 -1.599024e-006 2.586086e-009 -1.045969e-012  
 1.168784e-008 -1.887904e-011 7.170300e-015  
 5.359852e-005 -9.210926e-008 4.041911e-011  
 -1.845526e-006 3.307699e-009 -1.444052e-012  
 1.407784e-008 -2.568870e-011 1.110237e-014  
 8.122512e-006 -1.366546e-008 5.923505e-012  
 -2.872840e-007 5.206777e-010 -2.290429e-013  
 2.213356e-009 -4.094239e-012 1.792114e-015  
 9.730716e-006 -1.949758e-008 9.079747e-012  
 -3.194018e-007 7.212413e-010 -3.446272e-013  
 2.158743e-009 -5.040760e-012 2.467836e-015  
 1.338310e-005 -2.325780e-008 1.026643e-011  
 -4.893653e-007 1.082044e-009 -5.264175e-013  
 3.647244e-009 -8.248481e-012 4.107675e-015

-9.787244e-006 1.991643e-008 -9.306742e-012  
2.798924e-007 -4.921670e-010 2.044718e-013  
-1.973730e-009 3.416375e-012 -1.321691e-015

-9.782482e-006 1.819190e-008 -8.181199e-012  
3.233499e-007 -6.204495e-010 2.768091e-013  
-2.423141e-009 4.701553e-012 -2.072604e-015

-1.482886e-006 2.709792e-009 -1.207883e-012  
5.038654e-008 -9.764466e-011 4.389329e-014  
-3.821293e-010 7.508307e-013 -3.352759e-016

G 2 2 2 4 4  
-1.856464e-020 4.666973e-023  
2.248201e-022 -4.262005e-025

4.302749e-022 -1.124619e-024  
-5.296815e-024 1.107736e-026

-4.190313e-021 -3.169511e-024  
3.909063e-023 6.941786e-026

9.041899e-023 1.505595e-025  
-7.161923e-025 -2.425635e-027

1.970817e-020 -4.775422e-023  
-2.278287e-022 4.446044e-025

-5.321382e-022 1.277096e-024  
6.338663e-024 -1.294567e-026

3.524095e-021 -8.048441e-024  
-4.010611e-023 7.045664e-026

-9.589498e-023 2.155570e-025  
1.127712e-024 -2.098330e-027

4.692923e-020 -1.272605e-022

-5.645398e-022 1.195050e-024

-1.085057e-021 2.966177e-024  
1.363092e-023 -2.983440e-026

6.048185e-021 1.021969e-023  
-7.397864e-023 -1.835820e-025

-1.396907e-022 -3.624051e-025  
1.322073e-024 5.667216e-027

-5.107827e-020 1.313008e-022  
5.672558e-022 -1.229521e-024

1.425879e-021 -3.441519e-024  
-1.658943e-023 3.493323e-026

-8.846702e-021 2.148824e-023  
9.768604e-023 -1.900448e-025

2.529131e-022 -5.719237e-025  
-2.929097e-024 5.600417e-027

-3.479863e-020 1.028715e-022  
4.304755e-022 -9.860383e-025

8.376768e-022 -2.367306e-024  
-1.071766e-023 2.414718e-026

-5.024789e-021 -1.134194e-023  
5.981682e-023 1.711084e-025

1.013350e-022 3.321492e-025  
-9.096531e-025 -4.755404e-027

3.686663e-020 -1.050312e-022  
-4.125607e-022 9.932731e-025

-1.062088e-021 2.700802e-024  
1.245826e-023 -2.745042e-026

6.356841e-021 -1.706014e-023  
-7.079108e-023 1.534105e-025

-1.880589e-022 4.471288e-025  
2.196563e-024 -4.401617e-027

7.695646e-021 -2.432929e-023  
-9.767372e-023 2.378278e-025

-1.913376e-022 5.552551e-025  
2.487816e-024 -5.733071e-027

1.203223e-021 3.023271e-024  
-1.383657e-023 -4.320063e-026

-2.213381e-023 -8.374563e-026  
1.861989e-025 1.156259e-027

-7.974155e-021 2.459275e-023  
9.055163e-023 -2.345676e-025

2.349662e-022 -6.230741e-025  
-2.786419e-024 6.345173e-027

-1.375187e-021 3.997876e-024  
1.553976e-023 -3.642484e-026

4.162268e-023 -1.032443e-025  
-4.912934e-025 1.020500e-027

H 3 3 3 4 5  
-2.087249e-003 3.533194e-006 -1.380661e-009  
4.684017e-005 -7.386812e-008 2.650603e-011

-2.359034e-007 3.612947e-010 -1.185676e-013

1.615707e-004 -2.942357e-007 1.153650e-010  
-3.497159e-006 6.488422e-009 -2.460597e-012  
1.695876e-008 -3.357413e-011 1.252479e-014

-2.168610e-006 3.979394e-009 -1.513662e-012  
4.458164e-008 -8.510134e-011 3.117406e-014  
-1.979886e-010 4.147755e-013 -1.455706e-016

9.031052e-004 -7.498375e-007 1.133246e-010  
-1.732928e-005 1.050003e-009 7.344989e-012  
9.463325e-008 7.015460e-011 -9.487147e-014

-5.823086e-005 6.160278e-009 1.521783e-011  
8.352829e-007 1.955569e-009 -1.637750e-012  
-3.736368e-009 -1.957783e-011 1.499745e-014

7.718105e-007 3.037001e-010 -4.232426e-013  
-9.172730e-009 -4.256066e-011 3.161409e-014  
3.247511e-011 3.865024e-013 -2.762872e-016

1.389237e-003 -2.831345e-006 1.200791e-009  
-1.951886e-005 4.741366e-008 -1.925536e-011  
3.199187e-008 -1.401259e-010 4.505715e-014

-1.033451e-004 1.925464e-007 -8.360016e-011  
8.814175e-007 -2.054473e-009 8.048821e-013  
2.979959e-009 -1.681332e-012 1.834717e-015

1.285941e-006 -2.195181e-009 9.245126e-013  
-4.031095e-009 7.994068e-012 -1.038909e-015  
-1.097349e-010 1.849389e-013 -1.057322e-016

2.910395e-004 -6.478497e-007 2.898357e-010  
-4.794466e-006 1.303329e-008 -5.889040e-012  
1.338353e-008 -5.538637e-011 2.476338e-014

-2.266068e-005 4.784432e-008 -2.210761e-011  
2.954632e-007 -8.261206e-010 3.939424e-013  
-3.361756e-010 2.836476e-012 -1.420596e-015



2.955029e-007 -6.039882e-010 2.788393e-013  
-2.906571e-009 8.729621e-012 -4.193971e-015  
-5.634141e-012 -1.723964e-014 9.344635e-018

1.423872e-002 -2.292484e-005 9.177039e-009  
-3.823154e-004 6.025767e-007 -2.379918e-010  
2.349915e-006 -3.694388e-009 1.447042e-012

-1.090012e-003 1.896546e-006 -7.568974e-010  
2.916960e-005 -5.198206e-008 2.091893e-011  
-1.791679e-007 3.284865e-010 -1.337662e-013

1.473774e-005 -2.606754e-008 1.019056e-011  
-3.910947e-007 7.188619e-010 -2.859071e-013  
2.365375e-009 -4.500538e-012 1.806711e-015

-6.325594e-003 6.062433e-006 -1.331092e-009  
1.219789e-004 -2.860721e-008 -3.086757e-011  
-6.750093e-007 -2.825881e-010 4.713661e-013

4.413875e-004 -2.556777e-007 2.151176e-011  
-6.669049e-006 -7.553860e-009 7.184436e-012  
3.109503e-008 9.296477e-011 -7.295418e-014

-5.930740e-006 1.704755e-009 6.067200e-013  
7.597456e-008 1.875139e-010 -1.444446e-013  
-2.950789e-010 -1.924465e-012 1.369838e-015

-9.904587e-003 1.776493e-005 -7.354843e-009  
1.904732e-004 -3.609233e-007 1.531763e-010  
-8.217605e-007 1.606288e-009 -6.599564e-013

7.728428e-004 -1.332532e-006 5.773109e-010  
-1.227282e-005 2.206307e-008 -9.587857e-012  
4.152133e-008 -7.673556e-011 3.166969e-014

-1.016044e-005 1.662205e-008 -7.144223e-012  
1.351555e-007 -2.203731e-010 9.189025e-014  
-2.817903e-010 3.815453e-013 -1.046302e-016

-2.016229e-003 4.004621e-006 -1.761463e-009  
4.205714e-005 -9.228406e-008 4.231645e-011  
-1.966391e-007 4.759436e-010 -2.213661e-013

1.623479e-004 -3.158255e-007 1.447820e-010  
-3.034474e-006 6.681639e-009 -3.196883e-012  
1.294713e-008 -3.275601e-011 1.615291e-014

-2.205098e-006 4.206806e-009 -1.938721e-012  
3.774135e-008 -8.322288e-011 4.024809e-014  
-1.407200e-010 3.749106e-013 -1.884171e-016

-2.902538e-002 4.682001e-005 -1.954332e-008  
8.385707e-004 -1.365916e-006 5.758044e-010  
-5.439837e-006 8.920853e-009 -3.765442e-012

2.154403e-003 -3.658721e-006 1.498765e-009  
-6.227562e-005 1.096281e-007 -4.579421e-011  
4.057635e-007 -7.312721e-010 3.092971e-013

-2.922217e-005 5.015390e-008 -2.014484e-011  
8.469165e-007 -1.524827e-009 6.302253e-013  
-5.493227e-009 1.015828e-011 -4.248508e-015

1.317151e-002 -2.011621e-005 7.359091e-009  
-3.116847e-004 3.652841e-007 -1.224010e-010  
1.898953e-006 -1.705524e-009 4.345957e-013

-1.011676e-003 1.340647e-006 -5.132272e-010  
2.034910e-005 -1.376599e-008 2.518614e-012  
-1.133599e-007 1.658820e-011 2.520906e-014

1.434079e-005 -1.720729e-008 6.565116e-012  
-2.664959e-007 8.631386e-011 2.028688e-014  
1.402211e-009 6.609721e-013 -8.465382e-016

2.010069e-002 -3.631617e-005 1.488706e-008  
-4.936671e-004 9.196920e-007 -4.040559e-010  
2.766227e-006 -5.210831e-009 2.324915e-012

-1.617633e-003 2.872545e-006 -1.246280e-009  
 3.520591e-005 -6.418507e-008 2.894222e-011  
 -1.843717e-007 3.401427e-010 -1.548791e-013  
  
 2.220650e-005 -3.833813e-008 1.668714e-011  
 -4.538414e-007 7.988435e-010 -3.585956e-013  
 2.240704e-009 -3.940097e-012 1.766124e-015  
  
 3.818327e-003 -7.297088e-006 3.101567e-009  
 -9.588793e-005 1.937556e-007 -8.784579e-011  
 5.413087e-007 -1.137191e-009 5.269348e-013  
  
 -3.141217e-004 5.967985e-007 -2.674582e-010  
 7.238658e-006 -1.471490e-008 6.914740e-012  
 -3.934704e-008 8.417492e-011 -4.045988e-014  
  
 4.390295e-006 -8.231141e-009 3.717959e-012  
 -9.719972e-008 1.967034e-010 -9.313850e-014  
 5.111284e-010 -1.095846e-012 5.305997e-016  
  
 2.020610e-002 -3.252457e-005 1.395828e-008  
 -6.011418e-004 9.894861e-007 -4.337581e-010  
 3.961232e-006 -6.559773e-009 2.883997e-012  
  
 -1.450080e-003 2.416021e-006 -1.010941e-009  
 4.311737e-005 -7.464611e-008 3.201093e-011  
 -2.855649e-007 5.038397e-010 -2.184884e-013  
  
 1.957508e-005 -3.273004e-008 1.342405e-011  
 -5.849813e-007 1.027189e-009 -4.351284e-013  
 3.866108e-009 -6.937626e-012 2.971141e-015  
  
 -8.528494e-003 1.472093e-005 -5.933809e-009  
 2.264710e-004 -3.414621e-007 1.424130e-010  
 -1.448763e-006 1.956338e-009 -7.894678e-013  
  
 6.948499e-004 -1.118041e-006 4.759811e-010  
 -1.564484e-005 1.896609e-008 -7.404302e-012  
 9.185057e-008 -8.332317e-011 2.586673e-014

-1.015984e-005 1.569655e-008 -6.807818e-012  
2.129486e-007 -2.180988e-010 7.934557e-014  
-1.192118e-009 6.969114e-013 -1.040571e-016

-1.320455e-002 2.309253e-005 -9.207745e-009  
3.709669e-004 -6.811114e-007 3.006641e-010  
-2.278583e-006 4.256842e-009 -1.931521e-012

1.086471e-003 -1.925077e-006 8.252305e-010  
-2.714110e-005 4.971153e-008 -2.251777e-011  
1.584933e-007 -2.945697e-010 1.359216e-013

-1.522828e-005 2.658236e-008 -1.148957e-011  
3.641128e-007 -6.542505e-010 2.964237e-013  
-2.061960e-009 3.737801e-012 -1.714427e-015

-2.422968e-003 4.368535e-006 -1.767501e-009  
6.855201e-005 -1.315845e-007 5.849144e-011  
-4.202125e-007 8.324245e-010 -3.808146e-013

2.027037e-004 -3.728955e-007 1.620426e-010  
-5.221446e-006 1.018682e-008 -4.689284e-012  
3.092328e-008 -6.250414e-011 2.945668e-014

-2.874879e-006 5.251469e-009 -2.305346e-012  
7.181621e-008 -1.397018e-010 6.472223e-014  
-4.169769e-010 8.419805e-013 -3.985569e-016

-4.304205e-003 6.934375e-006 -3.061729e-009  
1.315702e-004 -2.197508e-007 9.996286e-011  
-8.735987e-007 1.466476e-009 -6.705461e-013

3.033175e-004 -5.021800e-007 2.156962e-010  
-9.207347e-006 1.590910e-008 -7.040231e-012  
6.137714e-008 -1.077360e-010 4.822614e-014

-4.078200e-006 6.745122e-009 -2.842967e-012  
1.243291e-007 -2.165222e-010 9.463632e-014  
-8.275373e-010 1.467869e-012 -6.489446e-016

1.692700e-003 -3.117887e-006 1.343553e-009  
-4.785233e-005 8.055260e-008 -3.644180e-011  
3.153545e-007 -4.972971e-010 2.235525e-013

-1.424346e-004 2.501447e-007 -1.116871e-010  
3.370139e-006 -4.896792e-009 2.133673e-012  
-2.025144e-008 2.482117e-011 -9.990082e-015

2.128777e-006 -3.665920e-009 1.668412e-012  
-4.672047e-008 6.183042e-011 -2.641239e-014  
2.672977e-010 -2.652825e-013 9.442426e-017

2.601569e-003 -4.366285e-006 1.680867e-009  
-8.005337e-005 1.455383e-007 -6.436629e-011  
5.167775e-007 -9.652847e-010 4.426790e-013

-2.195566e-004 3.848794e-007 -1.626230e-010  
5.942350e-006 -1.092216e-008 4.958724e-012  
-3.651425e-008 6.849284e-011 -3.188501e-014

3.119570e-006 -5.438017e-009 2.325692e-012  
-8.109775e-008 1.473722e-010 -6.704884e-014  
4.861883e-010 -8.974205e-013 4.165292e-016

4.657428e-004 -7.864553e-007 2.975029e-010  
-1.438168e-005 2.662628e-008 -1.158963e-011  
9.249256e-008 -1.776540e-010 8.034963e-014

-3.987343e-005 7.084298e-008 -2.965943e-011  
1.102908e-006 -2.096031e-009 9.461992e-013  
-6.830963e-009 1.343917e-011 -6.241824e-015

5.712039e-007 -1.013508e-009 4.298450e-013  
-1.533348e-008 2.911131e-011 -1.321746e-014  
9.335726e-011 -1.835015e-013 8.547969e-017

U 4 2 2 5 6  
-5.953284e-007 -4.222907e-010 2.140041e-012 -1.235061e-015  
1.030592e-008 -6.644359e-012 -2.787252e-014 1.900694e-017

9.921059e-009 2.404779e-011 -4.588040e-014 2.264637e-017  
-2.504181e-010 -1.996457e-013 1.088432e-015 -5.914654e-019

-1.054892e-006 -1.047161e-009 4.067053e-012 -2.247809e-015  
1.996533e-008 3.994313e-012 -6.498819e-014 3.829016e-017

1.715653e-008 2.844381e-011 -6.601440e-014 3.331726e-017  
-4.603241e-010 -2.136655e-013 1.717824e-015 -9.776040e-019

1.670888e-007 -8.822857e-010 5.399298e-013 -8.540639e-017  
2.153154e-009 2.148122e-011 -3.176395e-014 1.251033e-017

-7.150842e-009 -7.009713e-012 2.072176e-014 -8.332871e-018  
2.569108e-011 2.698618e-013 -9.106750e-017 -7.304051e-020

3.824729e-007 -4.323052e-010 -5.993588e-013 5.122122e-016  
-3.738606e-009 1.400494e-011 -5.182896e-015 -1.480970e-018

-9.610946e-009 -6.598597e-012 2.750318e-014 -1.388459e-017  
1.457560e-010 1.553921e-013 -4.605736e-016 2.074805e-019

6.218910e-008 -5.851825e-011 -1.126078e-013 8.993026e-017  
-6.879884e-010 1.980590e-012 -2.405333e-016 -5.206407e-019

-1.511509e-009 -8.565301e-013 4.223293e-015 -2.216336e-018  
2.476525e-011 1.896899e-014 -7.654036e-017 3.758863e-020

4.953068e-006 2.489522e-009 -1.803281e-011 1.077586e-014  
-7.917840e-008 3.161554e-011 2.575061e-013 -1.657889e-016

-1.036536e-007 -1.367593e-010 4.359244e-013 -2.446220e-016  
2.259387e-009 1.051202e-012 -9.756568e-015 5.564063e-018

8.564851e-006 6.646671e-009 -3.098027e-011 1.758356e-014  
-1.580220e-007 -2.898721e-011 5.311951e-013 -3.141400e-016

-1.700427e-007 -1.654874e-010 5.962191e-013 -3.300243e-016

4.304400e-009 7.460285e-013 -1.557314e-014 9.265900e-018  
  
 -9.482728e-007 4.023215e-009 -1.981962e-012 2.023983e-016  
 -2.828289e-008 -1.063630e-010 2.137834e-013 -9.773608e-017  
  
 4.607238e-008 6.736432e-011 -1.527035e-013 5.916945e-017  
 1.900809e-010 -2.039922e-012 -6.277858e-016 1.294012e-018  
  
 -2.807315e-006 1.555220e-009 5.916863e-012 -4.155563e-015  
 2.364331e-008 -6.710403e-011 6.962914e-015 1.704104e-017  
  
 7.627642e-008 5.707152e-011 -2.311777e-013 1.185951e-016  
 -1.091053e-009 -1.076571e-012 3.472925e-015 -1.620968e-018  
  
 -4.624505e-007 1.971238e-010 1.046504e-012 -7.170585e-016  
 4.711375e-009 -9.427890e-012 -3.340830e-015 5.079236e-018  
  
 1.221020e-008 7.651373e-012 -3.613541e-014 1.914781e-017  
 -1.947236e-010 -1.297777e-013 6.116707e-016 -3.113571e-019  
  
 -1.255750e-005 -2.803803e-009 4.662916e-011 -2.927765e-014  
 1.696885e-007 -7.558347e-011 -6.578931e-013 4.248310e-016  
  
 2.850494e-007 2.046534e-010 -1.171437e-012 7.181110e-016  
 -5.330515e-009 -1.146154e-012 2.429101e-014 -1.440206e-017  
  
 -2.189492e-005 -1.124699e-008 7.474222e-011 -4.427534e-014  
 3.691673e-007 2.741995e-011 -1.296720e-012 7.872481e-016  
  
 4.712084e-007 2.736304e-010 -1.564379e-012 9.264343e-016  
 -1.101292e-008 1.000547e-013 4.026677e-014 -2.477227e-017  
  
 4.783419e-007 -5.934367e-009 2.508240e-012 -3.258030e-017  
 9.820662e-008 1.672504e-010 -4.969788e-013 2.535165e-016  
  
 -6.029489e-008 -1.663422e-010 3.144947e-013 -1.212744e-016  
 -1.649237e-009 4.812961e-012 4.759656e-015 -4.864348e-018

5.867295e-006 -1.906866e-009 -1.571815e-011 1.051996e-014  
 -3.792110e-008 1.098593e-010 8.098621e-015 -4.005603e-017  
  
 -1.640973e-007 -1.299051e-010 5.572225e-013 -2.978184e-016  
 2.096307e-009 2.293446e-012 -7.335578e-015 3.520539e-018  
  
 9.989452e-007 -2.251321e-010 -2.728788e-012 1.802045e-015  
 -8.817292e-009 1.558290e-011 1.224561e-014 -1.257145e-017  
  
 -2.709959e-008 -1.753335e-011 8.845743e-014 -4.858563e-017  
 4.054480e-010 2.693007e-013 -1.377164e-015 7.255041e-019  
  
 1.232365e-005 -5.109011e-011 -4.927959e-011 3.189984e-014  
 -1.549034e-007 8.016691e-011 6.734759e-013 -4.380039e-016  
  
 -2.936839e-007 -1.007474e-010 1.270264e-012 -8.189785e-016  
 4.965828e-009 1.747051e-013 -2.409481e-014 1.457706e-017  
  
 2.181110e-005 6.884012e-009 -7.535390e-011 4.608209e-014  
 -3.572481e-007 1.192690e-011 1.306509e-012 -8.108923e-016  
  
 -4.909764e-007 -1.640771e-010 1.662739e-012 -1.030117e-015  
 1.115412e-008 -1.522155e-012 -4.181224e-014 2.629464e-017  
  
 3.176657e-007 3.752362e-009 -8.622027e-013 -6.142651e-016  
 -1.154094e-007 -1.129059e-010 4.909834e-013 -2.648112e-016  
  
 3.318281e-008 1.620645e-010 -2.829857e-013 1.134915e-016  
 2.416917e-009 -4.694776e-012 -7.026930e-015 6.032520e-018  
  
 -5.360991e-006 1.196794e-009 1.697116e-011 -1.125297e-014  
 2.604106e-008 -8.226712e-011 -2.156750e-014 4.171195e-017  
  
 1.507972e-007 1.145434e-010 -5.616428e-013 3.130121e-016  
 -1.703367e-009 -2.006172e-012 6.560902e-015 -3.279151e-018  
  
 -9.302365e-007 1.406291e-010 2.913325e-012 -1.912946e-015



7.208639e-009 -1.193714e-011 -1.465659e-014 1.319440e-017  
 2.539153e-008 1.532799e-011 -8.998936e-014 5.128136e-017  
 -3.561116e-010 -2.261837e-013 1.300626e-015 -7.123313e-019  
  
 -5.166866e-006 7.743884e-010 2.179444e-011 -1.428382e-014  
 6.370062e-008 -3.527882e-011 -2.928623e-013 1.907528e-016  
  
 1.280238e-007 1.412803e-011 -5.771012e-013 3.808301e-016  
 -1.976304e-009 1.133158e-013 1.000368e-014 -6.078033e-018  
  
 -9.152861e-006 -1.683898e-009 3.232615e-011 -2.013095e-014  
 1.514796e-007 -1.756366e-011 -5.689009e-013 3.582211e-016  
  
 2.142183e-007 3.660626e-011 -7.468864e-013 4.751266e-016  
 -4.839644e-009 1.068054e-012 1.849105e-014 -1.177951e-017  
  
 -1.842229e-007 -1.159410e-009 -4.475057e-013 7.434772e-016  
 5.353120e-008 3.505164e-011 -2.092185e-013 1.157849e-016  
  
 -9.951013e-009 -6.601639e-011 1.201460e-013 -5.209348e-017  
 -1.240148e-009 1.970028e-012 3.648094e-015 -2.904734e-018  
  
 2.235316e-006 -4.488217e-010 -7.847420e-012 5.216461e-015  
 -8.796767e-009 2.947938e-011 1.491786e-014 -2.047667e-017  
  
 -6.269781e-008 -4.232128e-011 2.483595e-013 -1.432464e-016  
 6.426404e-010 7.537898e-013 -2.675754e-015 1.400569e-018  
  
 3.896253e-007 -5.660592e-011 -1.331639e-012 8.774192e-016  
 -2.790367e-009 4.397158e-012 7.306492e-015 -6.188338e-018  
  
 -1.064299e-008 -5.572142e-012 3.992603e-014 -2.344199e-017  
 1.426727e-010 8.038114e-014 -5.507075e-016 3.128480e-019  
  
 7.663331e-007 -1.858817e-010 -3.351976e-012 2.208754e-015

-9.412591e-009 5.413296e-012 4.459644e-014 -2.905241e-017

-1.970196e-008 5.957861e-013 9.124160e-014 -6.085069e-017  
2.751455e-010 -2.544748e-014 -1.443446e-015 8.740460e-019

1.360543e-006 1.308653e-010 -4.897378e-012 3.082006e-015  
-2.320534e-008 4.127612e-012 8.863181e-014 -5.635079e-017

-3.309803e-008 -1.927483e-012 1.182519e-013 -7.643709e-017  
7.506477e-010 -2.091322e-013 -2.905793e-015 1.866069e-018

9.465012e-009 1.486142e-010 2.194288e-013 -2.114803e-016  
-8.512348e-009 -4.123138e-012 3.176250e-014 -1.779603e-017

1.470557e-009 9.500161e-012 -1.937661e-014 9.095802e-018  
2.105650e-010 -2.969120e-013 -6.263780e-016 4.785795e-019

-3.475745e-007 7.479270e-011 1.296754e-012 -8.657032e-016  
1.250836e-009 -4.088502e-012 -3.292773e-015 3.739919e-018

9.658900e-009 5.517480e-012 -3.972977e-014 2.351891e-017  
-9.296602e-011 -1.012654e-013 4.085365e-016 -2.231657e-019

-6.027212e-008 1.013989e-011 2.173563e-013 -1.438887e-016  
4.203034e-010 -6.266357e-013 -1.297438e-015 1.059225e-018

1.641611e-009 7.095744e-013 -6.388565e-015 3.836765e-018  
-2.147381e-011 -1.001195e-014 8.608191e-017 -5.042097e-020

‘calc\_rtcoef.pro’

Function calc\_rtcoef\_500, A1, a2, Q1, q2, RH

```
if q2 lt 0 then begin
    q2 = -q2
    Q1 = -Q1
endif
if q2 eq 0 and Q1 lt 0 then Q1 = -Q1

s = RH - 100.0

openr, lun , 'C:\parameter1.txt',/get_lun

    Var = create_struct('name','A','d1',2,'d2',2,'d3',3)
    readf,lun,Var,format='(A4,3I4)'
    B1 = fltarr(Var.d1,Var.d2,Var.d3)
    readf,lun,B1

    abc = "
    readf,lun,abc
    Var = create_struct('name','A','d1',2,'d2',2,'d3',3)
    readf,lun,Var,format='(A4,3I4)'
    B2 = fltarr(Var.d1,Var.d2,Var.d3)
    readf,lun,B2

    readf,lun,abc
    Var = create_struct('name','A','d1',2,'d2',2,'d3',3)
    readf,lun,Var,format='(A4,3I4)'
    C1 = fltarr(Var.d1,Var.d2,Var.d3)
    readf,lun,C1

    readf,lun,abc
    Var = create_struct('name','A','d1',2,'d2',2,'d3',3)
    readf,lun,Var,format='(A4,3I4)'
    C2 = fltarr(Var.d1,Var.d2,Var.d3)
    readf,lun,C2

    readf,lun,abc
    Var = create_struct('name','A','d1',2,'d2',2,'d3',3)
    readf,lun,Var,format='(A4,3I4)'
    D = fltarr(Var.d1,Var.d2,Var.d3)
    readf,lun,D
```

```

readf,lun,abc
Var = create_struct('name','A','d1',2,'d2',2,'d3',3)
readf,lun,Var,format='(A4,3I4)'
F = fltarr(Var.d1,Var.d2,Var.d3)
readf,lun,F

readf,lun,abc
Var = create_struct('name','A','d1',2,'d2',2,'d3',3)
readf,lun,Var,format='(A4,3I4)'
H = fltarr(Var.d1,Var.d2,Var.d3)
readf,lun,H

readf,lun,abc
Var = create_struct('name','A','d1',2,'d2',2,'d3',3)
readf,lun,Var,format='(A4,3I4)'
M = fltarr(Var.d1,Var.d2,Var.d3)
readf,lun,M

readf,lun,abc
Var = create_struct('name','A','d1',2,'d2',2,'d3',3)
readf,lun,Var,format='(A4,3I4)'
V = fltarr(Var.d1,Var.d2,Var.d3)
readf,lun,V

close,lun
free_lun,lun
;=====
;1)   calc the value of analytic solution, NB and Ncomb
;-----
;1.1) calc the value of N_brown
      NB = 10^( -14.6175 - 0.778360*alog10(a2) + 0.166410*alog10(a2)^2 $
          - 0.041937*alog10(a2)^3 )
;-----
;1.2) calc the value of N_comb
;-----
      x = (0.438-0.299*alog10(a2)^1+0.103*alog10(a2)^2-0.275*alog10(a2)^3 $
          -0.104*alog10(a2)^4)*0.01*Q1*q2 + (7.485-0.457*alog10(a2)^1 $
          -15.378*alog10(a2)^2-6.973*alog10(a2)^3+6.858*alog10(a2)^4 $
          +6.031*alog10(a2)^5+1.260*alog10(a2)^6)*s

      x_RH = (7.485-0.457*alog10(a2)^1-15.378*alog10(a2)^2-6.973*alog10(a2)^3 $
          +6.858*alog10(a2)^4+6.031*alog10(a2)^5+1.260*alog10(a2)^6)*s

      if x eq 0 then begin

```

```

    Ncomb = NB
endif else begin
    Ncomb = NB*x/(exp(x)-1)
endelse

if x_RH eq 0 then begin
    N_0_0_RH_500 = NB
endif else begin
    N_0_0_RH_500 = NB*x_RH/(exp(x_RH)-1)
endelse
;=====
; 2)   calc the value of R_0_0_RH_500
;-----
    if a2 le 0.2 then begin
        R_0_0_RH_500 = N_0_0_RH_500
        R_0_0_100_500 = NB
    endif else begin
        if RH le 100 then begin
            R_0_0_RH_500 = N_0_0_RH_500 + 10^( (-14.25 + 0.41*s + 0.030*s^2) $
                + ( 1.37 - 1.01*s - 0.1*s^2) * alog10(a2) )
        endif else begin
            R_0_0_RH_500 = N_0_0_RH_500 + 10^( (-14.25 - 0.47*s - 0.005*s^2) $
                + ( 1.37 + 1.35*s - 0.1*s^2) * alog10(a2) )
        endelse
        R_0_0_100_500 = NB + 10^(-14.25 + 1.37*alog10(a2))
    endelse
;=====
; 3)   calc the value of R_0_q2_RH_500
;-----
    if q2 eq 0 then begin
        R_0_q2_RH_500 = R_0_0_RH_500
    endif else begin
        if a2 le 0.2 then begin
            if RH lt 100 then begin
                z = 0
                for i = 0, (size(B1))(1)-1 do begin
                    for j = 0, (size(B1))(2)-1 do begin
                        for k = 0, (size(B1))(3)-1 do begin
                            z = z + B1(i,j,k)*s^i*alog10(a2)^j*alog10(q2)^k
                        end
                    end
                end
            end
        end
    end
end

```

```

    R_0_q2_RH_500 = R_0_0_RH_500 + 10^z
endif else begin
    z = 0
    for i = 0, (size(B2))(1)-1 do begin
        for j = 0, (size(B2))(2)-1 do begin
            for k = 0, (size(B2))(3)-1 do begin
                z = z + B2(i,j,k)*s^i*alog10(a2)^j*alog10(q2)^k
            end
        end
    end
    R_0_q2_RH_500 = R_0_0_RH_500 + 10^z
endelse
endif else begin
    if RH le 100 then begin
        z = 0
        for i = 0, (size(C1))(1)-1 do begin
            for j = 0, (size(C1))(2)-1 do begin
                for k = 0, (size(C1))(3)-1 do begin
                    z = z + C1(i,j,k)*s^i*alog10(a2)^j*alog10(q2)^k
                end
            end
        end
        R_0_q2_RH_500 = R_0_0_RH_500 + 10^z
    end
endif else begin
    z = 0
    for i = 0, (size(C2))(1)-1 do begin
        for j = 0, (size(C2))(2)-1 do begin
            for k = 0, (size(C2))(3)-1 do begin
                z = z + C2(i,j,k)*s^i*alog10(a2)^j*alog10(q2)^k
            end
        end
    end
    R_0_q2_RH_500 = R_0_0_RH_500 + 10^z
endelse
endelse
endelse

if q2 eq 0 then begin
    R_0_q2_100_500 = R_0_0_100_500
endif else begin
    if a2 le 0.2 then begin
        z=-15.608 - 0.437*alog10(a2) + 0.361*alog10(a2)^2 + $
        ( 1.265 + 0.152*alog10(a2) - 0.021*alog10(a2)^2 ) * alog10(q2)
    endif else begin

```

```

        z=-16.505-2.560*log10(a2)-0.285*log10(a2)^2+0.876*log10(a2)^3+(1.669 $
        +0.893*log10(a2)-0.552*log10(a2)^2-1.114*log10(a2)^3 )*log10(q2)
    endelse
        R_0_q2_100_500 = R_0_0_100_500 + 10^z
    endelse

    if s lt -5 or abs(q2) gt 100 then begin
        R_0_q2_RH_500 = R_0_0_RH_500 + R_0_q2_100_500 + R_0_0_100_500
    endif
;=====
; 4)   calc the value of R_Q1_0_RH_500
;-----
    if a2 ge 0.5 then begin
        z = 0
        for i = 0, (size(D))(1)-1 do begin
            for j = 0, (size(D))(2)-1 do begin
                for k = 0, (size(D))(3)-1 do begin
                    z = z + D(i,j,k) * s^i * a2^j * abs(Q1)^(k+1)
                end
            end
        end
        R_Q1_0_RH_500 = R_0_0_RH_500 + abs(z)

        R_Q1_0_100_500 = R_0_0_100_500 + (-5.571e-19 - 2.953e-18*a2)*Q1 + $
        (-1.974e-19 + 4.797e-19*a2)*Q1^2
        if s lt -5 or abs(Q1) > 100 then begin
            R_Q1_0_RH_500 = R_0_0_RH_500 + R_Q1_0_100_500 - R_0_0_100_500
        endif
    endif else begin
        R_Q1_0_RH_500 = R_0_0_RH_500
    endelse
;=====
; 5)   calc the value of R_Q1_q2_RH_500, Q1 and q2 are opposite-sign
;-----
    if Q1*q2 lt 0 then begin
        if a2 le 0.2 then begin
            E = fltarr(4)
            for i = 0,(size(F))(1)-1 do begin
                for j = 0,(size(F))(2)-1 do begin
                    for k = 0,(size(F))(3)-1 do begin
                        E(i) = E(i) + F(i,j,k)*log10(a2)^j*s^k
                    end
                end
            end
        end
    end

```

```

        end
    end
    end
    z = E(0) + E(1)*alog10(abs(Q1)) + E(2)*alog10(abs(q2)) $
        + E(3)*alog10(abs(Q1))*alog10(abs(q2))
    R_Q1_q2_RH_500 = R_0_q2_RH_500 + 10^z
endif else begin
    G = fltarr(4)
    for i = 0,(size(H))(1)-1 do begin
        for j = 0,(size(H))(2)-1 do begin
            for k = 0,(size(H))(3)-1 do begin
                G(i) = G(i) + H(i,j,k)*alog10(a2)^j*s^k
            end
        end
    end
    end
    if a2 gt 0.2 then begin
        z = G(0) + G(1)*alog10(abs(Q1)) + G(2)*alog10(abs(q2)) $
            + G(3)*alog10(abs(Q1))*alog10(abs(q2))
        R_Q1_q2_RH_500=R_0_q2_RH_500+R_Q1_0_RH_500-R_0_0_RH_500+10^z
    endif
endelse

if s lt -5 or abs(Q1) gt 100 or abs(q2) gt 100 then begin
    R_Q1_q2_RH_500=Ncomb+R_Q1_0_RH_500+R_0_q2_RH_500-R_0_0_RH_500-
    N_0_0_RH
endif

endif
;=====
; 6)   calc the value of R_Q1_q2_RH_500, Q1 and q2 are same-sign
;-----
    if Q1*q2 gt 0 then begin
        if a2 le 0.2 then begin
            L = fltarr(3)
            for i = 0,(size(M))(1)-1 do begin
                for j = 0,(size(M))(2)-1 do begin
                    for k = 0,(size(M))(3)-1 do begin
                        L(i) = L(i) + M(i,j,k)*alog10(a2)^j*s^k
                    end
                end
            end
            end
            z = L(0)*Q1*q2 + L(1)*Q1*q2^2 + L(2)*Q1^2*q2
            R_Q1_q2_RH_500 = R_0_q2_RH_500 / 10^z

```



```

endif else begin
    U = fltarr(3)
    for i = 0,(size(V))(1)-1 do begin
        for j = 0,(size(V))(2)-1 do begin
            for k = 0,(size(V))(3)-1 do begin
                U(i) = U(i) + V(i,j,k)*alog10(a2)^j*s^k
            end
        end
    end
    z = U(0)*Q1*q2 + U(1)*Q1*q2^2 + U(2)*Q1^2*q2
    R_Q1_q2_RH_500 = (R_0_q2_RH_500 + R_q1_0_RH_500 - R_0_0_RH_500) / 10^z
endelse

if s lt -5 or abs(Q1) gt 100 or abs(q2) gt 100 then begin
    y = 1 + exp(-x/(5.0+0.5*q2)) * (R_0_q2_100_500/NB - 1)
    R_Q1_q2_RH_500 = NB * x / (exp(x/y)-1)
endif

endif

if q2 eq 0 then R_Q1_q2_RH_500 = R_Q1_0_RH_500
if Q1 eq 0 then R_Q1_q2_RH_500 = R_0_q2_RH_500

return, [R_0_0_RH_500, R_0_q2_RH_500, R_Q1_0_RH_500, R_Q1_q2_RH_500]

end
=====
;
=====
;

Function calc_rtcoef_den, A1, a2, Q1, q2, RH, density

if q2 lt 0 then begin
    q2 = -q2
    Q1 = -Q1
endif
if q2 eq 0 and Q1 lt 0 then Q1 = -Q1

s = RH - 100.0

rtcoef500 = calc_rtcoef_500(A1, a2, Q1, q2, RH)
R_0_0_RH_500 = rtcoef500(0)
R_0_q2_RH_500 = rtcoef500(1)
R_Q1_0_RH_500 = rtcoef500(2)

```

```

R_Q1_q2_RH_500 = rtcoef500(3)

if a2 lt 0.2 then    return,  R_Q1_q2_RH_500

; 1)    read parameters
;-----
openr, lun , 'C:\parameter2.txt',/get_lun
  Var = create_struct('name','A','d1',2,'d2',2,'d3',3)
  readf,lun,Var,format='(A4,3I4)'
  A = fltarr(Var.d1, Var.d2, Var.d3)
  readf,lun,A

  abc = "
  readf,lun,abc
  Var = create_struct('name','A','d1',2,'d2',2,'d3',3)
  readf,lun,Var,format='(A4,3I4)'
  B = fltarr(Var.d1, Var.d2, Var.d3)
  readf,lun,B

  readf,lun,abc
  Var = create_struct('name','A','d1',2,'d2',2,'d3',3,'d4',4)
  readf,lun,Var,format='(A4,4I4)'
  C = fltarr(Var.d1, Var.d2, Var.d3, Var.d4)
  readf,lun,C

  readf,lun,abc
  readf,lun,abc
  Var = create_struct('name','A','d1',2,'d2',2,'d3',3,'d4',4)
  readf,lun,Var,format='(A4,4I4)'
  D = fltarr(Var.d1, Var.d2, Var.d3, Var.d4)
  readf,lun,D

  readf,lun,abc
  readf,lun,abc
  Var = create_struct('name','A','d1',2,'d2',2,'d3',3,'d4',4)
  readf,lun,Var,format='(A4,4I4)'
  E = fltarr(Var.d1, Var.d2, Var.d3, Var.d4)
  readf,lun,E

  readf,lun,abc
  readf,lun,abc
  Var = create_struct('name','A','d1',2,'d2',2,'d3',3,'d4',4)
  readf,lun,Var,format='(A4,4I4)'
  F = fltarr(Var.d1, Var.d2, Var.d3, Var.d4)

```

```

readf,lun,F

readf,lun,abc
readf,lun,abc
Var = create_struct('name','A','d1',2,'d2',2,'d3',3,'d4',4,'d5',5)
readf,lun,Var,format='(A4,5I4)'
G = fltarr(Var.d1,Var.d2,Var.d3,Var.d4,Var.d5)
readf,lun,G

readf,lun,abc
readf,lun,abc
readf,lun,abc
Var = create_struct('name','A','d1',2,'d2',2,'d3',3,'d4',4,'d5',5)
readf,lun,Var,format='(A4,5I4)'
H = fltarr(Var.d1,Var.d2,Var.d3,Var.d4,Var.d5)
readf,lun,H

readf,lun,abc
readf,lun,abc
readf,lun,abc
Var = create_struct('name','A','d1',2,'d2',2,'d3',3,'d4',4,'d5',5)
readf,lun,Var,format='(A4,5I4)'
U = fltarr(Var.d1,Var.d2,Var.d3,Var.d4,Var.d5)
readf,lun,U

close,lun
free_lun,lun
;=====

; 2)   calc R_0_0_RH_den
;-----
if density lt 1000 then begin
    z = 0
    for i = 0,(size(A))(1)-1 do begin
        for j = 0,(size(A))(2)-1 do begin
            for k = 0,(size(A))(3)-1 do begin
                z = z + A(i,j,k)*(density-500.0)^(i+1)*s^j*a2^k
            end
        end
    end
    R_0_0_RH_den = R_0_0_RH_500 + z
    if s lt -5 then R_0_0_RH_den = R_0_0_RH_500
endif else begin
    z = 0

```

```

for i = 0,(size(B))(1)-1 do begin
  for j = 0,(size(B))(2)-1 do begin
    for k = 0,(size(B))(3)-1 do begin
      z = z + B(i,j,k) * (density-500.0)^(i+1) * s^j * a2^k
    end
  end
end
R_0_0_RH_den = R_0_0_RH_500*10^z
if s lt -5 then R_0_0_RH_den = R_0_0_RH_500
endelse
;=====
; 3)   calc R_0_q2_RH_den
;-----
if density lt 1000 then begin
  z = 0
  for i = 0,(size(C))(1)-1 do begin
    for j = 0,(size(C))(2)-1 do begin
      for k = 0,(size(C))(3)-1 do begin
        for r = 0,(size(C))(4)-1 do begin
          z = z+C(i,j,k,r)*(density-500.0)^(i+1)*q2^(j+1)*s^k*a2^r
        end
      end
    end
  end
  R_0_q2_RH_den = R_0_q2_RH_500 + R_0_0_RH_den - R_0_0_RH_500 + z
  if s lt -5 or abs(q2) gt 100 then begin
    R_0_q2_RH_den = R_0_q2_RH_500 + R_0_0_RH_den - R_0_0_RH_500
  endif
endif else begin
  z = 0
  for i = 0,(size(D))(1)-1 do begin
    for j = 0,(size(D))(2)-1 do begin
      for k = 0,(size(D))(3)-1 do begin
        for r = 0,(size(D))(4)-1 do begin
          z = z+D(i,j,k,r)*(density-500.0)^(i+1)*q2^(j+1)*s^k*a2^r
        end
      end
    end
  end
  R_0_q2_RH_den = R_0_q2_RH_500 * R_0_0_RH_den / R_0_0_RH_500 * 10^z
  if s lt -5 then begin
    R_0_q2_RH_den = R_0_q2_RH_500
  endif
endif

```

```

endelse
;=====
; 4)   calc R_Q1_0_RH_den
;-----
      if density lt 1000 then begin
        z = 0
        for i = 0,(size(E))(1)-1 do begin
          for j = 0,(size(E))(2)-1 do begin
            for k = 0,(size(E))(3)-1 do begin
              for r = 0,(size(E))(4)-1 do begin
                z = z+E(i,j,k,r)*(density-500.0)^(i+1)*Q1^(j+1)*s^k*a2^r
              end
            end
          end
        end
        R_Q1_0_RH_den = R_Q1_0_RH_500 + R_0_0_RH_den - R_0_0_RH_500 + z
        if s lt -5 or abs(Q1) gt 100 then begin
          R_Q1_0_RH_den = R_Q1_0_RH_500 + R_0_0_RH_den - R_0_0_RH_500
        endif
      endif else begin
        z = 0
        for i = 0,(size(F))(1)-1 do begin
          for j = 0,(size(F))(2)-1 do begin
            for k = 0,(size(F))(3)-1 do begin
              for r = 0,(size(F))(4)-1 do begin
                z = z+F(i,j,k,r)*(density-500.0)^(i+1)*Q1^(j+1)*s^k*a2^r
              end
            end
          end
        end
        R_Q1_0_RH_den = R_Q1_0_RH_500 * R_0_0_RH_den / R_0_0_RH_500 * 10^z
        if s lt -5 then begin
          R_Q1_0_RH_den = R_Q1_0_RH_500
        endif
      endelse
;=====

; 5)   calc R_Q1_q2_RH_den   for opposite-sign charges, Q1*q2 < 0
;-----
      if Q1*q2 lt 0 then begin
        if density lt 1000 then begin
          z = 0
          for i = 0,(size(G))(1)-1 do begin

```

```

        for j = 0,(size(G))(2)-1 do begin
            for k = 0,(size(G))(3)-1 do begin
                for r = 0,(size(G))(4)-1 do begin
                    for t = 0,(size(G))(5)-1 do begin
                        z = z + G(i,j,k,r,t) * (density-500.0)^(i+1) $
                            * abs(Q1)^(j+1) * abs(q2)^(k+1) * s^r * a2^t
                    end
                end
            end
        end
        R_Q1_q2_RH_den = (R_0_q2_RH_den + R_Q1_0_RH_den - R_0_0_RH_den ) + $
            (R_Q1_q2_RH_500 - R_0_q2_RH_500 - R_Q1_0_RH_500 + R_0_0_RH_500 ) + z
        if s lt -5 or abs(Q1) gt 100 or abs(q2) gt 100 then begin
            R_Q1_q2_RH_den = R_0_q2_RH_den + R_Q1_q2_RH_500 - R_0_q2_RH_500
        endif
    endif else begin
        z = 0
        for i = 0,(size(H))(1)-1 do begin
            for j = 0,(size(H))(2)-1 do begin
                for k = 0,(size(H))(3)-1 do begin
                    for r = 0,(size(H))(4)-1 do begin
                        for t = 0,(size(H))(5)-1 do begin
                            z = z + H(i,j,k,r,t) * (density-500.0)^(i+1) * abs(Q1)^j $
                                * abs(q2)^k * s^r * a2^t
                        end
                    end
                end
            end
        end
        R_Q1_q2_RH_den=R_0_q2_RH_den+(R_Q1_q2_RH_500-R_0_q2_RH_500)*10^z
        if s lt -5 then begin
            R_Q1_q2_RH_den = R_0_q2_RH_den + R_Q1_q2_RH_500 - R_0_q2_RH_500
        endif
    endelse
end
=====
; 6)   calc R_Q1_q2_RH_den   for same-sign charges,   Q1*q2 > 0
;-----
    if Q1*q2 gt 0 then begin
        z = 0
        for i = 0,(size(U))(1)-1 do begin
            for j = 0,(size(U))(2)-1 do begin

```

```

        for k = 0,(size(U))(3)-1 do begin
            for r = 0,(size(U))(4)-1 do begin
                for t = 0,(size(U))(5)-1 do begin
                    z = z + U(i,j,k,r,t) * (density-500.0)^(i+1) * Q1^(j+1) $
                        * q2^(k+1) * s^r * a2^t
                end
            end
        end
    end
    R_Q1_q2_RH_den=(R_0_q2_RH_den*R_Q1_q2_RH_500/R_0_q2_RH_500)*10^z
end
;=====

if q2 eq 0 then    R_Q1_q2_RH_den = R_Q1_0_RH_den
if Q1 eq 0 then    R_Q1_q2_RH_den = R_0_q2_RH_den

return, R_Q1_q2_RH_den

end
;=====
;=====

pro calc_rate_rtcoef

; Set inputs
;-----
A1 = 3.0                ; Droplet radius
a2 = 1.0                ; Particle radius
Q1 = -20.0              ; Droplet Charge
q2 = 50.0               ; Particle Charge
RH = 99.0               ; Relative humidity
density = 1500.0         ; Particle density

rtcoef = calc_rtcoef_den(A1, a2, Q1, q2,RH, density)

print,'collision rate coefficient = ', rtcoef

end

```

## BIOGRAPHICAL SKETCH

Liang Zhang was born in October 2, 1985 in the city of Lanxi, Heilongjiang province in China. He was the second child of Fengxue Zhang and Shuxiang Wang, the first having been his sister, Lili Zhang. He attended ShuangFeng elementary school, then NO. 3 middle school Lanxi and NO.1 high school in Lanxi. In 2005, he entered the Peking University at Beijing and graduated with his B.S. in Space Physics in 2009. He later began to pursue his Master's degree in the National Space Science Center, Chinese Academy of Sciences in 2009 through 2012. He applied to UT Dallas to further his research in space science as a Physics PhD candidate in August 2012. He married his wife Xiumei Fan in 2015, and he is now in the progress of completing his degree and prepared to go back to China to unite with his wife and family.



## CURRICULUM VITAE

**Name:** Liang Zhang

**Gender:** Male

**Native place:** Heilongjiang, China

**Date of Birth:** October, 1985

### **Education:**

2005 – 2009:

University: Peking University

Department: School of Earth and Space Sciences

Major: Space Physics

Degree: Bachelor

2009 – 2012:

University: Chinese Academy of Sciences

Department: National Space Science Center

Major: Space Physics

Degree: Master

2012 – 2017:

University: The University of Texas at Dallas

Department: Physics Department

Major: Space Physics

Degree: Doctor

**Contact:** [lxz121930@utdallas.edu](mailto:lxz121930@utdallas.edu), 469-605-0670